THEORY OF SOUND GENERATION IN DUCTED COMPRESSIBLE FLOWS, WITH APPLICATIONS TO TURBOMACHINERY

by

C. L. MORFEY, B.A., M.Sc.(Eng.)

Thesis submitted for the degree of Doctor of Philosophy in the University of Southampton, Faculty of Engineering and Applied Science

Institute of Sound and Vibration Research
The University, Southampton, England

3 January 1970

ACKNOWLEDGMENTS

The author wishes to thank Dr. P.O.A.L.Davies (I.S.V.R.) who acted as supervisor, Mr. P.E.Doak (I.S.V.R.) and Prof. G.M.Lilley (Department of Aeronautics and Astronautics) for their encouragement in this work and for many helpful discussions.

Thanks are due also to the past and present Directors of the Institute, Prof. E.J.Richards and Prof. B.L.Clarkson, and the author's colleagues for their cooperation in arranging two periods of leave, during 1966-67 and 1969. The present thesis would not have been written otherwise.

Finally, it is a pleasure to thank Hawker-Siddeley Aviation Ltd. for financial support over the past five years, and the following establishments for providing the environment in which most of the thesis was actually written:

Bolt, Beranek and Newman Inc., Cambridge, Mass. (academic year 1966-67)

General Electric Co., Aircraft Engine Group, Evendale, Ohio (August 1968)

Cambridge University Engineering Department (September-October 1969).

ABSTRACT

FACULTY OF ENGINEERING AND APPLIED SCIENCE
INSTITUTE OF SOUND AND VIBRATION RESEARCH

Doctor of Philosophy

THEORY OF SOUND GENERATION IN DUCTED COMPRESSIBLE FLOWS, WITH APPLICATIONS TO TURBOMACHINERY

by Christopher Leonard Morfey

Theoretical results relating to sound in subsonic flows are obtained in part (A), and used in part (B) to estimate the sound power output of axial-flow machines. Topics covered in (A) are acoustic energy conservation in nonuniform flows, nonlinear sources of sound, and the generation of sound in ducts. The applications discussed in (B) include discrete-frequency sound generation due to rotor-stator interaction, and the radiation of sound from a subsonic rotor in turbulent flow. Finally, shock-wave radiation from supersonic rotors is described in terms of a simple theoretical model, and the predicted shock strengths are compared with measurements.

CONTENTS

LIST OF FIGURES

CHAPTER I

INTRODUCTION

1.1 HISTORICAL BACKGROUND

Lord Rayleigh, the founder of modern acoustic theory, died in 1919. For the last ten years of his life he had presided over the newly-formed Advisory Committee on Aeronautics - later to become the Aeronautical Research Council - and had seen aviation develop from Bleriot's cross-channel flight to the point where aircraft could cross the Atlantic. The association between acoustics and aerodynamics seems to have ended with Rayleigh's death, however; over the next twenty years the science of acoustics was developed by telecommunications engineers, and was largely neglected by natural philosophers in favour of electromagnetism and atomic physics.

During these years the growth of the aircraft industry was slow, at least compared with the immediately preceding period. Regular trans-atlantic flights had only just been inaugurated when the situation was transformed by World War II with the need to produce military aircraft on a large scale. As a result, civil aviation has grown rapidly in the post-war years and with it, the need to control the noise of aircraft.

Fortunately when the need became apparent, there was a certain amount of acoustical theory to turn to, largely as a result of wartime efforts in Russia and Germany to understand sound generation by ships and aircraft for detection purposes. With this background, and with the imminent

introduction of jet-powered aircraft threatening a rapid increase in noise levels around airports, research was begun in this country in 1949 into the sources of aircraft noise.

The result has been the emergence of aeroacoustics, dealing with sound generated aerodynamically, as a new and important branch of acoustics. By 1959, when the Boeing 707 entered airline service, enough was known about jet noise for exhaust nozzles to be designed which achieved some improvement, and more importantly Rolls-Royce were developing the bypass engine to take advantage of the strong dependence of jet noise on exhaust velocity. Further impetus to the new science came from the military sphere, where rocket launch noise and combustion instability raised similar fundamental problems involving a combination of acoustics and aerodynamics.

During the 1960's engine machinery - primarily turbojet compressors and fans - has become recognized as a source of aircraft noise comparable in importance with the exhaust jet; while there remains a number of unsolved problems in connection with jet noise at exhaust velocities below 0.4, or above 1.4, times the ambient speed of sound. The past twenty years' growth in the study of aeronautical acoustics seems likely to continue through the 1970's.

1.2 SCOPE OF THESIS

The following chapters are a theoretical study of one aspect of aircraft noise, namely the internal generation and transmission of sound in turbomachinery. The connecting theme is sound power, as the most important

single property of the various sources studied. Thus it is necessary to begin by considering such fundamental questions as the extent to which acoustic energy is conserved in high-speed flows, and the modifying effects of flow and a surrounding duct on different types of acoustic source.

Specific applications of the resulting acoustic theory are made to each in turn of the discrete-frequency source mechanisms in axial-flow machines, at subsonic and supersonic speeds. The acoustic analysis for ducted source distributions is combined for this purpose with simplified models of the unsteady aerodynamic flows responsible for sound generation, the aim in each case being to predict the acoustic power spectrum.

1.3 OUTLINE OF PRESENTATION

The acoustic theory basic to the present work is developed in the following three chapters, which make up part A of the thesis. Chapter 2 reviews and extends the use of acoustic energy conservation in moving media, and Chapter 3 does the same for aerodynamic sound generation with emphasis on second-order interactions as a source of sound. Chapter 4 develops a theoretical framework for analysing sound sources in ducts, and again flow effects are included.

Part B, consisting of the next four chapters, contains applications of the basic theory to turbomachinery noise. Periodic rotor-stator interaction, interaction of a rotor with turbulence, and radiation from steady blade loading and thickness are all considered quantitatively for subsonic machines. Finally shock-wave radiation from supersonic ducted

rotors is discussed in Chapter 8, and measurements of shock strength shown to agree with a simplified theory.

Previous relevant work is reviewed at the beginning of each chapter, and its relation to the present work discussed at the end of the chapter where appropriate. The thesis ends with a review in Chapter 9 of the main conclusions, and suggestions for further research.

CHAPTER 2

ACOUSTIC ENERGY IN NONUNIFORM FLOWS

In an ideal acoustic medium at rest, the sound power crossing any closed surface S is defined as

$$W = \int_S I_i \, dS_i \quad , \tag{1}$$

where $I_i = \langle p' v_i \rangle$ are the components of the acoustic intensity. The usefulness of sound power derives from its continuity property: if S_1 and S_2 are two surfaces enclosing the same sources of sound (Fig. 2.1), the same value of W is found for both surfaces.

This property is so useful that the question arises whether in a more general situation, such as a moving medium, a quantity can be found analogous to sound power in the classical situation. Two approaches are possible.

(a) For small-amplitude acoustic disturbances in an ideal fluid at rest, W is equal to the mean flow of energy across S[†], and the continuity of sound power appears as a consequence of energy conservation. A generalized acoustic intensity may therefore be defined in terms of the total energy flux $\underset{\sim}{N}$ in the flow as

$$\underset{\sim}{I} = \langle \underset{\sim}{N} - \underset{\sim}{N} \text{ (without sound)} \rangle \quad , \tag{2}$$

on the grounds that I_i in (1) represents the mean energy flux in the

---

[†]Provided on average no fluid enters or leaves the enclosed region. Cf. section 2.1.3.

i^{th} direction due to the acoustic disturbance. This is the definition of acoustic intensity adopted, for example, by Morse and Ingard in [1].

(b) Alternatively a vector intensity $\underset{\sim}{I}$ may be sought which is based on first-order estimates of the sound field, and reduces to the classical expression $\langle p'\underset{\sim}{v}\rangle$ in an ideal fluid at rest, but differs from this expression in that div $\underset{\sim}{I}$ vanishes (to second order in fluctuating quantities) over a wider range of conditions than $\mathrm{div}\langle p'\underset{\sim}{v}\rangle$. The wider the range of conditions, the more general is the continuity property and the more useful the definition.

The second approach, although it makes the definition of $\underset{\sim}{I}$ to some extent arbitrary,[†] has an important advantage over the first where linear acoustic theory is concerned. The intensity defined by (2) cannot in general be found from a solution of the linear acoustic equations, since it is of second order in fluctuating quantities - first-order terms disappear in the time-averaging operation. Thus while approach (b) specifically requires only first-order solutions, the energy flux approach (a) requires the equations of motion to be solved to second-order accuracy.

This difficulty has been pointed out by Andreev (who reviews the problem in [3]) and emphasized by Markham [4,5]. Andreev concludes from a second-order analysis that the classical intensity expression $\underset{\sim}{I} = \langle p'\underset{\sim}{v}\rangle$ is not generally valid in the sense of equation (2). Even for isentropic disturbances in a medium otherwise at rest, the energy flux interpretation of $\langle p'\underset{\sim}{v}\rangle$ holds only under certain boundary conditions.

[†] A similar situation arises [2] in the theory of power flow in electron beams.

The classical intensity expression does, on the other hand, satisfy the continuity equation

$$\frac{\partial I_i}{\partial x_i} \doteq 0 \qquad \text{(to 2nd order)} \tag{3}$$

in an ideal uniform fluid at rest, as Schoch [6] points out. Moreover generalized versions of (3), following approach (b) above, have been found by Bergmann [7] for a nonuniform fluid at rest, by Blokhintsev [8] in the geometric-acoustics approximation, and by Cantrell and Hart [9] for irrotational uniform-entropy flows. The present study† adopts the definition of $\underset{\sim}{I}$ given by Cantrell and Hart and applies it to an arbitrary nonuniform flow, in order to demonstrate the conditions under which acoustic energy is in fact conserved in the sense of equation (3).

---

†Parts of which first appeared in [10] in abbreviated form.

2.1 RELATION BETWEEN SOUND POWER AND MEAN ENERGY FLOW

The generalized definition of acoustic intensity used in the analysis is introduced below by an energy argument. Its usefulness in linear acoustics, however, is ultimately determined by the extent to which the continuity property (3) is valid, and the energy interpretation is dropped when this aspect is discussed in section 2.2.

2.1.1 Ideal uniform fluid at rest

If the time-averaged displacement of any fluid particle is zero, the mean energy flux across a fixed surface S may be estimated as the mean energy flux across a material surface, consisting of fluid particles whose mean position coincides with S. Any discrepancy will be of higher than second order in fluctuating quantities, and is therefore negligible for present purposes.

If p, V_n are the fluid pressure and velocity normal to S, defined for a particle of fluid, the instantaneous energy flux normal to S is $N_n = pV_n$ (for an inviscid nonconducting fluid), whose time-average value is

$$\langle N_n \rangle = \langle p' v_n \rangle \tag{4}$$

since the fluid is at rest on average, i.e. $\langle V_n \rangle = 0$. Reinterpreting p' and v_n as fluctuating field quantities, defined on the fixed surface S, gives the classical expression for acoustic intensity. It follows that under the conditions specified, the classical intensity expression - based on field variables which need be estimated only to first-order accuracy - equals the local mean energy flux to second order.

The same result may be derived without considering a material surface, in a way which leads on naturally to the Cantrell and Hart generalization. In terms of field variables, the normal energy flux crossing a fixed surface S is

$$N_n = Jm_n \quad , \tag{5}$$

where J is the stagnation enthalpy $(h + \tfrac{1}{2}V_i^2)$ and m_n is the normal component ρV_n of the mass flux. Time-averaging (5) and noting $\langle m_n \rangle = 0$ gives

$$\langle N_n \rangle = \langle J'm'_n \rangle, \doteq \langle p'v_n \rangle \qquad \text{(to 2nd order)} \tag{6}$$

provided there are no entropy fluctuations so that J' may be estimated to first order as (p'/ρ). This last assumption is justified since we are restricted to an ideal fluid free from entropy gradients; so the equivalence of $\langle p'v_n \rangle$ and the mean energy flux follows as before.

2.1.2 Acoustic energy dissipation

It is interesting to consider the extension of the above argument to non-ideal fluids, since it leads to a useful result relating acoustic energy dissipation to irreversible entropy production. Although the result is well-known, the derivation given in textbooks [11, 12] overlooks the fact that it is not valid locally but only in a space-average sense. An outline of the standard derivation, with emphasis on the assumptions involved, is given below; the result is compared in section 2·2 with that obtained from a more rigorous approach.

The production of entropy by irreversible processes in the fluid is characterized by a uniformly distributed mean production rate $\langle P_S \rangle$ per unit volume.† Thus in order to maintain a steady state, it would be necessary to extract heat from the fluid at a mean rate of approximately $\langle T \rangle \langle P_S \rangle$ per unit volume; cf. [13], section 5. Alternatively, the rate at which energy is fed into the entropy mode (represented here by gradual changes in mean entropy $\langle s \rangle$, density $\langle \rho \rangle$ etc.††), at constant mean pressure, is given by

$$\left.\frac{\partial \langle h \rangle}{\partial t}\right|_{\langle p \rangle = \text{const.}} \doteq \langle T \rangle \frac{\partial \langle s \rangle}{\partial t} \doteq \frac{\langle T \rangle}{\langle \rho \rangle} \langle P_S \rangle \qquad (8)$$

per unit mass of fluid.

In either case, the rate of energy loss from the acoustic mode is approximately $\langle T \rangle \langle P_S \rangle$ per unit volume. If it is further assumed that the mean energy flux associated with the acoustic mode is given by the same expression, $\underset{\sim}{I} = \langle p' \underset{\sim}{v} \rangle$, as in an ideal fluid, it follows that

$$\text{div } \underset{\sim}{I} \doteq -\langle T \rangle \langle P_S \rangle \quad . \qquad (9)$$

Equation (9) expresses the mean energy balance for the acoustic mode. Clearly the idea of weakly-coupled modes of disturbance [14] is basic to the present approach, and it breaks down if the viscosity or thermal conductivity is too large. Nevertheless the result is

---

†i.e. details of the local distribution of mean entropy changes, and the redistribution of entropy by heat transfer between fluid elements, are omitted from the model.

††Short-time averages are implied, as the fluid is no longer necessarily in a stationary state. Mean fluid properties such as $\langle s \rangle$ are therefore slowly-varying functions of time.

useful for estimating the space-average dissipation over regions comparable with the sound wavelength or larger, for example in weakly-attenuated sound waves [11], weak shock waves [15, 16], and acoustic boundary layers [11, 12].

2.1.3 Irrotational uniform-entropy flow

The energy flux expression (5) is valid for any inviscid, non-conducting fluid flow. However, its estimation to second order in fluctuating quantities poses the general difficulty mentioned earlier, that linearized solutions for these quantities are inadequate except in certain special cases.†

Cantrell and Hart [9] have shown how the difficulty may be avoided for irrotational, uniform-entropy flows by going directly to the total energy flow across a closed surface, rather than working out the local energy flux and subtracting its unperturbed value. The total energy flow, as shown below, has a time-average value which can be expressed to second-order accuracy in terms of first-order fluctuations; moreover its continuity is ensured by energy conservation.

For any closed surface S fixed in the flow, the total outward energy flow is

$$\dot{E} = \int_S N_i \, dS_i = \int_S Jm_i \, dS_i \quad . \tag{10}$$

If the flow is irrotational and of uniform entropy over S, it follows

---

†Ribner [17] has studied one such case; see section 2.3.

that the time-average value $\langle J \rangle$ is also uniform over S. If in addition the amount of fluid enclosed by S remains constant on average, so that

$$\int_S \langle m_i \rangle \, dS_i = 0 \quad , \tag{11}$$

equation (10) gives the time-average energy flow out of S as

$$\langle \dot{E} \rangle = \int_S \langle J' m_i' \rangle \, dS_i \quad . \tag{12}$$

Finally, if the specific entropy does not fluctuate with time on S, the quantity $\langle J' m_i' \rangle$ appearing in (12) may be written in terms of the velocity fluctuation components $v_i = V_i - \langle V_i \rangle$ and the pressure fluctuation p'. To second order in fluctuating quantities,

$$\langle J' m_i' \rangle \doteq \langle p' v_i \rangle + \frac{V_i}{\rho c^2} \langle p'^2 \rangle + \frac{V_i V_j}{c^2} \langle p' v_j \rangle + \rho V_j \langle v_i v_j \rangle . \tag{13}$$

The assumption $s' = 0$ is justified provided the flow over S is free from any entropy gradients.

The main point of interest here is that the collection of second-order terms on the right-hand side of (13) meets all the requirements for a generalized definition of acoustic intensity, as listed for approach (b) in the introduction. In particular, defining sound power as the surface integral in (12) extends the continuity property of sound power to all irrotational uniform-entropy flows, provided diffusion effects are negligible and the flow is statistically stationary in time.

2.2 CONTINUITY EQUATION FOR ACOUSTIC ENERGY IN GENERAL FLOWS

A continuity equation for acoustic energy, which covers the previous situations as special cases, can be derived from the linearized equations for unsteady flow as follows. A quantity corresponding to acoustic energy flux is defined by

$$N_i^* = J^* m_i^* \quad , \tag{14}$$

where

$$J^* = V_j u_j + (1/\rho)p' \quad , \quad m_i^* = \rho u_i + (V_i/c^2)p' \tag{15}$$

are first-order quantities which coincide with (J', m_i') in a region of irrotational flow free from entropy fluctuations; here

$$\underset{\sim}{u} = \underset{\sim}{v} - \underset{\sim}{w} \tag{16}$$

is the irrotational velocity field obtained by subtracting the fluctuating velocity field $\underset{\sim}{w}$ induced by vorticity (div $\underset{\sim}{w} = 0$) from the total velocity fluctuation $\underset{\sim}{v}$. The above definition of N_i^* is chosen in the light of the previous section, and is a straightforward generalization of the quantity $J'm_i'$ appearing in Cantrell and Hart's analysis for irrotational uniform-entropy flows.

2.2.1 Linearized equations of motion

The full equations of motion for a viscous heat-conducting fluid may be written as

$$\frac{\partial \rho}{\partial t} + \frac{\partial(\rho V_i)}{\partial x_i} = 0 \quad , \quad \frac{DV_j}{Dt} = R_j - \frac{1}{\rho}\frac{\partial p}{\partial x_j} \quad , \quad \frac{Ds}{Dt} = S/\rho \ . \tag{17}$$

The quantities (R_j, S) include the effects of viscosity and thermal conductivity; thus R_j contains the viscous force component $(-1/\rho)\,\partial/\partial x_i\,(P_{ij} - p\delta_{ij})$ on a fluid element per unit mass, in addition to any external force field. Likewise S represents the rate at which a fluid element gains entropy, per unit volume of the flow, and includes a term

$$S_{diff} = -\frac{1}{T}\left\{\tfrac{1}{2}(P_{ij} - p\delta_{ij})e_{ij} + \frac{\partial q_i}{\partial x_i}\right) \tag{18}$$

due to diffusion effects.

If the equation of state for the fluid is taken as

$$\ell n\ \rho = \theta(p,s) \quad , \tag{19}$$

the fluctuating parts of equations (17) are given to first order by

$$\frac{\partial \rho'}{\partial t} \doteq -\frac{\partial m_i^*}{\partial x_i} - \frac{\partial}{\partial x_i}\,(\rho w_i + \rho V_i \theta_s s') \quad , \tag{20}$$

$$\frac{\partial v_j}{\partial t} \doteq -\frac{\partial J^*}{\partial x_j} - \zeta_{ij}\,u_i - (\theta_s/\rho)\,\left(\frac{\partial s}{\partial x_j}\,p' - \frac{\partial p}{\partial x_j}\,s'\right)$$

$$- \frac{\partial V_j}{\partial x_i}\,w_i - V_i\,\frac{\partial w_j}{\partial x_i} + R_j' \quad , \tag{21}$$

$$\frac{Ds'}{Dt} \doteq -\frac{\partial s}{\partial x_i}\,v_i + (S/\rho)' \quad . \tag{22}$$

2.2.2 The acoustic energy equation

Equation (20) can be further expanded using (19), (22) and the time-averaged continuity and entropy equations from (17). If the resulting equation is then multiplied by J^*, and equation (21) by m_j^*, the sum of the resulting second-order equations can be put in the form

$$\frac{\partial E^*}{\partial t} + \frac{\partial N_i^*}{\partial x_i} = P \quad . \tag{23}$$

Here E^* represents a generalized acoustic energy density, and N_i^* are the components of a generalized acoustic energy flux, given respectively by

$$E^* = \frac{1}{2\bar{\rho}c^2}(p'^2) + \frac{V_j}{c^2}(p'u_j) + \tfrac{1}{2}\rho(u_j^2) \tag{24}$$

and

$$N_i^* = (p'u_i) + \frac{V_i}{\rho c^2}(p'^2) + \frac{V_i V_j}{c^2}(p'u_j) + \rho V_j(u_i u_j) \quad ; \tag{25}$$

(note that $c^2 = 1/\rho\theta_p$ in terms of the state equation - cf. Appendix I). It should be emphasized that these quantities do not in general correspond to any actual energy density or flux in the fluid flow.

On the right-hand side of (23), P represents the rate of acoustic energy production per unit volume, and is given to second-order accuracy by

$$P = P_o + P_1 \quad ;$$

$$P_o \doteq m_i^* R_i' - \theta_s J^* S' \quad ,$$

$$P_1 \doteq (\theta_p \theta_s S V_i - \rho\theta_p \zeta_{ij} V_j)(p'u_i) + \rho\theta_s V_j \frac{\partial s}{\partial x_i}(u_i u_j)$$

$$+ \left[\frac{1}{\rho}(\theta_s^2 - \theta_{ss})S + (\theta_p \theta_s - \theta_{ps})V_i \frac{\partial p}{\partial x_i}\right](p's')$$

$$+ \left[(\theta_s^2 - \theta_{ss})SV_j - \rho\theta_{ps} V_i V_j \frac{\partial p}{\partial x_i} + \theta_s \frac{\partial p}{\partial x_j}\right](u_j s')$$

$$- \rho\theta_p(\zeta_{ij}V_j + R_i)(p'w_i) - \left(\frac{\partial \rho V_j}{\partial x_i} - \rho\theta_s V_j \frac{\partial s}{\partial x_i}\right)(u_j w_i) - m_j^* \frac{Dw_j}{Dt} . \tag{26}$$

The significance of these terms is discussed in detail in the following section.

The main conclusion to be drawn from equations (23-26) is that in a nonuniform flow, defining acoustic energy according to (24) and (25) leads in general to a nonzero production term in the energy balance. This holds both instantaneously and in the time-average; taking the time-average of equation (23) for a statistically stationary flow gives

$$\frac{\partial I_i}{\partial x_i} = \langle p \rangle \tag{27}$$

where $I_i = \langle N_i^* \rangle$ are the components of the generalized acoustic intensity.[†]

It follows that the sound power $W = \int_S I_i \, dS_i$ crossing two surfaces S_1 and S_2 (Fig. 2.1) is in general different by an amount

[†]The intensity as defined here differs from that given by (13) only in that $\underset{\sim}{u}$ replaces $\underset{\sim}{v}$; the flow was assumed irrotational in section 2.1.3.

$$W_2 - W_1 = \int_V \langle P \rangle \, dV \quad , \tag{28}$$

corresponding to the generation or loss of acoustic energy in the intervening space V. The volume integral in (28) can be estimated from a knowledge of the sound field in V, as the analysis below demonstrates.

2.2.3 Acoustic energy production terms

In equation (26), the production rate P per unit volume is divided into two parts. For sound waves in a uniform fluid at rest, only the first part (P_o) remains; it accounts for the losses due to viscosity and heat conduction which occur under these conditions. The second part (P_1) represents the additional production of acoustic energy which occurs when sound travels through a rotational mean flow, or through a medium in which mean entropy gradients are combined with mean pressure gradients or flow. As expected, both P_o and P_1 vanish in an irrotational uniform-entropy flow which is free from diffusion effects or external sources.

For the simple case of plane sound waves in a uniform fluid at rest, it is interesting to compare the acoustic energy dissipation given by (26) with the usual result based on an energy argument (section 2.1.2). The wave motion is taken in the x_1 direction, with velocity components $\{u_1(x_1,t),\ 0,\ 0\}$. The acoustic energy loss rate per unit volume is then given by (26) as

$$-P_o = -m_1 * R_1' + \theta_s J * S' \quad , \tag{29}$$

where

$$R_1' \doteq \frac{4}{3}\frac{\mu}{\rho}\frac{\partial^2 u_1}{\partial x_1^2} \tag{30}$$

and

$$S' \doteq \frac{k}{T}\frac{\partial^2 T'}{\partial x_1^2} \doteq -\frac{k\theta_s}{\rho T}\frac{\partial^2 p'}{\partial x_1^2} \quad .$$

In equation (30), the expression for S' in terms of T' and the thermal conductivity k follows from (18). Neglecting any contribution of s' to T' - which would lead to a k^2 term in the dissipation - then gives $T' \doteq -(\theta_s/\rho)p'$ (cf. Appendix I).

Since $m_1^* \doteq \rho u_1$ and $J^* \doteq (1/\rho)p'$ in this case, it follows from (29) that

$$-P_o \doteq -\frac{4}{3}\mu u_1 \frac{\partial^2 u_1}{\partial x_1^2} - \frac{k\theta_s^2}{\rho^2 T} p' \frac{\partial^2 p'}{\partial x_1^2} \quad ;$$

or, using Appendix I to substitute for θ_s and writing $C_p\mu/k = Pr$,

$$-P_o \doteq \mu\left\{\frac{4}{3}\left(\frac{\partial u_1}{\partial x_1}\right)^2 + \frac{\gamma-1}{\rho^2 c^2 Pr}\left(\frac{\partial p'}{\partial x_1}\right)^2\right\} - \frac{1}{2}\mu\frac{\partial^2}{\partial x_1^2}\left(\frac{4}{3}u_1^2 + \frac{\gamma-1}{\rho^2 c^2 Pr}p'^2\right) . \tag{31}$$

The time-average of (31) is the mean rate of acoustic energy dissipation, per unit volume, at any point in the fluid.

This result differs from that obtained by the entropy-production approach, equation (9), since the latter gives only the space-average dissipation and the $\partial^2/\partial x_1^2$ term does not appear. For weakly-attenuated

waves, the two approaches give the same total dissipation of acoustic energy over a region large compared with the acoustic wavelengths involved. Finally, for weakly-attenuated progressive waves the $\partial^2/\partial x_1^2$ term in (31) is zero in the present approximation, and only the first term remains - cf. Lighthill [18].

2.3 COMPARISONS WITH PREVIOUS WORK

Acoustic-energy equations of the same form as (23) have been developed by several authors, using various expressions for the energy density E^* and energy flux components N_i^*. In some cases the short-time averages $\langle E^* \rangle = D$ and $\langle N_i^* \rangle = I_i$ are used to formulate a mean acoustic energy equation, on the understanding that any change in these quantities over a typical fluctuation period is negligible.

It is convenient to review this earlier work under three headings, in order of increasing generality. Section 2.3.1 covers classical acoustics, where sound waves travel through a uniform medium at rest. Section 2.3.2 progresses to geometric acoustics, where gradual variations in the medium are permitted. Section 2.3.3 deals with small disturbances in a general nonuniform flow. Where appropriate, comparisons are made with the results developed in this paper.

2.3.1 Classical acoustics

For small perturbations in a fluid otherwise at rest - the situation of classical acoustics - it has been usual to regard the acoustic energy equation as a direct result of the conservation of energy. The difficulties associated with this view have already been discussed in the introduction.

Bergmann [7] and Blokhintsev [8], on the other hand, use the

linearized equations of motion to derive the classical acoustic-energy equation for an inviscid, nonconducting fluid. The energy density and flux are

$$E^* = \frac{1}{2}\,(1/\rho c^2)\; p'^2 + \frac{1}{2}\,\rho v_j^{\,2} \quad , \quad N_i^* = p' v_i \quad ; \tag{32}$$

the production rate P is zero to second order under these conditions (see section 3 of [8]: Energy and energy flow in Acoustics). Bergmann's analysis furthermore shows that density (or entropy) gradients leave the acoustic-energy balance unaffected in a stationary medium, in agreement with equation (26).

Schoch [6] likewise shows that this classical result - while not a complete expression of energy conservation in the fluid - provides a valid second-order relationship between the quantities of linear acoustics. While it is convenient, and traditional, to use the names "acoustic-energy density" and "acoustic-energy flux" for the quantitive E^* and N_i^* given by equation (32), Schoch makes it clear that a true statement of energy conservation would have to contain additional terms to be accurate to second order.

2.3.2 Geometric acoustics

The theory of geometric acoustics applies only in media whose state changes little over one wavelength, and is based on the assumption of quasi plane-wave propagation at any point in the sound field.

Within this approximation, Blokhintsev [8, section 7] derives a time-averaged acoustic-energy equation in which the mean energy density

D and acoustic intensity $\underset{\sim}{I}$ are[†] (in the present notation)

$$D = (1/\rho c^2)(1+V_n/c)\langle p'^2\rangle \quad ,$$
$$\underset{\sim}{I} = (1+V_n/c)\{\langle p'\underset{\sim}{u}\rangle + (\underset{\sim}{V}/\rho c^2)\langle p'^2\rangle\} \quad ; \tag{33}$$

the production term is zero to second order, as in the classical-acoustics case. Here, V_n is the flow velocity component normal to the local wavefronts; note that the concept of a wavefront direction applies only under quasi plane-wave conditions.

The velocity fluctuation $\underset{\sim}{u}$ is related to p', in geometric acoustics, by

$$\rho c u_n = p' \quad , \quad u_t = 0 \quad , \tag{34}$$

(where n and t denote normal and tangential components referred to a wavefront). This fact allows Blokhintsev's expressions, equation (33), to be rearranged in several different ways. One such arrangement is

$$D = \frac{1}{2}(1/\rho c^2)\langle p'^2\rangle + (V_n/c^2)\langle p'u_n\rangle + \frac{1}{2}\rho\langle u_n^2\rangle \quad ,$$
$$I_n = \langle p'u_n\rangle + (V_n/\rho c^2)\langle p'^2\rangle + (V_n/c)^2\langle p'u_n\rangle + \rho V_n\langle u_n^2\rangle \quad ,$$
$$I_t = (V_t/\rho c^2)\langle p'^2\rangle + (V_t V_n/c^2)\langle p'u_n\rangle \quad . \tag{35}$$

A comparison of equation (35) with (24) and (25) shows that Blokhintsev's D and I_i are time averages of the quantities E^* and N_i^*

[†]The mean flow makes it necessary to specify the irrotational velocity fluctuation u_i in equation (33); this ensures that the vorticity mode does not contribute to the acoustic intensity defined above.

defined in Section 2.2.2. In other words, the mean energy density and intensity of geometric acoustics are obtainable from the analysis of that section as a special case.†

2.3.3 General nonuniform flow

Apart from the work of Cantrell and Hart (outlined in Section 2.1.3), which is restricted to irrotational, uniform-entropy flows, the acoustic energy concept has previously been limited to geometric and classical acoustics. In view of this limitation, Ribner [20] proposed that equations (33) for mean energy density and intensity be carried over from geometric acoustics to the general situation. There is no reason to suppose, however, that the mean production rate would vanish in the resulting acoustic energy balance. Moreover, it is not clear how V_n would be interpreted.

Although the use of acoustic energy in moving media has generally involved a restriction to geometric acoustics, one exception occurs in an earlier paper by Ribner [17]. By limiting the mean flow to a uniform stream Ribner derived an expression that gave the cross-stream component of the mean energy flux to second order, without requiring second-order solutions of the equations of motion. No assumptions were made about the structure of the sound field.

If vorticity fluctuations are excluded, the mean energy flux found in this case by Ribner coincides with the acoustic intensity given in

---

†Hayes' generalization [19] of Blokhintsev's acoustic energy equation, for a moving medium whose undisturbed motion varies slowly with time, follows in the same way if D, I_i are defined as short-time averages.

Section 2.2.2. In general, however, the approach which starts from an overall energy balance and seeks to extract an acoustic-energy balance does not lead to useful results.

Examples of the latter approach are provided by Ryshov and Shefter [21] and Guiraud [22]. Without restricting the flow any more than is done in Section 2.2.2 of the present analysis (except to omit the diffusion terms R_j, S), they arrived at a form of second-order energy-balance equation. Their energy-flux term, for example, takes the form

$$N_i^* = p'v_i + V_i \left[\frac{1}{2}(1/\rho c^2)\, p'^2 + \frac{1}{2}\rho v_j^2\right] \quad , \tag{36}$$

which has a certain intuitive appeal; for, if the first term is interpreted as the flux of energy relative to the fluid, then the second term appears to represent the convected energy density (potential plus kinetic).

The difficulty with this type of equation is the production term in the energy balance. Included in the energy production rate, for instance, are terms like

$$\rho \frac{\partial V_j}{\partial x_i} v_i v_j$$

which vanish only where the mean velocity is uniform.† The approach of Section 2.2.2, on the other hand, leads to an energy production rate that vanishes (apart from diffusion effects) wherever the flow is irrotational and of uniform specific entropy.

---

†In the papers mentioned [21, 22] this was no disadvantage, since the energy balance was used only within the framework of geometric acoustics, where flow gradients are assumed small.

Finally, it is necessary to point out that Pridmore-Brown's calculation [23] of streamwise energy flux in a one-dimensional flow omits certain second-order terms (as Cantrell and Hart [9] have shown). What the calculation does, in effect, is to derive a mean acoustic energy balance equation in which the intensity is given by the time-average of (36); but as with all equations of this type, it is incorrect to identify the intensity with the local mean energy flux (or its increase due to the acoustic perturbation) except in special circumstances.

2.4 CONCLUSIONS

(a) The concept of acoustic energy is extended to nonuniform fluid flows. Acoustic energy density and energy flux are defined for this purpose by equations (24) and (25).

(b) An important consequence of this definition is that in an irrotational uniform-entropy flow, there is no production or dissipation of acoustic energy (apart from molecular diffusion effects such as viscosity).

(c) In general the resulting energy balance equation exhibits acoustic energy production within the flow, at a rate given by equation (26).

(d) The acoustic energy equations used in classical and geometric acoustics appear as special cases of the general acoustic energy balance given in section 2.2.2.

(e) Although there are other ways of generalizing Rayleigh's classical definition of acoustic energy (equation 32) to moving media, the present approach - based on the work of Cantrell and Hart - has the advantage of leading to conclusion (b).

(f) The acoustic energy balance can be expressed in spectral density form by the standard procedure of inserting a variable time delay in the analysis.

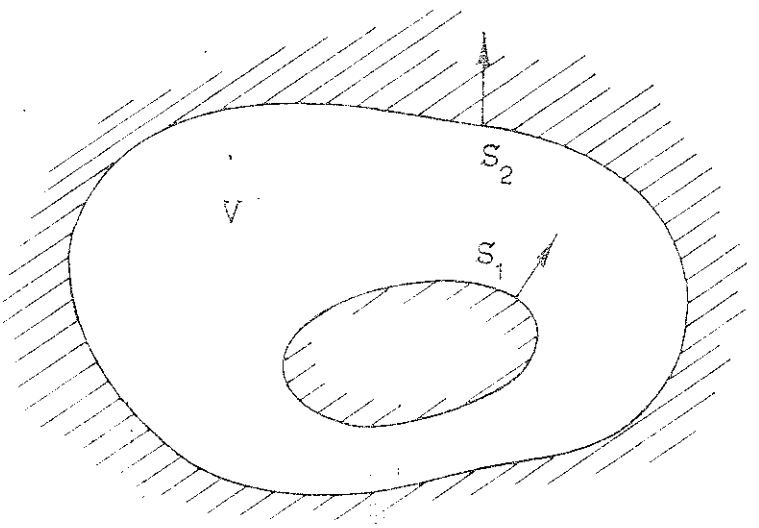

Fig. 2.1 Definition sketch for surfaces S_1 and S_2 separated by a region V of flow.

CHAPTER 3

SECOND-ORDER ANALYSIS OF SOUND SOURCES

In the previous chapter the concept of acoustic energy was generalized for use in compressible flows, the aim being to identify the sound power associated with a specified sound field in a moving medium. The question of how the sound field is generated is taken up in this chapter.

The analysis follows Lighthill [24] in representing the fluid density field - or in this case the pressure perturbation - as a linear sound field in a uniform fluid, free from viscosity and heat conduction. The main differences are:

(1) The idealized reference fluid is here taken as moving with a uniform steady velocity $\bar{\underset{\sim}{V}}$, whereas Lighthill's acoustic analogy refers to a uniform fluid at rest. In this way the reference fluid is identified as closely as possible with the actual mean flow without the need for moving axis transformations. The advantage becomes apparent in Chapter 4 when ducted flows with fixed boundary conditions are considered.

(2) The equivalent acoustic source terms are found to second order by expanding the equations of motion about the unperturbed reference flow, as was done by Chu and Kovasznay [14]. This process leads to explicit expressions for other second-order sources besides the $v_i v_j$ interaction on which Lighthill's analysis focuses.

(3) Nonlinear interactions between external sources and flow perturbations are included among the second-order source terms studied.

The final aim is an acoustic wave equation for the dimensionless pressure perturbation, $p^* = (p-p_o)/\rho_o c_o^2$, of the form

$$L(p^*) = Q \tag{1}$$

where L is the convected wave operator $(\bar{D}^2/Dt^2 - c_o^2\nabla^2)$. The left-hand side is linear with constant coefficients, so if Q is given the equation can be solved analytically; Chapter 4, which concludes the part of the thesis concerned with general theory, studies the solution of (1) for sources contained in ducts.

3.1 EQUATIONS OF MOTION WITH EXTERNAL SOURCES

The inclusion of external sources in the flow model has three uses. First, it provides a physical interpretation of the acoustic source terms due to fluid motion; Chu and Kovasznay discuss this aspect in detail, and it will not be pursued further here. Second, there may actually be body forces (for example) acting on the fluid, which are represented by external source terms in the equations of motion. Third, the flow may include regions in which the equations of motion used elsewhere do not apply (for example, foreign bodies or boundary layers); it is sometimes desirable to regard the equations as applicable throughout these regions, in which case their effect on the surrounding flow can be modelled by means of source distributions. The source distributions are applied within each region in such a way as to match the boundary conditions at the interface with the surrounding fluid.

Examples of the last application are Curle's theory of aerodynamic sound in flows with fixed boundaries [25], and Ffowcs Williams' extension to arbitrarily moving boundaries [26]. These theories permit, in principle, the replacement of any shape or size of boundary by an equivalent acoustic source distribution over the surface in question; equivalent here means that the resulting density field outside the boundaries is identical to that in the actual flow.

With this type of application in mind (see Chapters 5 and 6), distributed sources are introduced as follows:

Volume displacement	z	(per unit volume)
External force field	$\rho \underset{\sim}{g}$	(per unit volume)
Entropy input rate	H	(per unit volume)

Combinations of these three types of input can in principle produce any desired modification of the flow field, since they influence the continuity, momentum and energy equations of the fluid. In the analysis which follows, z, $\underset{\sim}{g}$ and H are regarded as perturbations which have only a first-order effect on the flow (i.e. the order of magnitude of any perturbed quantity is unaltered.)

Introduction of the volume displacement z leads to a two-fluid continuum model, in which unit volume of space contains mass $\rho(1-z)$ of the real fluid. The dynamics of the fictitious fluid occupying the displaced volume are of no interest; it is simply necessary to specify continuity of pressure with the surrounding real fluid (here assumed inviscid and nonconducting).

The equations of motion of the real fluid are conveniently formulated on a mass basis, by considering the volume, momentum and energy of a fluid mass element. The volume occupied per unit mass of real fluid is $1/[\rho(1-z)]$, so the equations per unit mass are:

$$\text{(Volume)} \qquad \frac{D}{Dt}\frac{1}{\rho(1-z)} = \frac{1}{\rho(1-z)}\frac{\partial V_i}{\partial x_i} \; ; \quad \frac{D}{Dt} \equiv \frac{\partial}{\partial t} + V_i \frac{\partial}{\partial x_i} \tag{2}$$

$$\text{(momentum)} \qquad \frac{DV_j}{Dt} = \frac{1}{\rho(1-z)}\left(-\frac{\partial p}{\partial x_j} + \rho g_j\right) \; ; \tag{3}$$

$$\text{(energy)} \qquad \frac{D}{Dt}\left(e + \tfrac{1}{2}V_j^2\right) = \frac{-1}{\rho(1-z)}\frac{\partial pV_i}{\partial x_i} + p\frac{D}{Dt}\frac{z}{\rho(1-z)} + \frac{g_j V_j}{1-z} + \frac{TH}{\rho(1-z)} \; . \tag{4}$$

The energy equation has been included explicitly, to show how the input terms affect the energy balance. The terms on the right-hand side of (4) account for, respectively, (i) the energy input to the fluid element <u>via</u> stresses on the external boundary; (ii) the energy input due to expansion of the displaced volume within the element; (iii) the work done by external forces ρg_j per unit volume acting on the fluid element; (iv) the energy input as heat, TH per unit volume.

Equations (2) through (4) may be rearranged as follows:

$$\frac{Ds}{Dt} = \frac{H}{\rho(1-z)} \; ; \tag{5}$$

$$\frac{D\theta}{Dt} - \theta_s \frac{Ds}{Dt} = \theta_p \frac{Dp}{Dt} = -\frac{\partial V_i}{\partial x_i} + \frac{1}{1-z}\frac{Dz}{Dt} - \frac{\theta_s}{\rho} H \; ; \tag{6}$$

$$\frac{DV_j}{Dt} = \frac{-1}{\rho(1-z)}\frac{\partial p}{\partial x_j} + \frac{g_j}{1-z} \; . \tag{7}$$

These equations provide the basis of the present analysis. The next stage is to consider perturbations about a uniform mean flow, with the aim of finding an equation for p* in terms of other quantities.

3.2 SECOND-ORDER INTERACTIONS AS A SOURCE OF SOUND

In a uniform flow, perturbations in vorticity (turbulence), entropy (hot spots) and pressure (sound) are to a certain extent propagated independently [14]. The only coupling, in fact, arises from viscosity and heat conduction (here neglected) and from second-order interactions.

Of interest here are pressure perturbations due to nonlinear interactions among the following first-order flow disturbances: velocity ($v_i = V_i - \bar{V}_i$), entropy ($s' = s - s_o$), pressure ($p' = p - p_o$) and the external source terms z, $\underset{\sim}{g}$. Any pair of these quantities is regarded as a possible source of sound, except that second-order products of the external source terms are not considered[†].

With this simplification, the divergence of (7) is subtracted from D/Dt (6) to give a wave-type equation for the case H = 0.

$$\theta_p \frac{D^2p}{Dt^2} - \frac{1}{\rho(1-z)} \frac{\partial^2 p}{\partial x_j^2} = \frac{\partial V_i}{\partial x_j} \frac{\partial V_j}{\partial x_i} - \theta_{pp} \left(\frac{Dp}{Dt}\right)^2 - \frac{1}{\rho(1-z)} \frac{\partial \theta}{\partial x_j} \frac{\partial p}{\partial x_j}$$

$$+ \frac{1}{\rho} \frac{\partial z}{\partial x_j} \frac{\partial p}{\partial x_j} + \frac{D^2 z}{Dt^2} - \frac{\partial g_j}{\partial x_j} . \qquad (8)$$

The source term Q in (1) is found by noting that the above equation reduces to L(p*) = 0, in the idealized case of infinitesimal perturbations to a uniform, steady, source-free flow. Equation (8)

[†]The entropy input H is omitted for simplicity at this stage, since it is not required in subsequent chapters. The corresponding acoustic source terms are quoted for completeness at the end of the chapter.

is therefore expanded in terms of (p', s', $\underset{\sim}{v}$, z, $\underset{\sim}{g}$), and all terms other than L(p*) taken over to the right-hand side. Two further approximations are made at this stage:

(a) Source terms which contain the pressure perturbation (either explicitly or in the form $\partial v_i/\partial x_i$) are approximated to second order in perturbed quantities.

(b) Source terms which explicitly involve z or $\underset{\sim}{g}$ are also approximated to second order.

These approximations affect all the terms in (8) except $\partial g_j/\partial x_j$ and $(\partial V_i/\partial x_j)(\partial V_j/\partial x_i)$. They lead to the following result[†] for the source term in (1):

$$Q \doteq \frac{\bar{D}^2 z}{Dt^2} - \frac{\partial g_j}{\partial x_j} + I \ , \quad \left(\frac{\bar{D}}{Dt} \equiv \frac{\partial}{\partial t} + \bar{V}_i \frac{\partial}{\partial x_i}\right) \ , \tag{9}$$

where I represents a series of second-order interaction terms.

$$I = \frac{\partial^2 v_i v_j}{\partial x_i \partial x_j} - \tfrac{1}{2}(\theta_{pp} + \theta_p^2)_o \frac{\bar{D}^2}{Dt^2}(p'p') - (\theta_{ps} + \theta_p \theta_s)_o \frac{\bar{D}^2}{Dt^2}(p's')$$

$$- (\theta_s/\rho)_o \frac{\partial s'}{\partial x_j}\frac{\partial p'}{\partial x_j} + \theta_{po}\frac{\bar{D}^2}{Dt^2}(p'z) + \theta_{so}\frac{\bar{D}^2}{Dt^2}(s'z) - \theta_{po}\frac{\partial}{\partial x_j}(p'g_j) - \theta_{so}s'\frac{\partial g_j}{\partial x_j} \ . \tag{10}$$

Since turbulent velocity fluctuations occur independently, to first order, of p' and s', the only source term in (10) which involves turbulent

---

[†]The analysis makes use of the linearized equations corresponding to (5), (6) and (7).

velocities is $\partial^2 v_i v_j / \partial x_i \partial x_j$. This result justifies Lighthill's treatment of jet noise at high subsonic Mach numbers, in which sound radiation is attributed to a quadrupole distribution $v_i v_j$ in a fluid at rest.

On the other hand, turbulent velocities in the presence of solid surfaces - e.g. blades - can give rise to fluctuating forces and hence to sound radiation, as shown by the $\partial g_j / \partial x_j$ term.

The thermodynamic derivatives occurring in the equations above are given for a perfect gas with constant specific-heat ratio γ by

$$\theta_p = \frac{1}{\rho c^2} = \frac{1}{\gamma p} \quad ; \quad \theta_s = -1/C_p$$

$$\theta_{pp} = -\frac{1}{\gamma p^2} \quad ; \quad \theta_{ps} = 0 \quad , \tag{11}$$

as shown in Appendix I.

3.3 ANALYSIS OF THE ACOUSTIC SOURCE DISTRIBUTION

The source distribution Q given by (9) may be rearranged in the form

$$Q = Q^{(o)} - \frac{\partial Q_i}{\partial x_i} + \frac{\partial^2 Q_{ij}}{\partial x_i \partial x_j} \quad , \tag{12}$$

where $Q^{(o)}$ is a distribution of monopole order, $\partial Q_i / \partial x_i$ is of dipole order and $\partial^2 Q_{ij} / \partial x_i \partial x_j$ is of quadrupole order. Explicit recognition of the different orders of source distribution is required in Chapter 4, where the basic solution of the wave equation is given in terms of an actuator-disk source region whose thickness tends to zero.

The following values of $Q^{(o)}$, Q_i, Q_{ij} are obtained from equations (9) to (12) for the case of a perfect gas with γ constant. As in Chapter 2, the irrotational velocity perturbation $\underset{\sim}{u}$ is defined by $\underset{\sim}{u} = \underset{\sim}{v} - \underset{\sim}{w}$.

$$Q^{(0)} \doteq \frac{\partial^2 z}{\partial t^2} + \frac{1}{\rho c^2} \frac{\partial^2}{\partial t^2} (p'z) - \frac{1}{C_p} \frac{\partial^2}{\partial t^2} (s'z) - \frac{1}{C_p} \left(\frac{\partial s'}{\partial x_i} g_i\right)$$

$$+ \tfrac{1}{2} \frac{\gamma-1}{\rho^2 c^4} \frac{\partial^2}{\partial t^2} (p'p') + \frac{1}{C_p \rho c^2} \frac{\partial^2}{\partial t^2} (s'p') - \frac{1}{C_p \rho} \frac{\partial^2 s'}{\partial x_i^2} p' \quad , \quad (13)$$

$$Q_i \doteq - 2\bar{V}_i \frac{\partial z}{\partial t} - 2 \frac{V_i}{\rho c^2} \frac{\partial}{\partial t} (p'z) + 2 \frac{V_i}{C_p} \frac{\partial}{\partial t} (s'z)$$

$$+ g_i + \frac{1}{\rho c^2} (p'g_i) - \frac{1}{C_p} (s'g_i)$$

$$- (\gamma-1) \frac{V_i}{\rho^2 c^4} \frac{\partial}{\partial t} (p'p') - 2 \frac{V_i}{C_p \rho c^2} \frac{\partial}{\partial t} (s'p') - \frac{1}{C_p \rho} \left(\frac{\partial s'}{\partial x_i} p'\right) \quad , \quad (14)$$

$$Q_{ij} \doteq \bar{V}_i \bar{V}_j z' + \frac{V_i V_j}{\rho c^2} (p'z) - \frac{V_i V_j}{C_p} (s'z)$$

$$+ (w_i w_j) + 2(u_i w_j) + (u_i u_j) + \tfrac{1}{2}(\gamma-1) \frac{V_i V_j}{\rho^2 c^4} (p'p') + \frac{V_i V_j}{C_p \rho c^2} (s'p'). \quad (15)$$

These are accurate to second order, within the limitations noted. Equations (13) to (15) are used to identify sources of turbomachinery noise in Chapter 5.

3.4 SOUND SOURCES ASSOCIATED WITH THE ENTROPY INPUT H

If the above analysis is repeated with $H \neq 0$, additional acoustic source terms are found as follows. A linear term

$$Q = -\left(\frac{\theta_s}{\rho}\right)_o \frac{\bar{D}H}{Dt} \quad , \quad = \frac{\bar{D}H/Dt}{\rho_o C_p} \qquad \text{(perfect gas, } \gamma \text{ const.)} \qquad (16)$$

describes the generation of sound by the direct heating effect; a set of second-order terms,

$$Q \doteq 2\left(\frac{\theta_p \theta_s}{\rho}\right)_o \frac{\bar{D}p'}{Dt} H - \frac{1}{\rho_o}\left(\theta_s^2 + \theta_{ss}\right)_o \frac{\bar{D}}{Dt}(s'H) + \left(\frac{\theta_s}{\rho}\right)_o \frac{\partial}{\partial x_i}(v_i H) \quad ,$$

$$\doteq -\frac{1}{C_p \rho}\left\{\frac{2}{\rho c^2}\left(\frac{Dp'}{Dt} H\right) + \frac{1}{C_p}\frac{D}{Dt}(s'H) + \frac{\partial}{\partial x_i}(v_i H)\right\} \text{ (perfect gas, } \gamma \text{ const.)} \qquad (17)$$

describes the generation of sound by interaction between the entropy input H and the (independent) flow perturbations p', s', $\underset{\sim}{v}$. Equations (16) and (17) involve exactly the same approximations as (9) and (10); they are included here for completeness, but are not used in subsequent chapters.

3.5 CONCLUSIONS

A convected wave equation is derived for the pressure, in a uniform steady flow with superimposed perturbations in pressure, specific entropy and velocity. Additional perturbations arise from external sources of volume, momentum and entropy. The resulting source terms in the wave

equation are evaluated to second order in the perturbations, neglecting molecular diffusion effects and second-order interactions among the external forcing terms.

CHAPTER 4

SOUND TRANSMISSION AND GENERATION IN DUCTS

The aim of this chapter is toprovide a theoretical framework for estimating the sound power output of ducted sources. The theory has been developed for application to turbomachinery noise sources in aircraft turbofan engines; it is presented here in general terms, however, since the results obtained are valid for any type of acoustic source whose environment may be represented one-dimensionally, as a uniform duct with specified end conditions.

The present chapter is an extension of earlier work by the author [27] which considered sound generation in the absence of flow. Emphasis is placed on the effects of axial flow on the transmission and generation of a single duct mode; the model adopted for this purpose consists of a uniform straight duct of arbitrary cross section, with rigid impervious walls, containing a uniform flow. In the particular case where the duct section is axisymmetric, swirl effects are modelled by a uniform solid-body rotation of the flow.

Additional assumptions made in the analysis are that the fluid is inviscid and non-conducting, and that relative density changes due to pressure fluctuations are small. This last requirement may be expressed as

$$p^* = p'/\rho_o c_o^2 << 1 ; \qquad (1)$$

it implies that linearized theory may be used as a first approximation in describing the unsteady pressure field.

A typical solution for p' is therefore studied in the single-frequency, single-mode form

$$p' = \mathrm{Re}(P) ; \quad P = A_N e^{i(k_x x - \omega t)} E_N(y) \qquad (2)$$

which has the advantage that separate factors express the dependence of the complex pressure P on time (t), axial position (x) and transverse position (y).

Any pressure distribution $p'(\underset{\sim}{y},t)$ over the duct cross-section may be built up by superposition of distributions of this type; section 4.1 considers the transmission along the duct of a single modal component as given by (2).

The question of sound generation is taken up in section 4.2 and a general solution for the pressure field is given in terms of axial moments of the source distribution. This is a generalization of an approach used by Mani [28] in a paper on axial flow fan noise generated by unsteady blade forces.

The chapter concludes with an application of the theory to a three-dimensional version of Mani's problem, and an outline of an alternative approach which can be applied to sources situated at a mean-flow discontinuity.

4.1 TRANSMISSION OF FORWARD AND REFLECTED WAVES

Under the conditions described above, the propagation of sound in a region free from sources is governed by the linear convected wave equation:

$$Lp^* \doteq 0, \tag{3}$$

where $L = \left(\frac{\partial}{\partial t} + \bar{\underset{\sim}{V}} \cdot \nabla \right)^2 - c_o^2 \nabla^2$ is the convected wave operator. For uniform axial flow along a duct, the mean velocity $\bar{\underset{\sim}{V}} = (c_o M_x, 0, 0)$ with c_o, M_x constant.

Substitution of equation (2) for the pressure field gives the following equation for the axial wavenumber k_x corresponding to a single mode and frequency:

$$\left(\frac{\omega}{c_o} \right)^2 - 2M_x \left(\frac{\omega}{c_o} \right) k_x - (1 - M_x^2) k_x^2 = k_N^2 , \quad (N = 0, 1, 2 \text{ etc.}) , \tag{4}$$

Here the k_N are a set of discrete values characteristic of the duct section, such that the corresponding functions E_N given by

$$(\nabla_t^2 + k_N^2) E_N = 0 \tag{5}$$

also meet the wall boundary conditions.

It follows from equation (4) that

$$\left.\begin{aligned} k_x &= \left(\frac{\pm\alpha - M_x}{1 - M_x^2} \right) \frac{\omega}{c_o} = k^{\pm}_x \quad ; \\ \alpha &= \left[1 - \left(\frac{k_N c_o}{\omega} \right)^2 (1 - M_x^2) \right]^{\frac{1}{2}} . \end{aligned}\right\} \tag{6}$$

4.1.1. The cut-off condition

Equation (6) shows that the axial wavenumber of any mode† may be either real or complex, depending on whether the frequency is above or below the cut-off value given by

$$\frac{\omega}{k_N c_o} = (1 - M_x^2)^{\frac{1}{2}} . \qquad (7)$$

For real values of α (i.e. above cutoff), it is worth noting that the + and - signs in equation (6) do not necessarily correspond to positive and negative phase velocities in the x direction. What they do correspond to, as will be shown below, is the direction of energy transmission along the duct.

4.1.2 Forward and reflected wave combinations

When wave systems in the same mode travel in both directions along a duct, the associated sound pressures in the forward (k_x^+) and reflected (k_x^-) waves may be written as

$$\left.\begin{aligned} P^+ &= A(y)\, e^{i(k_x^+ x - \omega t)} , \\ P^- &= B(y)\, e^{i(k_x^- x - \omega t)} . \end{aligned}\right\} \qquad (8)$$

The complex ratio P^-/P^+ is called the reflection factor; its value at any axial position x is given by

$$\frac{P^-}{P^+} = \frac{B}{A} e^{i(k_x^- - k_x^+)x}$$

$$= \frac{B}{A} \exp\left(\frac{-2i\alpha kx}{1 - M_x^2}\right) \qquad (k = \omega/c_o) . \qquad (9)$$

† Footnote: Other than the plane-wave mode, for which $k_N = 0$.

If the reflection phase ψ (x) is defined by:

$$\frac{P^-}{P^+} = e^{2i\psi} \quad ; \quad \frac{B}{A} = e^{2i\psi_o} \quad , \tag{10}$$

then equation (9) gives

$$\psi = \psi_o - \frac{\alpha\, kx}{1-M_x^2} \quad . \tag{11}$$

Finally, the resultant sound pressure at any position can be conveniently expressed in terms of ψ as †

$$P = (P^+ + P^-) = 2A \exp i \left(\psi_o - \frac{M_x k x}{1-M_x^2} - \omega t \right). \cos \psi \quad . \tag{12}$$

4.1.3 Axial admittance of duct modes

The axial velocities U^+, U^- corresponding to the forward and reflected waves are found from the linearized momentum equation:

$$U^+ = \frac{P+}{\rho_o c_o} \left(\frac{\alpha - M_x}{1 - \alpha M_x}\right) , \qquad U^- = \frac{-P^-}{\rho_o c_o} \left(\frac{\alpha + M_x}{1 + \alpha M_x}\right) \tag{13}$$

It is useful to express the axial velocity U ($=U^+ + U^-$) in terms of the modal pressure P at the same point. The complex ratio U/P is the modal admittance in the axial direction, and is independent of position y in the duct cross-section.

† Footnote: Compare the zero-flow result in [1], equation (3.3)

In non-dimensional form, the modal admittance ratio $\beta(x)$ is given by

$$\beta = \rho_o c_o \frac{U}{p} = \frac{-i\alpha(1 - M_x^2)\tan\psi - M_x(1 - \alpha^2)}{1 - \alpha^2 M_x^2} , \qquad (14)$$

as follows from equations (10) and (13) above. Once β is known at any position in the duct, its value at other positions can be calculated using equation (14).

4.1.4 Sound power transmitted along the duct

In calculating the sound power transmitted by the modal pressure field described above, it is necessary to take account of the mean flow in the duct. A generalized definition of acoustic intensity, which preserves the continuity property of sound power in any flow which is isentropic and irrotational, is given in Chapter 2:

$$I_i = \langle p' v_i \rangle + \frac{\bar{V}_i}{\rho_o c_o^2} \langle p'p' \rangle + \frac{\bar{V}_i \bar{V}_j}{c_o^2} \langle p' v_j \rangle + \rho_o \bar{V}_j \langle v_i v_j \rangle . \qquad (15)$$

In the present case, $\{\bar{V}_i\} = (c_o M_x, 0, 0)$; and the pressure and axial-velocity fluctuations are expressed in complex form as $p' = \mathrm{Re}(P)$, $v_x = \mathrm{Re}(U)$, with U and P related by equation (14) for a single mode. It follows that the modal acoustic intensity in the axial direction is

$$I_x = \frac{|P|^2}{2\rho_o c_o} \left[(1 + M_x^2)\,\mathrm{Re}\,\beta + M_x (1 + |\beta|^2) \right] . \qquad (16)$$

The total sound power is found by integrating I_x over the duct cross-section S. For this purpose the modal pressure P is written as:

$$P(x, y, t) = \bar{P}(x)\, E(y)\, e^{-i\omega t} , \qquad (17)$$

and the mode shape functions are understood to be normalized so that

$$\int_S E_N^* E_{N'} \, dS(\underline{y}) = \begin{cases} S & (N' = N) \\ 0 & (N' \neq N) \end{cases} . \tag{18}$$

This gives the sound power W in a single mode, in terms of the modal pressure amplitude $\bar{P}$:

$$W = \frac{S |\bar{P}|^2}{2\rho_o c_o} \left[(1 + M_x^2) \operatorname{Re} \beta + M_x (1 + |\beta|^2) \right] . \tag{19}$$

The power in different modes at the same frequency can be added, because of the orthogonality of the mode shape functions.†

4.1.5 Energy transmission coefficient

Above the mode cut-off frequency, the sound power W transmitted along the duct is simply the difference, $(W^+ - W^-)$, between the forward- and backward-transmitted sound powers associated with the separate wave systems P^+, P^-. It is convenient to define an energy transmission coefficient q as the ratio between the actual and forward-wave sound powers, or intensities, under these conditions:

$$W = qW^+ \; ; \; I_x = q I_x^+ , \quad \text{(above cut-off)} . \tag{20}$$

The forward and backward-wave intensities at any frequency follow from equations (13) and (19). These give

† Footnote: This no longer applies if the eigenvalues k_N^2 are complex, as occurs with non-rigid duct walls.

$$\left.\begin{aligned} I_x^{\pm} &= \pm \frac{|P^{\pm}|^2}{2\rho_o c_o}\ \alpha\ \left(\frac{1 - M_x^2}{1 \pm \alpha M_x}\right)^2 \qquad \text{(above cut-off; } \alpha \text{ real)} \\ I_x^{\pm} &= 0 \qquad\qquad\qquad\qquad\qquad\quad \text{(below cut-off; } \alpha \text{ imaginary)} \end{aligned}\right\} \quad (21)$$

Clearly the P^+ wave system corresponds above cut-off to energy transmission in the +x direction, and the P^- system to energy transmission in the -x direction. This distinction applies at all frequencies for which α is real.

The combined intensity in general is given by:

$$I_x = \frac{|P^+|^2}{2\rho_o c_o}\ |\alpha|\ q\ \left|\frac{1 - M_x^2}{1 - \alpha M_x}\right|^2 . \qquad (22)$$

The modulus signs in equation (22) generalize the definition of q to cover the whole frequency range above and below cut-off, although equation (20) and the physical interpretation in terms of forward-wave intensity are valid only above cut-off.

The value of q at any position in the duct † may be related to the reflection phase ψ ($= \xi + i\eta$) at the same position, by comparing equations (16) and (22). With the aid of equations (10) and (14), it now follows that:

above cut-off

$$\begin{aligned} q &= \frac{2e^{-2\eta}}{(1 + \alpha M_x)^2}\ \left[(1 + \alpha^2 M_x^2)\ \text{sh:}\ + 2\alpha M_x\ \text{ch:}\right] \\ &= 1 - r^2\left(\frac{1 - \alpha M_x}{1 + \alpha M_x}\right)^2 \end{aligned} \qquad (23)$$

where $r = e^{-2\eta}$ is the modal reflection coefficient;

† Footnote: In comparing the results of this section with equations (3.9) and (3.10) of reference 27, it should be noted that the transmission coefficient T defined in [27] corresponds to q at x = 0. Below the cut-off frequency, $q(x) \neq q(0)$.

below cut-off

$$q = \frac{2e^{-2\eta}}{1+|\alpha|^2 M_x^2}\left[(1-|\alpha|^2 M_x^2)\, s: - 2\,|\alpha| M_x c:\right]. \qquad (24)$$

In the expressions above

$$\begin{aligned} sh: &= \sinh 2\eta & s: &= \sin 2\xi \\ ch: &= \cosh 2\eta & c: &= \cos 2\xi \end{aligned} \qquad (25)$$

Comparisons of equations (23) and (24) shows that whereas the energy transmission coefficient q above cut-off is independent of x - η being constant in this case, as follows from (11) - the same is not true below cut-off. Equation (11) then gives $\eta = \eta_o - i|\alpha|kx/(1 - M_x^2)$, so that

$$q(x) = q(0) \exp \frac{2|\alpha|kx}{1 - M_x^2} \qquad \text{(below cut-off)}. \qquad (26)$$

However, the intensity I_x in either case is independent of x, as follows from acoustic energy conservation.

In many cases of practical importance, the duct is terminated by an open end, and it is useful to know the modal transmission coefficient of the opening as a function of frequency and flow Mach number. In the high-frequency limit - which means well above the cut-off frequency of the mode concerned [29] - q will approach 1 for all subsonic Mach numbers (i.e. $r \to 0$). Information is lacking on the behaviour of q with M_x at lower frequencies around cut-off and below.†

† Footnote: Carrier [30] has constructed a theoretical model in which the duct is surrounded by a uniform flow at the same Mach number as inside. His results for transmission of an incident plane wave out through a circular opening may be stated in terms of the zero-flow transmission coefficient q' at a frequency $(1-M_x^2)^{-\frac{1}{2}}$ times higher than the actual frequency:

$$q = q' \ (M_x < 0, \text{ duct inlet}); \quad q = q'\left(\frac{1-M_x}{1+M_x}\right)^2 + \frac{4M_x}{(1+M_x)^2} \ (M_x > 0, \text{ outlet}).$$

Qualitative support for these predictions is provided by Mechel, Schilz and Dietz [31] who report measurements of the plane-wave reflection factor (and hence q) for a baffled circular opening in the frequency range $0 < ka_o < 1.5$. Except in the low frequency limit, the measurements show somewhat larger effects due to flow than are predicted.

The problem is complicated by the coupling between modes which occurs at an opening, although in practice this can often be neglected [29]. For the frequency range above cut-off, working hypotheses as to the flow dependence of q are put forward in section 4.2.3.

4.1.6 Relation between transmission coefficient and admittance ratio

In some cases it may be possible to estimate the modal admittance ratio β at a given cross-section, and it is then useful to have an explicit expression for q in terms of β. Such an expression can be found from (14), (23) and (24) with the aid of the relations:

$$\tan 2\xi = \frac{2X}{1 - X^2 - Y^2} \quad , \quad \mathrm{Re}\ (e^{2i\psi}) = \frac{1 - X^2 - Y^2}{(1 + Y)^2 + X^2} \tag{27}$$

where $X + iY = \tan(\xi + i\eta)$. The result, for frequencies above or below cut-off, is:

$$q = \frac{4|\alpha|\left[(\sigma + M_x)(1 + \sigma M_x) + M_x \phi^2\right]}{|(\alpha + M_x) + \beta(1 + \alpha M_x)|^2} \qquad (\beta = \sigma + i\phi). \tag{28}$$

In the high-frequency limit $\alpha \to 1$, $\sigma \to 1$ and $\phi \to 0$, so $q \to 1$ as expected. Another check is provided by the zero-flow case, for which (28) gives

$$q\,(M_x = 0) = \frac{4\,|\alpha|\sigma}{|\alpha + \beta|^2} \tag{29}$$

This agrees with equation (3.10) of [27].

4.2 SOUND GENERATION IN DUCTS

The duct-mode approach developed in the previous section is applied below to describe the excitation of sound by source distributions inside a duct. Provided the mean flow is uniform as previously, the linear wave equation (3) still applies with the addition of a source term $Q\ (\underset{\sim}{x})$ on the right-hand side; Q is of second order in fluctuating quantities, except in regions where external sources are applied (e.g. volume displacement, applied forces [32]).

The resulting inhomogeneous wave equation may be written formally as:

$$Lp^* = Q = Q^{(o)} - \frac{\partial Q_i}{\partial x_i} + \frac{\partial^2 Q_{ij}}{\partial x_i \partial x_j} - \ldots \ ; \qquad (3o)$$

The inclusion of specifically higher-order source distributions $\frac{\partial Q_i}{\partial x_i}$, $\frac{\partial^2 Q_{ij}}{\partial x_i \partial x_j}$, etc. is a reminder that these distributions require special treatment, if the source region is to be approximated as compact in terms of the sound wavelength.

4.2.1 Actuator-disk source representation

The following analysis considers the excitation of sound by source distributions which are acoustically compact in the x direction. Such distributions may be represented as area source-distributions over the duct cross-section; thus

$$Q^{(o)} = s^{(o)}\ \delta(x - x_s) \qquad (31)$$

is a volume source-distribution of monopole order† confined to the duct cross section $x = x_s$, and similarly

† Footnote: In the sense of having zero dipole and higher-order moments in the x direction.

$$Q_x = s_x \delta(x - x_s), \quad Q_{xx} = s_{xx} \delta(x - x_s) \tag{32}$$

represent the axial components of dipole- and quadrupole-type distributions in the actuator-disk limit. These area distributions $s^{(o)}$, s_x, s_{xx} may in fact be interpreted as the successive axial moments of the corresponding volume source distribution Q (cf. [33] Sec.1.5):

$$s^{(o)} = \int_{x_s^-}^{x_s^+} Q \, dx; \quad s_x = \int_{x_s^-}^{x_s^+} xQ \, dx; \quad s_{xx} = \int_{x_s^-}^{x_s^+} \tfrac{1}{2} x^2 Q \, dx. \tag{33}$$

Once a solution has been found for the sound field set up in a uniform duct by an $s^{(o)}$ source distribution, the solutions for higher-order axial moments follow by differentiation [27,34,35]. The immediate aim of the analysis is therefore to find the basic $s^{(o)}$ solution. A method applied by Mani [28] to a similar problem is adopted here, in which the jumps in p^* and $\partial p^*/\partial x$ across the source plane are related to the source distribution through equation (1).

4.2.2 Single-frequency modal response function

The first step is to replace $s^{(o)}$ by a complex source amplitude $S^{(o)}$ (proportional to $e^{-i\omega t}$), whose spatial variation over the duct cross-section corresponds to one of the normal modes of the cross-section. The coupling between $S^{(o)}$ and the sound pressure P in the same mode then turns out to have a particularly simple form, namely:

$$P(x) = S^{(o)} G(x, x_s) \tag{34}$$

In order to find the single-frequency modal response function G, equation (30) is integrated twice in the x direction through the source plane, with Q given by (31): thus

$$\frac{1}{\rho_o c_o^2}\int_{x_s-}^{x_s+} dx\,(LP) = S^{(o)}\ ;\ \frac{1}{\rho_o c_o^2}\int_{x_s-}^{x_s+} dx \int_{x_s-}^{x} dx'\,(LP) = 0\ , \quad (35)$$

The dominant terms in LP are those involving the axial gradients $\partial P/\partial x$ and $\partial^2 P/\partial x^2$, since the source plane represents a discontinuity in the sound field. Equation (35) therefore reduces to:

$$-2ikM_x\left[\,P\,\right]_-^+ - (1-M_x^2)\left[\frac{\partial P}{\partial x}\right]_-^+ = \rho_o S^{(o)};\quad \left[\,P\,\right]_-^+ = 0\ , \quad (36)$$

where the notation $\left[\ \right]_-^+$ denotes the jump in value from x_s- to x_s+.

The axial pressure gradient on either side of the source plane follows from equation (12) as:

$$\frac{\partial P}{\partial x} = P\left(\frac{\alpha k}{1-M_x^2}\tan\psi - \frac{iM_x k}{1-M_x^2}\right)\ ; \quad (37)$$

different values of ψ ($=\psi_o^{\pm} - \alpha k x$) apply on the two sides ($x \gtrless x_s$), so the jump in pressure gradient is:

$$\left[\frac{\partial P}{\partial x}\right]_-^+ = P_s\,\frac{\alpha k}{1-M_x^2}\,(\tan\psi_s^+ - \tan\psi_s^-). \quad (38)$$

Here P_s is written for the pressure at the source plane, which is the same at x_s- and x_s+ by virtue of equation (36).

Combining (36) and (38) gives:

$$P_s = \frac{-\rho_o S^{(o)}}{\alpha k\,(\tan\psi_s^+ - \tan\psi_s^-)}\ , \quad (39)$$

and the mode response function at the source plane follows from equation (34):

$$G(x_s, x_s) = -\rho_o/\alpha k \,(\tan\psi_s^+ - \tan\psi_s^-) = \frac{i\rho_o/k}{\beta_+ - \beta_-} \left(\frac{1 - M_x^2}{1 - \alpha^2 M_x^2}\right). \dagger \qquad (40)$$

The value of $G(x, x_s)$ for any field point x in the duct can be found by using equation (12) for the axial pressure variation. The final result, for the +x side of the source plane, is:

$$G(x, x_s) = \frac{-\rho_o}{\alpha k} \frac{1}{\tan\psi_s^+ - \tan\psi_s^-} \frac{\cos\psi^+}{\cos\psi_s^+} \exp\frac{iM_x k\,(x_s - x)}{1 - M_x^2}, (x > x_s), \qquad (41)$$

Equation (41) gives the response, in any duct mode, to a single-frequency source distribution in that mode. The duct pressure field may therefore be calculated for an arbitrary source distribution over the duct cross-section by superposition of different modes and frequencies. In addition, the sound field due to a source distribution of finite extent in the x direction may be found by summing the effects of elemental area distributions spread along the duct [36].

The response to the higher-order source moments S_x, S_{xx} - again confined to a single mode and frequency - may be expressed in terms of equivalent zero-order moments defined as follows [35, Appendix II].

$$S^{(x)} = \frac{1}{G}\frac{\partial G}{\partial x_s} S_x \quad ; \quad S^{(xx)} = \frac{1}{G}\frac{\partial^2 G}{\partial x_s^2} S_{xx} . \qquad (42)$$

† Footnote: The expression in terms of the modal admittance ratios $\beta_\pm$, derived from equation (14), permits comparison with the zero-flow result given in reference 27, section 6.2.

Further discussion of dipole and quadrupole excitation is deferred to section 4.3 which also considers a particular application of the above results in detail.

4.2.3 Special case: no reflected waves on -x side of source plane

This situation corresponds to case (b) of reference 27, section 6; it would occur, for example, if the duct were of infinite length on the -x side of the source, or (more realistically) at frequencies well below and above cut-off in an open-ended duct.

The vanishing of the reflected wave implies Im $\psi^- \to -\infty$ in equation (41), and hence $\tan \psi_s^- = -i$. The mode response function on the +x side therefore becomes:

$$G(x,x_s) = \frac{i\rho_o}{\alpha k} \cos\psi \cdot e^{i\psi_s} \exp \frac{iM_x k(x_s - x)}{1 - M_x^2}$$

$$= \frac{i\rho_o}{\alpha k} \cos\psi \cdot \exp i\left(\psi_o - \frac{M_x kx}{1-M_x^2}\right) \cdot e^{-ik_x^+ x_s}, \quad (x > x_s) \qquad (43)$$

where the + superscript has been dropped from ψ^+, ψ_s^+ and ψ_o^+ on the understanding that from now on, all values of the reflection phase refer to the region $x > x_s$.

Equation (43) gives:

$$\frac{1}{G}\frac{\partial G}{\partial x_s} = -ik_x^+ ; \quad \frac{1}{G}\frac{\partial^2 G}{\partial x_s^2} = -(k_x^+)^2 \qquad (x > x_s) . \qquad (44)$$

Under the present conditions, therefore, axial dipole and quadrupole distributions S_x, S_{xx} produce the same sound field in the region $x > x_s$ as simple-source distributions $-ik_x^+ S_x$, $-(k_x^+)^2 S_{xx}$.

The modal intensity in the +x direction can be calculated by evaluating equation (23) at the source plane. This requires a knowledge of the forward-wave amplitude P_s^+ excited at the source plane. For a simple-source distribution $S^{(o)}$,

$$P_s^+ = \frac{P_s}{2e^{i\psi_s}\cos\psi_s} = S^{(o)}\,\frac{G(x_s, x_s)}{2e^{i\psi_s}\cos\psi_s} \quad ; \tag{45}$$

in the present case with G given by equation (43),

$$P_s^+ = S^{(o)}\,\frac{i\rho_o}{2\alpha k} \quad . \tag{46}$$

The axial sound intensity corresponding to each of the source distributions $S^{(o)}$, S_x, S_{xx} is therefore related to the modal transmission coefficient q_s at the source plane as follows:

<u>simple source</u> $$I_x = \frac{1}{8}\,\frac{q_s}{|\alpha|}\,\frac{\rho_o c_o}{\omega^2}\left|\frac{1 - M_x^2}{1 - \alpha M_x}\right|^2 |S^{(o)}|^2 \quad ;$$

<u>axial-dipole source</u> $$I_x = \frac{1}{8}\,\frac{q_s}{|\alpha|}\,\frac{\rho_o}{c_o}\left|\frac{\alpha - M_x}{1 - \alpha M_x}\right|^2 |S_x|^2 \quad ;$$

<u>axial-quadrupole source</u> $$I_x = \frac{1}{8}\,\frac{q_s}{|\alpha|}\,\frac{\omega^2\rho_o}{c_o^3}\left|\frac{(\alpha - M_x)^2}{(1 - M_x^2)(1 - \alpha M_x)}\right|^2 |S_{xx}|^2 \quad . \tag{47}$$

These results give the sound intensity transmitted forward from the source plane, i.e. into the region $x > x_s$. They are valid (as the modulus signs imply) for all frequencies above or below cut-off; the high-frequency limiting case is of particular interest since it provides a rough approximation to the whole frequency range above cut-off, where the mode is able to radiate efficiently.

High-frequency limit $(\alpha \to 1)$ †

$$I_x \to \frac{1}{8} q_s \frac{\rho_o c_o}{\omega^2} (1+M_x)^2 |S^{(o)}|^2 \ , \ \frac{1}{8} q_s \frac{\rho_o}{c_o} |S_x|^2 \ , \ \frac{i}{8} q_s \frac{\omega^2 \rho_o}{c_o^3} (1+M_x)^{-2} |S_{xx}|^2 . \tag{48}$$

For higher-order modes, equation (48) becomes valid at frequencies well above cut-off, and under these conditions $q_s \to 1$ for an open-ended duct. It follows that an $S^{(o)}$ distribution, for example, radiates less sound from the inlet than from the exit end, in the presence of a subsonic mean flow.

At frequencies which are above cut-off, but not far enough above for (48) to be valid, a rough estimate of the energy transmission coefficient q_o for an open-ended duct may be obtained from either of the following assumptions:

Assumption (a) $q_o = \alpha$ (49)

This is an extrapolation from the zero-flow case. When $M_x = 0$, q_o/α varies from $4\tau_o$ at cut-off (where $\tau_o = \text{Re } 1/\beta_o$; cf. equation 29) to 1 in the high-frequency limit, and may be approximated by 1 over the whole range. The same approximation is assumed to hold in the presence of flow.

Assumption (b) $\beta_o = 1$ (50)

Calculations for the zero-flow case in [29] suggest that for high-order modes at axisymmetric openings, $\tau_o \sim 1$ over the whole range above cut-off. If the reactance of the opening is neglected equation (50) is obtained, which when extrapolated to the general case ($M_x \neq 0$) gives:

$$q_o = \frac{4\alpha}{(1+\alpha)^2} \tag{51}$$

from equation (28).

† Footnote: For the plane-wave mode, $\alpha = 1$ at all frequencies.

It should be emphasized that both these assumptions are speculative. The main merit of equations (49) and (51) is that they are correct in the high-frequency limit, give plausible results at cut-off and vary monotonically in between. The main difference between the equations is that (49) implies $\tau_o = \frac{1}{4}$ at cut-off, while (51) is based on the assumption $\tau_o = 1$; the former is perhaps therefore more suitable for low-order modes - cf. [29] - and the latter for high-order modes. Neither is realistic for the plane-wave mode, but here Carrier's solution gives some guidance (see Section 4.1.5.

4.3 EXAMPLE: SOUND GENERATED BY A FLUCTUATING FORCE DISTRIBUTION

To illustrate the application of the foregoing theory, it is used in the present section to calculate the sound power generated in a duct by a force distribution applied at one cross-section. Such a situation has practical significance in connection with axial-flow fan noise, as it provides a model of sound excitation by blade forces.

The calculation is preceded by a discussion of model analysis techniques needed for the source moment distributions of section 4.2.1.

4.3.1 Modal analysis of axial source moments

The first step in the modal approach to sound generation is to analyse the axial moments $s^{(o)}$, s_x, s_{xx} etc. of the volume source distribution Q into normal-mode components. This is accomplished by the usual process of multiplying by the conjugate mode function E_N^* and integrating over the duct cross-section; for example,

$$s^{(o)} = \sum_N s_N^{(o)} \tag{52}$$

where

$$s_N^{(o)} = \frac{E_N}{S} \int_S s^{(o)} E_N^* \, dS \tag{53}$$

Although equation (53) gives the modal components for any zeroth-moment distribution $s^{(o)}$, it is convenient to treat separately the special cases where $s^{(o)}$ contains derivatives with respect to the transverse co-ordinates y_i. Area distributions of the form

$$s^{(o)} = \frac{-\partial s_i}{\partial y_i} \, , \quad \frac{\partial^2 s_{ij}}{\partial y_i \partial y_i} \, , \text{ etc.} \tag{54}$$

in fact arise from volume source distributions of the form

$$Q = -\frac{\partial Q_i}{\partial y_i} \quad , \frac{\partial^2 Q_{ij}}{\partial y_i \partial y_i}, \text{ etc.} \tag{55}$$

as follows from the definition of the source moment $s^{(o)}$ in equation (33).

Equation (53) gives the modal components corresponding to (54) as

$$s_N^{(o)} = \frac{E_N}{S} \int_S s_i \frac{\partial E_N^*}{\partial y_i} \, dS, \quad \frac{E_N}{S} \int_S s_{ij} \frac{\partial^2 E_N^*}{\partial y_i \partial y_j} \, dS, \text{ etc.}; \tag{56}$$

these results are obtained on integrating by parts, and noting that the distributions $s_i = \int Q_i \, dx$, $s_{ij} = \int Q_{ij} \, dx$, etc., are confined to the duct cross-section and vanish outside. Exactly similar results apply to the higher-order axial moments s_x, s_{xx}, etc. (cf. [35], Appendix II).

In the present application, a fluctuating force distribution $\underset{\sim}{f}(\underset{\sim}{y}, t)$ per unit area is specified over the duct cross-section $x = x_s$. The axial (x) and transverse (y_i) components of $\underset{\sim}{f}$ are denoted by f_x, f_i. The corresponding force distribution $\underset{\sim}{g}$ per unit mass therefore has components:

$$g_x \doteq \frac{1}{\rho_o} f_x \, \delta(x - x_s) \, , \quad g_i \doteq \frac{1}{\rho_o} f_i \, \delta(x - x_s), \tag{57}$$

and the acoustic source distribution in equation (30) is:

$$Q = - \operatorname{div} \underset{\sim}{g} = - \frac{\partial g_x}{\partial x} - \frac{\partial g_i}{\partial y_i} \, . \tag{58}$$

It follows from (57) and (58) that the axial moments of Q may be written as:

$$s^{(o)} \doteq -\frac{\partial}{\partial y_i}\,(f_i/\rho_o)\quad,\quad (\text{i.e. } s_i \doteq f_i/\rho_o)$$

and $\quad s_x \doteq f_x/\rho_o\ .$ (59)

The normal-mode components of $s^{(o)}$ and s_x are then given by equations such as (53) and (56).

4.3.2 Equivalent source distribution for single-frequency excitation

If any higher-order source moment, for example s_x, is confined to a single frequency and duct mode, the response function G can be used to define an equivalent zero-order source moment distribution (equation 42). Thus if f_x in the present case is given by:

$$f_x = \mathrm{Re}\ (F_x)\ ;\ F_x \propto e^{-i\omega t}\ E_N(\chi)\ , \tag{60}$$

the equivalent source distribution in complex form is:

$$S^{(x)} = \frac{1}{G}\ \frac{\partial G}{\partial x_s}\ \cdot\ \frac{F_x}{\rho_o} \tag{61}$$

as follows from equations (59) and (42).

The total Nth-mode excitation is represented by the sum $S^{(x)} + S^{(o)}$ of the axial and transverse contributions. Equations (56) and (59) show that $S^{(o)}$ is not related to the modal components of the transverse force distribution itself, but rather to the modal components of $(\frac{1}{E^*_N}\frac{\partial E^*_N}{\partial y_i})\ f_i$; so to proceed further it is necessary to specify the variation of f_i over the duct cross-section.

4.3.3 Axial and tangential forces in an axisymmetric duct

For an axisymmetric duct bounded by the cylinders $r = a_o$ (outer wall) and $r = a_1$ (inner wall), the mode shape functions E_N are best expressed in polar co-ordinates:

$$E_{mn}(r,\theta) = e^{im\theta} R_{mn}(r). \tag{62}$$

The two mode numbers m and n replace the single index N used above; m is the circumferential mode number, and n is the radial order of the mode†.

A force distribution with the following components is assumed to act over the cross-section $x = x_s$:

Axial force/unit area = f_x, as given by (60) with $E_N = E_{mn}$;

Tangential force/unit area $f_\theta = (\frac{r}{a_o})\, \varepsilon f_x$. (63)

Physically, ε is related to the angle δ_o between the resultant force (at $r = a_o$) and the x direction by $\varepsilon = \tan \delta_o$.

The corresponding equivalent source distributions in the (m,n) mode are given by (61) for the axial contribution, and by:

$$S^{(o)} = \frac{E_{mn}}{S} \int_S (\frac{r}{a_o})\, \varepsilon \frac{F_x}{\rho_o} (\frac{-im}{r}) E^*_{mn}\, dS = -\frac{im\varepsilon}{a_o} \frac{F_x}{\rho_o} \tag{64}$$

for the tangential contribution. The latter follows from (56) on noting that F_x is proportional to E_{mn}.

Equations (61) and (64) together give the total (m,n) mode excitation for the particular force distribution assumed above. No restriction has so far been placed on the modal admittances either side of the source; for purposes of illustration it is now assumed that the duct on the -x side provides a non-reflecting termination for the mode in question.

† Footnote: The properties of axisymmetric-duct modes are discussed in detail in [37], [27] and [38].

The same assumption was shown in section 3.3 to give

$$\frac{1}{G}\frac{\partial G}{\partial x_s} = -ik_x^+ \qquad (x > x_s) \tag{65}$$

on the +x side of the source; so the combined source distribution becomes

$$S^{(x)} + S^{(o)} = -i\left(k_x^+ + \frac{m\varepsilon}{a_o}\right)\frac{F_x}{\rho_o} \qquad (x > x_s)\,. \tag{66}$$

At this stage the problem is solved in principle, since the sound field in the duct and the radiated sound power can be found by the methods of sections 2 and 3. It is of some interest, however, to work out the sound power explicitly for the special case where the duct provides a non-reflecting termination on <u>both</u> sides of the source; this is a rough approximation to the situation in an open-ended duct for frequencies above cut-off. (Compare the slightly more sophisticated approximations discussed in section 4.2.3).

4.3.4 <u>Upstream and downstream sound power in a rotating mean flow</u>

The preceding analysis has implicitly assumed the mean flow in the duct to be axial. If there is in addition a solid-body rotation, with a peripheral Mach number $M_\theta = \Omega a_o/c_o$ such that $M_\theta^2 << 1$, this can be allowed for according to Appendix II by treating ω as the radian frequency relative to the swirl; i.e.

$$\omega = \omega_o - m\Omega\,, \tag{67}$$

where ω_o is the absolute radian frequency. The sound power expressions also have to be multiplied by a factor

$$\frac{\omega_o}{\omega} = 1 + \frac{m}{ka_o}M_\theta\,, \quad \text{(from Appendix II)}\,. \tag{68}$$

Putting $q_s = 1$ in equation (47) and using (66) gives the sound power radiated to the +x side of the force distribution as:

$$W_+ = \frac{1}{8}\,\frac{\omega o}{\omega}\,\frac{|\bar{F}_x|^2 S}{\alpha \rho_o c_o}\,(1 - \alpha M_x)^{-2}\left[(\alpha - M_x) + \frac{m\varepsilon}{ka_o}(1-M_x^2)\right]^2. \qquad (69)$$

Here $\bar{F}_x$ is the normal-mode coefficient of the axial force distribution, so that $F_x = \bar{F}_x E_{mn}(r,\theta)$. Equation (69) shows that the modal power radiated to the +x side can be made to vanish by an appropriate choice of ε (so that the factor in brackets is zero). However, the same choice of ε does not make the power vanish on the other side of the source, because the expression for W_- differs from W_+ (equation 69) by having $-\alpha$ in place of α.

The ratio of the sound powers on the two sides is

$$\frac{W_+}{W_-} = \left\{\frac{1 + \alpha M_x}{1 - \alpha M_x}\cdot\frac{(m\varepsilon/ka_o)(1-M_x^2) + \alpha - M_x}{(m\varepsilon/ka_o)(1-M_x^2) - \alpha - M_x}\right\}^2, \qquad (70)$$

which tends to 1 in the high-frequency limit (cf. equation 48). Comparison with Mani's two-dimensional result [28] shows agreement for the case $M_\theta = 0$ (no swirl), but there appears to be an error in Mani's analysis for the sound intensity with swirl (cf. Appendix II).

4.4 USE OF JUMP CONDITIONS FOR SOUND GENERATION AT A FLOW DISCONTINUITY

An alternative approach to finding the sound excited by a fluctuating force distribution is to consider the jump conditions across the source plane. If the specific entropy of the fluid is the same on both sides, as assumed below, the reamining jump conditions are determined by continuity of mass and momentum flow.

The following analysis demonstrates the approach by using it to calculate the sound field due to an axial fluctuating-force distribution in an axial mean flow. This is a case already considered by the source-moment approach, which in fact gives the same answer with less trouble. The advantage of the present method is that it remains valid when there is a discontinuity in the mean flow across the actuator disk†, as well as in the fluctuating flow.

4.4.1 Linearized jump conditions

The jump conditions across an actuator disk normal to the duct axis are obtained from continuity of mass and axial momentum across the disk in the x direction. Thus:

$$\left[\, m \,\right]_-^+ = 0 \quad : \qquad \left[\, p \,\right]_-^+ + m\left[\, V_x \,\right]_-^+ = f_x \,, \tag{71}$$

where $m = \rho V_x$ is the mass flux, and f_x is the applied force per unit disk area in the x direction. These equations are next linearized and expressed in phasor form, on the understanding that a single frequency and duct mode are being considered; this means that f_x is also restricted to a single mode. If the mean flow is the same on both sides,

† Footnote: The source-moment method no longer applies in this situation, since the wave equation on which it is based is not uniformly valid through the disconuity. Mani's results using this approach [28] are therefore valid only when the mean-flow discontinuity vanishes.

$$M_x \left[P \right]_-^+ + \rho_o c_o \left[U + U_v \right]_-^+ \doteq 0 , \tag{72}$$

and

$$\left[P \right]_-^+ + \rho_o c_o \, M_x \left[U + U_v \right]_-^+ \doteq F_x . \tag{73}$$

In equations (72) and (73), the axial velocity $U = \beta P/\rho_o c_o$ due to the acoustic mode is distinguished from the axial velocity U_v induced by vorticity in the flow. Even if the upstream flow is irrotational, vorticity is produced downstream of the actuator disk by nonuniformities in the force distribution f_x.

An equation due to Berndt [39, eq.(11)] gives the jump in vorticity due to an arbitrary axial-force distribution f_x, based on consideration of the transverse fluid momentum on the two sides of the disk. If $\underset{\sim}{\zeta}$ is the vorticity,

$$\left[\underset{\sim}{\zeta} \right]_-^+ = \underset{\sim}{n} \times \left(\left[1/\rho \right]_-^+ \nabla_t m - \underset{\sim}{a}_t \left[\rho \right]_-^+ / m \right) - \frac{1}{m} \left(\underset{\sim}{n} \times \nabla_t f_x \right). \tag{74}$$

Here $\underset{\sim}{n}$ is the unit vector in the axial direction (normal to the disk), and $\underset{\sim}{a}_t$ is the acceleration of a point moving with the transverse fluid velocity $\underset{\sim}{V}_t$; thus

$$\underset{\sim}{a}_t = \left(\frac{\partial}{\partial t} + \underset{\sim}{V}_t \cdot \nabla \right) \underset{\sim}{V}_t . \tag{75}$$

If the mean flow is axial and uniform over the actuator disk, linearization of the vorticity jump equation (74) gives:

$$\left[\underset{\sim}{\zeta}' \right]_-^+ \doteq \underset{\sim}{n} \times \nabla_t \left\{ \left(\frac{1}{\rho_2} - \frac{1}{\rho_1} \right) m' - \frac{1}{m} f_x' \right\} - \left(\frac{\rho_2 - \rho_1}{m} \right) \underset{\sim}{n} \times \underset{\sim}{a}'_t \tag{76}$$

where ρ_1, ρ_2 are the densities on the $-x$ and $+x$ sides of the discontinuity.

Finally, if there is no discontinuity in the mean flow, $\rho_2 = \rho_1$ and equation (76) is simplified considerably. Expressed in phasor form in the same way as equations (72) and (73), the vorticity jump is

$$\left[\underset{\sim}{Z} \right]_-^+ \doteq \left(\frac{-1}{\rho_o c_o M_x} \right) \underset{\sim}{n} \times \nabla_t F_x \ . \tag{77}$$

Equations (72), (73) and (77) are the basic equations from which the sound field is derived below; they apply only to a uniform axial flow which is subjected to axial fluctuating forces. More general jump conditions may be obtained by returning to equations (71) and (74), although for non-axial force distributions it is necessary to use Berndt's full equation for the vorticity jump.

4.4.2 Solution for the vorticity field

The velocity field $\underset{\sim}{V}_v$ associated with the vorticity $\underset{\sim}{\zeta}$ is defined by

$$\text{curl } \underset{\sim}{V}_v = \underset{\sim}{\zeta} \ ; \quad \text{div } \underset{\sim}{V}_v = 0 \tag{78}$$

and may be represented by the curl of a vector potential:

$$\underset{\sim}{V}_v = \text{curl } \underset{\sim}{b} = \nabla \times \underset{\sim}{b} \ . \tag{79}$$

Equations (78) and (79) give an equation for $\underset{\sim}{b}$:

$$\nabla^2 \underset{\sim}{b} = - \underset{\sim}{\zeta} \qquad (\text{div } \underset{\sim}{b} = 0 \ ; \text{ cf. } [\ 40], \text{ Section 2.4}). \tag{80}$$

In the present case,

$$\left.\begin{aligned} \nabla^2 &\equiv \frac{\partial^2}{\partial x^2} + \nabla_t^2 \quad , \\ \text{where} \quad \frac{\partial^2}{\partial x^2} &\doteq \frac{1}{c_o^2 M_x^2} \frac{\partial^2}{\partial t^2} \end{aligned}\right\} \tag{81}$$

sin ce the vorticity field consists of perturbations which are convected at the mean flow velocity. If the solution is specialized to a single frequency ($\partial/\partial t = -i\omega$) and duct mode ($\nabla_t^2 = -k_N^2$), (80) and (81) combine to give the phasor equation

$$\left(\frac{\omega^2}{c_o^2 M_x^2} + k_N^2\right) \underset{\sim}{B} = \underset{\sim}{Z}$$

or, in terms of the axial wavenumber parameter α (equation 6),

$$\underset{\sim}{B} = \frac{M_x^2 (1 - M_x^2)}{1 - \alpha^2 M_x^2} \left(\frac{c_o}{\omega}\right)^2 \underset{\sim}{Z} \quad . \tag{82}$$

In order to eliminate the axial velocity U_v from the jump equations (72) and (73), what is needed is an expression for the jump

$$\left[U_v \right]_-^+ = \left(\nabla \times \left[\underset{\sim}{B} \right]_-^+\right)_x \qquad \text{(cf. equation 79)} \quad , \tag{83}$$

in terms of the force distribution F_x. Such an expression is provided by (77) and (82), which give

$$\left.\begin{aligned} \left[\underset{\sim}{B} \right]_-^+ &= \underset{\sim}{n} \times \nabla_t G \\ \text{where} \quad G &= - \frac{c_o F_x}{\omega^2 \rho_o} \frac{M_x (1 - M_x^2)}{1 - \alpha^2 M_x^2} \quad . \end{aligned}\right\} \tag{84}$$

It follows from (83) and (84) that

$$\left[U_v \right]_-^+ = \nabla_t^2 \, G = - \left(\frac{\omega}{c_o}\right)^2 G. \, \frac{1 - \alpha^2}{1 - M_x^2} \quad ,$$

i.e.

$$\left[U_v \right]_-^+ = \frac{F_x}{\rho_o c_o} \cdot \frac{M_x (1 - \alpha^2)}{1 - \alpha^2 M_x^2} \quad . \tag{85}$$

This is the required solution.

4.4.3 Solution for the pressure field

If the velocities U, U_v are eliminated from equations (72) and (73), by expressing the acoustic component U in terms of the admittance ratios β_-, β_+ on the two sides of the actuator disk and using (85) for the vorticity component, the following result is obtained:

$$P_{\mp} = - \frac{\left[M_x (2 - \alpha^2 - M_x^2) + \beta_{\pm} (1 - \alpha^2 M_x^2) \right]}{(1 - M_x^2)(1 - \alpha^2 M_x^2)(\beta_+ - \beta_-)} F_x \quad ;$$

$$P_+ - P_- = \frac{F_x}{1 - M_x^2} \quad . \tag{86}$$

Equation (86) gives the sound pressure on each side of the actuator disk. It may alternatively be written in terms of the reflection phase ψ for waves either side, by using equation (14) to express β in terms of ψ. For the special case treated in section 4.2.3, where there are no reflected waves on the $-x$ side, the pressure at any position on the $+x$ side is given by the present method as

$$P\,(x > x_s) \;=\; \frac{k_x^+}{\alpha k}\; F_x \cos\psi . \exp i\left(\psi_o - \frac{M_x kx}{1 - M_x^2}\right) . e^{-ik_x^+ x_s} \quad ; \qquad (87)$$

this agrees with the value $(\partial G/\partial x_s)\;\; F_x/\rho_o$ found by the method of section 4.2 (where S_x is given by F_x/ρ_o).

4.5 CONCLUSIONS

The theory of sound transmission and generation in hard-walled ducts has been extended to include axial and swirling mean flow. Situations previously considered by Davies and Ffowcs Williams (sound generated by turbulence in an infinite duct of square cross-section, Ref.41) and Mani (fluctuating forces in a narrow annular duct, Ref.28) appear as particular applications of the present theory, which is based on the idea of a single-frequency mode response function rather than a Green function as used in [41].

The main conclusions are summarized below.

(a) The effect of an axial mean flow on the sound power transmitted by a single mode, at frequencies well above cut-off, is to multiply the power by $(1 \pm M_x)^2$ for a given pressure amplitude. The $\pm$ signs refer to waves travelling in the $\pm$ x directions. This is the same factor as predicted by geometric acoustics, and corrects the result given in [23].

(b) Solid-body rotation of the flow in an axisymmetric duct further modifies the modal sound power by a factor ω_o/ω, where ω_o is the radian frequency in fixed co-ordinates and ω is the frequency in co-ordinates rotating with the flow. It is assumed that the rotation is subsonic with angular velocity $\Omega \ll \omega_o$, so that the sound propagates relative to the swirl in the same way as in a non-rotating flow.

(c) In a duct with non-reflecting terminations, the sound power radiated upstream and downstream from a fixed monopole source-distribution is proportional to $(1 \pm M_x)^2$, under the conditions given in (a). The corresponding factors for axial-dipole and axial-quadrupole source-distributions are 1 (i.e. no convective effect) and $(1 \pm M_x)^{-2}$. This last result differs from the one given in [41] because the sound power in that paper was defined relative to the mean flow.

(d) The effects of finite duct length are incorporated in the general theory, since axial standing waves are allowed for. However, there is very little information on the modal reflection factors at the open end of a duct in the presence of flow.

(e) In turbomachinery applications the axial gradients of the mean flow may not be negligible. A possible model to include this effect would be an actuator disk across which both the mean and unsteady components of the flow were discontinuous. The problem of sound generation by unsteady forces applied at a mean-flow discontinuity has been studied by Mani [28], but without considering the downstream vorticity. An outline solution which takes account of the vorticity in this situation is presented in section 4.4.

CHAPTER 5

IDENTIFICATION OF SOUND SOURCES IN SUBSONIC TURBOMACHINERY

In the last eight years our understanding of the sound generated in turbomachinery, as a by-product of unsteady internal aerodynamic flows, has greatly increased. Consequently we may shortly expect to see, in airline service, aircraft engines which have been designed from the outset with some knowledge of factors affecting noise.

These advances, however, are still not sufficient to ensure acceptably quiet airport operations in the face of increasing air traffic. Two main difficulties stand in the way of quietening aircraft propulsive machinery.

The first difficulty is one of finding which design parameters have a significant effect on the sound output of a fan or compressor. That is, for a machine with a given mass flow and pressure rise, what means are available for controlling the noise? As a result of empirical investigations combined with fundamental research, there is a growing list of qualitative answers to this question [42].

A more serious difficulty remains. In the absence of any breakthrough, engine noise reductions will have to be achieved by a combination of several techniques. An optimum engine design can then be reached only from a knowledge of how each item in the combination affects (i) the sound output, and (ii) the aerodynamic performance.

Here the existing knowledge is inadequate[†], and it is the purpose of the following chapters to review and extend the theory of turbomachinery noise sources so as to provide explicit relations between sound output and aerodynamic parameters. Analytical relations of this type, however approximate, provide a basis for interpreting experimental data in a systematic way. Hopefully, further advances in understanding will follow which will indicate methods of noise reduction at source.

5.1 PREVIOUS STUDIES OF TURBOMACHINERY NOISE GENERATION

Central to most early studies of turbojet engine noise was the idea of fluctuating blade forces as the primary source of sound. Thus Hetherington [43], discussing the discrete-frequency radiation from a rotor-stator combination, used the work of Kemp and Sears [44, 45, 46] to estimate the unsteady loading - and hence radiated sound - due to aerodynamic interaction between the blade rows. This same approach was followed up by Bragg and Bridge [47], and was also developed independently by Slutsky, in work only recently published [48]. Studies by Lilley [49] and Sharland [50] of broadband noise generation likewise attributed the sound radiated from a rotor to fluctuating forces.

The analysis which follows differs in two respects from these papers. First, certain new mechanisms of sound generation are identified in addition to fluctuating blade forces. One such mechanism has already been described

---

[†]The author's review [35] of published methods for predicting fan and compressor noise shows that errors of over 10 dB can occur, when any of these methods is applied to a new machine.

by Ffowcs Williams [51] and shown to account for appreciable sound radiation from subsonic multibladed rotors.

Second, once the source mechanisms have been identified, the calculation of sound power is based on the theory of Chapter 4. It is interesting in this context to notice that all of the papers mentioned use different acoustic models to calculate the sound power output from given blade forces. These are listed below.

Broadband	[50]	Blades replaced by point forces in free field. Effects of motion neglected
	[49]	As above, but approximate correction made for blade rotation
Discrete frequency	[47]	As [50], but allowance made for cancellation between blades
	[43]	Blades replaced by line forces in free field. No allowance for cancellation
	[48]	Blades replaced by line vortices in infinite axisymmetric duct. Correct phase relations included.

The present study concentrates on discrete-frequency sources, so that phase relationships between different blades have to be taken into account as indicated by Slutsky [48] and Tyler and Sofrin [37]. The point-force representation is inadmissible, as the blade span is not generally small compared with the sound wavelength. Finally, Slutsky's line-vortex representation does not correctly account for vorticity shed downstream of a blade row.

5.2 IDENTIFICATION OF SOURCE MECHANISMS

The general theory of Chapter 3 makes it possible to identify all of the various sound-producing mechanisms in subsonic turbomachinery. Equations (3.9) and (3.10) show that apart from the classical mechanisms of fluctuating volume velocity ($\tilde{D}^2z/Dt^2$) and fluctuating forces ($\partial g_j/\partial x_j$), sound is generated by certain nonlinear interactions between flow perturbations.

Three types of nonlinear interaction source are expected on the basis of equation (3.10).

(a) Nonlinear sources due to pressure-field interaction between blade rows. The first two terms of (3.10) account for interaction between the pressure fields; the fifth and seventh terms account for interaction between the pressure field of one blade row and the thickness or loading of the other.

(b) Nonlinear terms associated with turbulence or velocity wakes. The first term of (3.10) includes both interaction between turbulent velocity components, and interaction of turbulence with the potential field of a blade row.

(c) Nonlinear terms associated with hot spots or entropy wakes. The third and fourth terms of (3.10) account for interaction between pressure and entropy perturbations; such interactions may be particularly important in turbines, where the flow entering a rotor may contain appreciable temperature gradients arising from combustion. Finally, the

sixth and eighth terms account for interactions between entropy perturbations and the thickness and loading of a blade row.

A classification of the acoustic source terms according to multipole order is shown below, for each of the mechanisms identified above. The numbers in each column of the table refer to terms in equations (3.13), (3.14) and (3.15) respectively; for example, $Q_i(4)$ denotes the g_i term in (3.14).

TABLE

Source type:	$Q^{(0)}$	Q_i	Q_{ij}	Spectrum
Linear source terms	(1)	(1,4)	(1)	Discrete
	"Propeller" mechanisms-steady load & thickness			
		(4)		Discrete or continuous
	Fluctuating blade loads			
Nonlinear terms due to pressure-field interaction between blade rows	(2)	(2)	(2)	Discrete
	Pressure-field interaction with rotor blade thickness			
		(5)		
	Pressure field/rotor loading			
	(5)	(7)	(6,7)	
	Interaction between two pressure fields			
Nonlinear terms associated with turbulence			(4) Turbulence/ turbulence	Discrete (wake profile interactions) or Continuous (random disturbances)
			(5) Turbulence/ potential field	
Nonlinear terms associated with entropy fluctuations (turbine)	(3)	(3)	(3)	
	Entropy interaction with rotor blade thickness			
	(4)	(6)		
	Entropy/rotor loading			
	(6,7)	(8,9)	(8)	
	Entropy/rotor pressure field			

Each of the sound-generating mechanisms in the table is investigated in detail in the two following chapters. Chapter 6 considers the spatially periodic flow disturbances due to blade-row wakes and pressure fields as a source of interaction noise; the flow disturbances themselves are related to the lift and drag forces on the blade row. Interaction of a rotor with incident turbulence is studied in Chapter 7, and the radiated sound power is compared with that radiated from the steady blade loading in an undisturbed flow.

CHAPTER 6

PERIODIC ROTOR-STATOR INTERACTION AS A SOURCE OF SOUND

In this chapter, the general theory set out in the first part of the thesis is applied to rotor-stator interaction noise. Specifically, the discrete-frequency sound power output due to blade-row interaction is estimated for an axial compressor or turbine stage. Some of the results are then generalized in Chapter 7 to describe sound generation by a rotor in turbulent flow. Subsonic flow is assumed throughout; the question of sound radiation from a supersonic rotor is taken up in Chapter 8.

6.1 PERIODIC DISTURBANCE FIELD OF A BLADE ROW

Before the sound output can be calculated, it is necessary to define the unsteady flow components in terms of the geometry and operating parameters of a fan or turbine. The complexity of the problem makes it desirable to begin with the simplest possible model relevant to the situation; the present section aims to provide such a model.

The blade row is represented by a two-dimensional cascade of thin airfoils, and compressibility effects are neglected. The flow deflection through the blade row is assumed small, so that the pressure field can be estimated by the same linearized theory as is used for the radiated sound field. For practical applications, as in section 6.2, the rotor and stator flow angles β, α are given their values on the side nearer the interacting blade row.

Spatial harmonic components of the rotor and stator fields are characterized by tangential wavenumbers $2\pi p/d_R$, $2\pi s/d_S$ in the direction of rotor motion (y). This implies spatial factors exp $i(2\pi py/d_R)$, exp $i(2\pi sy/d_S)$.

6.1.1 Rotor pressure field

Particularly simple results are obtained for the two extreme cases of low and high solidity.

(a) Low solidity ($\pi|p|\sigma_R << 1$)

The following expressions give the pressure and velocity harmonic components in the rotor plane†, due to rotor loading†† (blade lift coefficient = $\pi\phi_R$). Here as elsewhere, the harmonic index p may take +ve or -ve values (p = ±1, ±2 etc.) Where results are quoted for $p > 0$, replacement of i by -i gives the result for $p < 0$.

$$\left|\frac{\tilde{P}_p}{\rho c^2}\right| = \frac{\pi}{4}\sigma_R\phi_R M_x^2 . \sec^2\beta \quad ; \quad \frac{P_{-p}}{P_{+p}} = e^{-2i\beta} \qquad (p>0) \tag{1}$$

$$\left|\frac{\tilde{U}_p}{c}\right| = \frac{\pi}{4}\sigma_R\phi_R M_x . \sec\beta \quad ; \quad \frac{U_{-p}}{U_{+p}} = 1 \quad . \tag{2}$$

---

†The axial extent of the rotor is neglected in the low-solidity approximation; thus the rotor is regarded as an actuator disk.

††For rotor thickness pressure field, $\phi_R \to 4p\sigma_R\varepsilon_R$ and $P_{-p}/P_{+p} = e^{-4i\beta}$. Here ε_R is the mean thickness/chord for the rotor blade.

The transverse velocity component is given, on either side of the rotor, by

$$\frac{V_p}{U_p} = \begin{cases} i & (x < x_R) \\ -i & (x > x_R) \end{cases}, \quad (p > 0). \tag{3}$$

All quantities have a wavenumber in the x direction of

$$k_x = \begin{cases} -ik_p & (x < x_R) \\ ik_p & (x > x_R) \end{cases} \quad (\text{decay constant } k_p = 2\pi|p|/d_R); \tag{4}$$

thus at distance $\bar{x}$ either side of the rotor plane,

$$\left|U_p/\bar{U}_p\right|^2 = e^{-2k_p\bar{x}} = K_p. \tag{5}$$

For a stator with blade angle α, exactly similar expressions apply except that $P_s^+/P_s^- = e^{-2i\alpha}$ $(s>0)$. The decay constant is $k_s = 2\pi|s|/d_s$ for the s th spatial harmonic of the pressure field.

(b) <u>High solidity</u> $(\exp 2\pi|p|\sigma_R >> 1)$

The pressure fields either side of the rotor in this case are equivalent to those produced by an actuator disk in the LE plane, the pressure and velocity in that plane being given by $(for\ p > 0)$

$$\left|\frac{\bar{P}_p}{\rho c^2}\right| = \left|\frac{2\sigma_R}{p}\right|^{\frac{1}{2}} \phi_R M_x^2 \cdot \tfrac{1}{4}\sec^2\beta \; ; \quad \frac{P_p^-}{P_p^+} = i\, e^{-i\beta} \tag{6}$$

$$\left|\frac{\bar{U}_p}{c}\right| = \left|\frac{2\sigma_R}{p}\right|^{\frac{1}{2}} \phi_R M_x \cdot \tfrac{1}{4}\sec\beta \; ; \quad \frac{U_p^-}{U_p^+} = i\, e^{i\beta} \; . \tag{7}$$

In other respects the description given in (a) above applies here.

For a stator, the phase changes through the actuator disk are (for $s > 0$) $P_s^+/P_s^- = -i\,e^{-i\alpha}$; $U_s^+/U_s^- = -i\,e^{i\alpha}$. Equations (6) and (7) apply to a rotor or stator with a flat-plate steady lift distribution over the blade chord.

6.1.2 Rotor velocity wake (Figure 6.1)

At low Mach numbers, the rotor wake momentum thickness $\bar{e}_R$ (measured in the tangential direction) is related to the rotor loss coefficient π_R by [52]

$$\frac{\bar{e}_R}{d_R} \doteq \tfrac{1}{2}\pi_R \quad , (\pi_R << 1). \tag{8}$$

Here π_R is based on the dynamic pressure downstream of the rotor; and $\bar{e}_R$ is measured ~1 chord downstream of the trailing edge where the pressure is almost uniform, but adjacent wakes have not begun to merge.

The wake displacement thickness e_R at this position ($X = 1$) can be estimated from (8) by assuming a form parameter $H \doteq 1$; thus

$$\frac{e_R}{d_R} = \frac{-1}{V_\infty d_R} \int_{\text{wake}} v\,dy \text{ (evaluated at } X = 1) \doteq \tfrac{1}{2}\pi_R, \tag{9}$$

and in general, if $e_R(X) \propto f(X)$ defines the downstream variation of displacement thickness,

$$\frac{e_R(X)}{d_R} \doteq \tfrac{1}{2}\pi_R \frac{f(X)}{f(1)} . \tag{10}$$

The harmonic components of the wake velocity field at any downstream [position

follow from (10), provided the wake is thin enough to be approximated by a delta function ($k_p e_R < 1$).

Thus

$$\left|\frac{U_p}{c}\right|^2 \doteq K_w \cdot \tfrac{1}{4}\pi^2 R^2 M_x^2 \; ; \quad \frac{V_p}{U_p} = -\tan\beta \qquad (11)$$

gives the axial and transverse velocity components downstream of the rotor. The wake decay factor K_w is defined as

$$K_w = [f(X)/f(1)]^2 \quad , (\underline{c.f.} \text{ equation 10}). \qquad (12)$$

Because of this decay in the downstream direction, the axial wavenumber of each harmonic component is complex:

$$\mathrm{Re}(k_x) = k_p \tan\beta; \quad \mathrm{Im}(k_x) \sim 1/b_{xR} = \frac{\sec\beta}{\sigma_R d_R} \; (0<X<1). \qquad (13)$$

6.1.3. Rotor entropy wake

On the assumption that pressure variations through the wake in the transverse direction are negligible, specific-entropy perturbations s' are related to temperature perturbations by

$$s' \doteq (C_p/T)T' \quad , (\text{to 1st order}). \qquad (14)$$

Harmonic components of the wake temperature profile, at any downstream position, will be denoted by T_p. For thin wakes, these may be estimated from the integrated temperature defect in a wake (c.f. use of displacement thickness for velocity wake).

If we define a temperature defect parameter - by analogy with (9) - as

$$\theta_R = \frac{-1}{Td_R} \int_{\text{wake}} T' \, dy \quad \text{(evaluated at } X = 1\text{)}, \tag{15}$$

and a wake decay factor K_w is applied as before to give the temperature defect at other values of X, then the result is

$$\left|\frac{T_p}{T}\right|^2 \doteq K_w \theta_R^2 , \quad (2\pi p/\theta_R < 1). \tag{16}$$

Finally, the axial wavenumber of each harmonic component is given by

$$\mathrm{Re}(k_x) = k_p \tan\beta; \quad \mathrm{Im}(k_x) \simeq O(1/b_{xR}), \tag{17}$$

(decay assumed of some order as for velocity wakes).

A special case relevant to compressors is that of isoenergetic wakes, where the stagnation enthalpy is uniform through the wake in the transverse direction. The temperature-defect parameter θ_R is then related to the pressure-loss coefficient π_R by

$$\theta_R \doteq (\gamma - 1)M_R^2 . \tfrac{1}{2}(e_R + \bar{e}_R)/d_R \quad \text{(for perfect gas, to order } M_R^2\text{)}^{\dagger};$$

i.e. from (9),

$$\theta_R \doteq \tfrac{1}{2}(\gamma - 1)\, \pi_R M_x^2 \sec^2\beta \; ; \quad \text{(for m parameter} \doteq 1 \text{ in wake at } X = 1\text{)}. \tag{18}$$

† For a general fluid, $(\gamma - 1)$ is replaced by $(c^2/C_p T)$.

6.2 ESTIMATES OF INTERACTION TONE INTENSITY

The particular case of a rotor-stator stage (Figure 6.2), of medium to high solidity, is studied in detail in the present section. The aim is to provide estimates of the sound power output associated with the more important of the mechanisms which operate in such a situation. For this purpose the various mechanisms are considered independently, without regard to phase; it will be seen that cancellation can occur only under special circumstances.

Three types of periodic rotor-stator interaction are considered: (1) interaction mechanisms which depend on the pressure field of either blade row for bridging the gap between the rows; (2) those which depend on the velocity wake from the upstream row entering the downstream row; (3) those which depend on the entropy wake entering the downstream blade row.

6.2.1 Pressure-field interaction mechanisms

If both rotor and stator have a flat-plate steady lift distribution and a solidity of order 1 or more, section 6.1.1 shows that the pressure field is much weaker at the trailing edge than in the inlet plane. The only mechanism under this heading which is not affected is the rotor lift fluctuation due to the pressure field upstream of the stator; all other pressure-field interaction mechanisms are weaker by an order of magnitude, equivalent to the decay of the pressure field in the axial width of a blade row. This mechanism is analysed below.

(a) Rotor lift fluctuations due to stator potential velocity field:

The relationship between sound intensity I_{sp}, radiated in either direction from the rotor, and the axial component L_{xs} of the lift fluctuation

on a rotor blade, follows from equations (4.48) and (4.61).

$$I_{sp} \doteq \frac{1}{2\rho c} \left| \frac{L_{xs}}{d_R} \right|^2 , \text{ (well above cutoff);} \qquad (19)$$

here I_{sp} refers to sound radiated at $|p| \times$ blade-passing frequency, through interaction with the s th spatial harmonic of the stator velocity field.† Equation (19) assumes that the chordwise distribution of the unsteady blade loading is compact in terms of the radiated sound wavelength.

The fluctuating blade force L_{xs} at s × vane-passing frequency is dominated by the upwash component V_R of the velocity at the rotor trailing edge (Appendix III, equation 12)

$$L_{xs} \doteq -\pi b_R \rho c M_x \tan\beta_2 \, (K_L'' \, V_R)_s , \quad (K_L'' \text{ referred to trailing edge}). \qquad (20)$$

The upwash V_R is related to the axial and transverse velocity fluctuations U, V by

$$V_R = -(U \sin \beta_2 + V \cos \beta_2) = - i \, e^{-i\beta_2} U, \qquad (s > 0) \quad (21)$$

since V/U = i for each spatial harmonic of the stator field on the upstream side.

The lift response function can be approximated as follows, in terms of the reduced frequency n and reduced wavenumber q for the rotor (see Appendix III).

$$K_L'' \doteq \frac{1 - n/q}{(2\pi q)^{\frac{1}{2}}} e^{-i\frac{1}{4}\pi} \qquad (|n| > 1) \qquad (22)$$

---

† The corresponding mode is given by $m = |p|(B + \frac{s}{p} V)$, with the convention that m is +ve for modes spinning in the same direction as the rotor. The contributions for (p, s) and $(-p, -s)$ have been combined to give the modal intensity I_{sp}.

where

$$n = -\pi\, s\, (b_R/d_S).\ M_t/M_R \tag{23}$$

and

$$q = -i\pi|s|(b_R/d_S)\, e^{\mp i\beta_2} \quad (s \gtrless 0). \tag{24}$$

Equations (23) and (24) give

$$|1 - n/q|^2 = \frac{\cos^2\beta_2}{\cos^2\alpha_1} \quad . \tag{25}$$

If the stator potential velocity field is caused by the steady-state blade loading, equation (7) may be used to estimate U_s. Combining this result with equations (19) through (25) gives the sound intensity, for each interaction mode above cutoff ($|s|V \doteq |pB$).

$$\text{(a)}\quad \frac{I_{sp}}{\rho c^3} \doteq \frac{K_p}{32p^2}\ \frac{V}{B}\ \sigma_R\sigma_S\phi_S^2 M^4 x\ \ \frac{\sin^2\beta_2}{\cos^4\alpha_1} \quad . \tag{26}$$

The decay factor K_p accounts for the decay of the stator (or rotor) pressure field over the distance $\bar{x}$ separating adjacent blade rows. It leads to a much more rapid fall-off of sound power with axial separation than occurs for any of the remaining mechanisms (b) through (f).

6.2.2 Velocity wake interaction mechanisms

The periodic wake pattern downstream of the rotor interacts with the stator to produce three sources of sound. These are described below (mechanisms b, c, d).

(b) Stator lift fluctuations due to rotor wake:

Corresponding to equation (19)

$$I_{ps} \doteq \frac{1}{2\rho c} \left| \frac{L_{xp}}{d_S} \right|^2 \quad \text{(well above cutoff)} \tag{27}$$

relates the sound intensity for a single mode $|p|(\mathcal{B} + \frac{s}{p}\mathcal{V})^{\dagger}$ to the lift fluctuation on a stator blade at p × blade-passing frequency. In terms of the unsteady-lift response functions H_L' and K_L' referred to the leading edge,

$$L_{xp} \doteq \pi b_S \rho c M_x \tan\alpha_1 . \quad (H_L'/K_L' + V_S/U_S)(K_L' U_S)_p \tag{28}$$

where U_S, V_S are the longitudinal and upwash components of the rotor-wake velocity perturbation entering the stator. Figure 6.3 gives the following relations between velocity components:

$$U_S = U \frac{\cos(\beta_2+\alpha_1)}{\cos \beta_2} \; ; \; V_S/U_S = -\tan(\beta_2 + \alpha_1). \tag{29}$$

For reduced frequencies $|n| > 1$, the unsteady-lift response functions may be approximated by

$$|K_L'|^2 \doteq \frac{1}{2\pi|n|} \; ; \; H_L'/K_L' \doteq \phi_S \text{ (frozen gust convected over stator blade)} \tag{30}$$

where

$$n = \pi p \frac{b_S}{d_R} \frac{M_t}{M_S} = \pi p \frac{b_S}{d_R} (t_1 + t_2) \cos \alpha_1 . \tag{31}$$

Combining equations (27) through (31) with equation (11) for U_p gives

---

† Made up of contributions from the (p, s) and $(-p, -s)$ interactions.

(b) $$\frac{I_{ps}}{\rho c^3} \doteq \frac{K_w}{16}\,\frac{V}{|p\beta}\;\pi_R^{\,2}\sigma_S M_x^{\,4}(t_1+t_2)^{-1}\;\frac{\sin^2(\beta_2+\alpha_1)\sin^2\alpha_1}{\cos^2\beta_2\;\cos^3\alpha_1}\left[\phi_S\cot(\beta_2+\alpha_1)-1\right]^2. \tag{32}$$

(c) Interaction of rotor and stator wake profiles:

Interaction of the p th harmonic component of the rotor wake pattern with the sth spatial harmonic of the stator wake gives a quadrupole source distribution

$$(\overline{S}_{xx})_{ps} = 2\int_{x_S}^{\infty} U_p\,U_s\,dx \quad \text{(retarded time neglected)} \tag{33}$$

over the stator disk. The axial variation of U_pU_s may be represented approximately by a complex wavenumber K (see rotor wake description, equation (13).

$$U_pU_s \propto e^{iKx} \;;\quad (x > x_S)$$

$$\text{Re } K \doteq k_p(t_1+t_2) \quad (\text{using } k_s \doteq k_p \text{ and } \tan\alpha_2 \doteq \tan\alpha_1),$$

$$\text{Im } K \sim (1/b_{xR} + 1/b_{xs}). \tag{34}$$

Since $(k_p\,b_x)^2 \sim (2\pi)^2$ is a large quantity, the exact value of Im K has little effect on the modulus of the source integral. Thus

$$|\overline{S}_{xx}|^2_{ps} = \left|\frac{2i}{K}\,(U_pU_s)_S\right|^2$$

$$\doteq \frac{4}{k_p^2}\,(t_1+t_2)^{-2}\,c^4K_w\cdot\frac{1}{16}\,\pi_R^2\pi_S^2M_x^4, \tag{35}$$

where the wake description in terms of pressure-loss coefficients has been used, and K_w allows for the decay of the rotor wake before it reaches the stator. The sound intensity follows from Section 4.3.3; combining the (p,s) and $(-p,-s)$ interactions gives

$$\frac{I_{ps}}{\rho c^3} \doteq \frac{1}{2}\,\frac{\omega^2}{c^6}\,|\bar{S}_{xx}|^2_{ps} \qquad (\omega = cM_t\,k_p),$$

i.e.

$$\text{(c)} \qquad \frac{I_{ps}}{\rho c^3} \doteq \frac{K_w}{8}\,\pi_R^2\pi_S^2 M_x^6 \quad . \tag{36}$$

Although this result is apparently independent of harmonic number $|p|$, it will generally overestimate the higher harmonics, for which the wakes can no longer be regarded as delta functions.

(d) Interaction of rotor wakes with stator potential velocity field:

The dominant source is again the axial quadrupole $Q_{xx} = v_x v_x$, with one velocity factor derived from the rotor wake and the other from the stator potential field. The axial wavenumber of the source distribution either side of the stator - - for the U_p wake component and the U_s potential velocity component - - is given by

$$\text{Re } K \doteq k_p \tan\beta_2 \qquad (p > 0) \;;$$

$$|\text{Im } K| = k_s + O(1/b_{xR}) \doteq k_p \quad \begin{matrix}\text{(positive downstream of stator,}\\ \text{negative upstream).}\end{matrix} \tag{37}$$

If the source distribution is integrated on the upstream side of the stator only, the resultant source strength is given by

$$|\overline{S}_{xx}|^2_{ps} \doteq \left|\frac{2i}{K}(U_p U_s)_S\right|^2 \quad (\text{provided } k_p \overline{x} > 1)$$

$$= \frac{4c^4}{k_p^2 \sec^2\beta_2} \left|\frac{U_p}{c}\right|^2_S \left|\frac{\overline{U}_s}{c}\right|^2 \quad . \qquad (38)$$

The omission of the downstream contribution from (38) may be justified on the grounds that for a high-solidity stator, the pressure field downstream of the trailing edge will be weak compared with that upstream of the leading edge†. On the other hand if $\sigma_S << 1$, equation (38) should be multiplied by $\left|1 + e^{2i\beta_2}\right|^2 = 4\cos^2\beta_2$ to allow for the downstream contribution (as follows from (37) and the continuity of U_s through the stator disk in this case, where the velocity is that due to stator loading).

In the high-solidity case, the stator potential velocity $\overline{U}_s$ is given by equation (7), while the rotor wake is specified by section 6.1.2. Substitution in (38) gives the sound intensity associated with each interaction mode as in (36),

i.e.

(d) $$\frac{I_{ps}}{\rho c^3} \doteq \frac{K_w}{16} \frac{V}{|B|} \pi^2 \phi_R^2 \phi_S^2 \sigma_S M_x^6 (t_1 + t_2)^2 \frac{\cos^2\beta_2}{\cos^2\alpha_1} \quad . \qquad (39)$$

6.2.3 Entropy Wake Interaction Mechanisms

In view of the restriction to low Mach numbers, only the lowest-order source of each type (in terms of M_x dependence) will be considered here.

† This still leaves the pressure field actually within the stator row unaccounted for.

The present model provides two types of rotor-stator interaction which involve entropy wakes, as shown by the table in Chapter 5.

(Entropy/stator pressure field:) source term $Q^{(0)} = -\frac{1}{C_p \rho}\left(\frac{\partial^2 s'}{\partial x_i^2}\, p'\right)$ (40)

(Entropy/stator loading:) source term $Q^{(0)} = -\frac{1}{C_p}\left(\frac{\partial s'}{\partial x_i}\, g_i\right)$. (41)

The sound output from each of these mechanisms is estimated below, assuming a stator solidity of order 1 or more.

(e) Entropy wake/stator pressure field interaction:

An analysis exactly parallel to the velocity wake case gives, from (40) above,

$$\left|\bar{S}^{(0)}\right|^2_{ps} \doteq c^4 k_p^2 \sec^2\beta_2 \left|\frac{T_p}{T}\right|^2_S \left|\frac{\bar{P}_s}{\rho c^2}\right|^2 \qquad (42)$$

where, as before, only the contribution from upstream of the rotor has been included. Substituting for T_p (from equation 16) and $\bar{P}_s$ (from equation 6) gives the interaction source amplitude, in terms of the coefficients θ_R and ϕ_S.

Finally, the sound intensity associated with each interaction mode follows from

$$\frac{I_{ps}}{\rho c^3} \doteq \frac{1}{2\omega^2 c^2} \left|\bar{S}_{ps}\right|^2; \qquad (43)$$

thus

(e) $$\frac{I_{ps}}{\rho c^3} \doteq \frac{K_w}{16}\frac{V}{pB}\,\theta_R^2 \phi_S^2 \sigma_S M_x^2\, \frac{(t_1 + t_2)^{-2}}{\cos^2\beta_2 \cos^4\alpha_1} \quad . \qquad (44)$$

(f) Entropy wake/stator loading interaction:

Since in this case the source distribution is confined to the stator blades, it is convenient to integrate first over each blade section to obtain a line source distribution.† The stator row is then regarded as a series of line sources, whose relative phase must be taken into account when the spatial harmonic components of the source distribution are calculated. (Compare the representation of rotor and stator by fluctuating line forces, in mechanisms (a) and (b) respectively.)

Integration over a blade section gives, from (41),

$$\int_{\substack{\text{blade}\\ \text{section}}} Q^{(0)}\, dS = A = -\, C_p^{-1} \int (\partial s'/\partial x_n)\, g_n\, dS, \qquad (45)$$

where subscript n denotes the component in the lift direction (normal to the stator chord). The entropy perturbation can be expressed in terms of the temperature perturbation using equation (14), and Figure 6.3 gives the angle between the stator lift direction and the rotor wake normal as $(\beta_2 + \alpha_1)$. Thus the contribution from the p th harmonic component of the rotor wake is

$$A_p = -\frac{ik_p}{T}\,\frac{\cos(\beta_2+\alpha_1)}{\cos\beta_2} \int_{\substack{\text{blade}\\ \text{section}}} T_p\, g_n\, dS \qquad (p > 0)$$

$$= -\frac{ik_p}{T}\,\frac{\cos(\beta_2+\alpha_1)}{\cos\beta_2\cos\alpha_1} \cdot \tfrac{1}{2}\, b_S c M_x \int_{-1}^{1} T_p\, k(\xi)\, d\xi\ ; \qquad (46)$$

† The chordwise loading distribution is assumed compact in terms of the radiated sound wavelength.

here $k(\xi)$ is the steady-state circulation distribution† over the stator chord, and ξ is the chordwise coordinate normalized by half the blade chord.

The integral in (46) is of the same form as the unsteady-lift integral for longitudinal gust velocities. It may therefore be expressed in terms of the response function $H_L(n)$, where $n = \omega b_S/2cM_S$ is the stator reduced frequency††.

$$\int_{-1}^{1} T_p \, k(\xi) \, d\xi \doteq \frac{2\pi c M_x}{\cos\alpha_1} H_L'(n) \cdot (T_p)_S, \quad (H_L' \text{ referred to leading edge}). \tag{47}$$

An approximation valid for the present model ($n^2 >> 1$) is

$$|H_L'(n)|^2 \doteq \phi_S^2/2\pi|n|. \tag{48}$$

Finally, the spatial harmonic components, $\propto \exp i(pB + sV)\theta$, of the source distribution in the stator disk are given by

$$\bar{S}_{ps}^{(0)} \doteq A_p/d_S. \tag{49}$$

The sound intensity produced by this mechanism follows from equations (43) and (46) through (49), with the temperature perturbation entering the

---

†In (46), the integral over the blade thickness has been estimated holding T_p constant: $\int g_n \, dx_n$ = (1/ρ) × (pressure difference across blade) = k × (free-stream velocity).

†† Here, as for velocity wakes, the wake pattern is taken as being convected with the free-stream velocity, i.e. $q = n$.

stator given by (16). Thus for each interaction mode above cutoff,

$$(f)\quad \frac{I_{ps}}{\rho c^3} = \frac{K_w}{4}\,\frac{V}{|p|B}\,\theta_R^2\phi_S^2\sigma_S M_x^2\,(t_1+t_2)^{-3}\,\frac{\cos^2(\beta_2+\alpha_1)}{\cos^2\beta_2\,\cos^5\alpha_1}. \qquad (50)$$

In fans and compressors, entropy variations associated with the rotor wakes may be estimated on the assumption that the pressure and stagnation enthalpy are uniform. The parameters θ_R and π_R are then related by (18), and equations (44) and (50) become

Isoenergetic wakes

$$(e)\quad \frac{I_{ps}}{\rho c^3} \doteq (\gamma-1)^2\,\frac{K_w}{64}\,\frac{V}{|p|B}\,\pi_R^2\phi_S^2\sigma_S M_x^6\,\frac{(t_1+t_2)^{-2}}{\cos^6\beta_2\,\cos^4\alpha_1}, \qquad (51)$$

$$(f)\quad \frac{I_{ps}}{\rho c^3} \doteq (\gamma-1)^2\,\frac{K_w}{16}\,\frac{V}{|p|B}\,\pi_R^2\phi_S^2\sigma_S M_x^6\,(t_1+t_2)^{-3}\,\frac{\cos^2(\beta_2+\alpha_1)}{\cos^6\beta_2\,\cos^5\alpha_1}. \qquad (52)$$

These results may be compared with mechanism (d), equation (39).

6.3 CONCLUSIONS

(a) From the results given in section 6.2, the discrete-frequency sound power output of a subsonic rotor-stator stage can be estimated in terms of steady-flow operating parameters.

Six different mechanisms are identified as being significant.

(b) For interaction between a stator and downstream rotor, mechanisms (a) through (f) of section 6.2 are modified as follows:

B,V interchanged; also subscripts R,S

$\beta_2 \rightarrow -\alpha_2$ $(t_2 \rightarrow \tan \alpha_2)$; $\alpha_1 \rightarrow -\beta_1 (t_1 \rightarrow \tan \beta_1)$

Harmonic number $p \rightarrow pB/V$.

(c) The results are quoted in the form of sound intensity per propagating mode. The number of such modes, for a given blade-passing harmonic, depends on the interacting blade and vane numbers and the rotor tangential Mach number; it is not likely to be large†, but may be zero - - in which case the sound power is still finite, but the present results do not apply.

(d) The model on which the estimates are based is two-dimensional and assumes low Mach number flow. The sound power results are therefore expected to become inaccurate at low hub-tip ratios and Mach numbers approaching 1. In addition, the estimates for higher harmonics ($|p| > 1$) will be less accurate than that for the fundamental blade-passing frequency.

(e) In fans and compressors at sufficiently low Mach numbers, the

†For example, if $M_t < 0.5$ and $V > \frac{1}{2}B$, not more than two modes can propagate at blade passing frequency.

dominant mechanisms of tone generation are those associated with lift fluctuations on one of the blade rows (sound power per mode $\propto M_x^4$). The relative significance of pressure field interaction (mechanism a) and velocity wake interaction (mechanism b) depends largely on the blade-row separation; if the separation is large enough, mechanism (b) will always predominate.

(f) The effect on mechanism (b) of lift fluctuations due to longitudinal gusts is generally to increase the sound output from a rotor-stator stage.† However, as Horlock [53] has pointed out, the longitudinal and upwash contributions are able to cancel for an IGV stator followed by rotor: the condition is

$$\phi_R \cot(\alpha_2 + \beta_1) = 1.$$

(g) In turbines, the presence of temperature gradients in the flow entering a blade row leads to additional sound generation (mechanisms e,f). Estimation of the sound output requires a knowledge of wake temperature profiles.

(h) Finally, although explicit results are derived only for discrete-frequency sound, each of the wake interaction mechanisms (b) through (f) can give rise to broadband sound if the steady wake pattern is replaced by a randomly fluctuating flow entering either rotor or stator.

---

†Specifically, if $\beta_2 + \alpha_1 > \frac{1}{2}\pi$, the sound is increased; otherwise it is decreased.

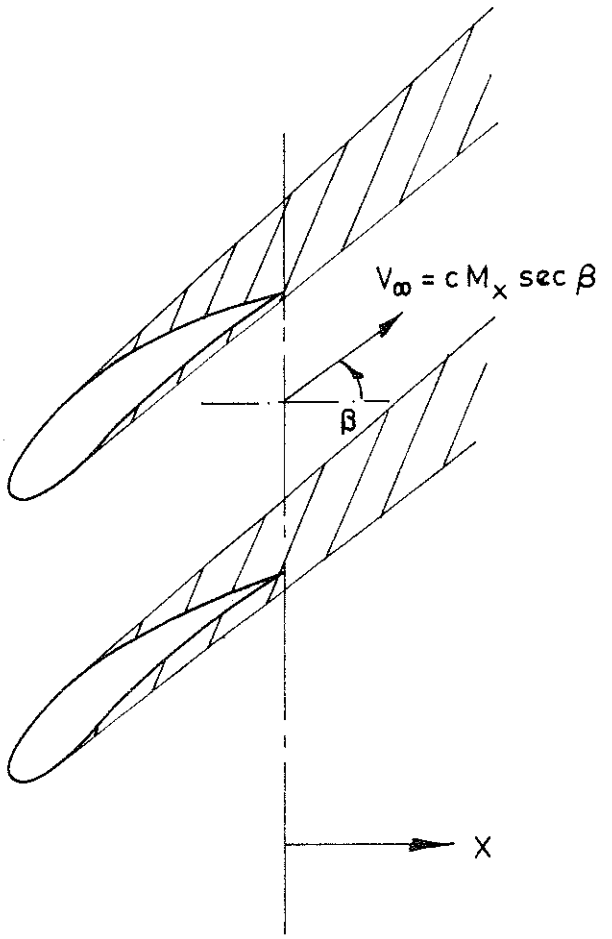

Fig. 6.1 Rotor wakes.

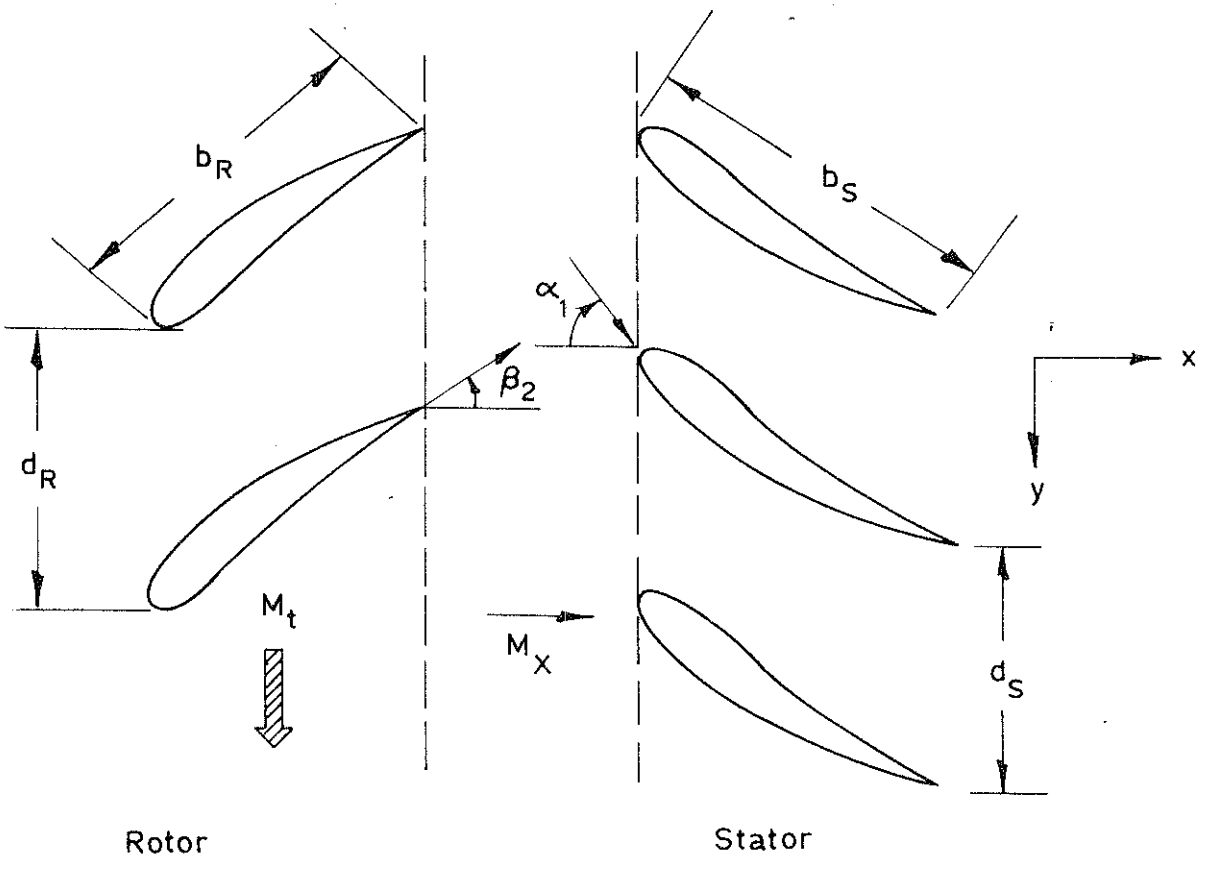

Fig. 6.2 Rotor-stator stage.

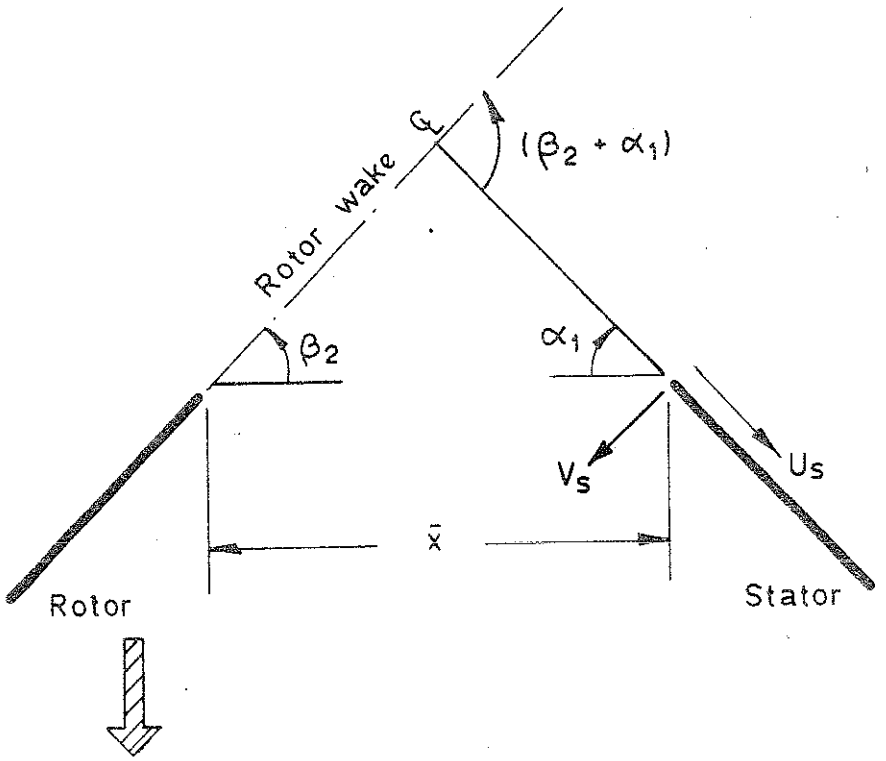

Fig. 6.3 Wake interaction geometry.

CHAPTER 7

SOUND OUTPUT FROM A SUBSONIC ROTOR OPERATING IN UNIFORM MEAN FLOW

A rotor can generate blade-passing tones in at least three different ways apart from the rotor-stator interaction mechanisms discussed in the previous chapter. These are

(a) Interaction with low-frequency turbulence in the incident flow;

(b) Radiation from the steady blade loading and thickness at subsonic speeds;

(c) Shock-wave radiation at supersonic speeds.

The present chapter is concerned with (a) and (b); radiation from a supersonic rotor is studied in Chapter 8.

Strictly, the frequency spectrum associated with mechanism (a) is not discrete, but consists of a series of narrow peaks at the blade-passing harmonics. The width of the spectral peaks depends on the bandwidth of the incident turbulence, and in the analysis which follows the latter will be assumed small compared with the blade-passing frequency.

Similarly, if the rotor blades are unevenly spaced around the disk, the radiated spectrum will not be confined to the blade-passing harmonics but will contain other multiples (n) of the disk rotational frequency. This is particularly important, for different reasons, in mechanisms (b) and (c).

In case (b), the radiation efficiency of a subsonically rotating pattern falls off rapidly with increasing n. It follows that multiples $n < B$ which are weakly present in the source spectrum may radiate as much sound as the blade-passing component ($n = B$).

In the supersonic case (c), the decay rate associated with a repeated shock pattern is less for widely-spaced shocks than for closely-spaced shocks. This suggests that low-order multiples ($n < B$) corresponding to blade nonuniformity will again be accentuated, in terms of radiated power, relative to the blade-passing frequency.

The following analysis and Chapter 8 assume a rotor with identical equally-spaced blades, the aim being to estimate the blade-passing harmonic content of the sound power spectrum for each of the three mechanisms. A fourth possible mechanism, in which turbulent boundary layers on each blade contribute to the low-frequency loading fluctuations, is similar in some respects to mechanism (a) and will not be considered here.

7.1 INTERACTION OF A ROTOR WITH LOW-FREQUENCY TURBULENCE

Turbulent velocity fluctuations incident on a subsonic rotor will generate sound in exactly the same way as the velocity wake profiles described in Chapter 6. The following assumptions will be made in order to estimate the sound output.

(a) The turbulent velocity spectrum is confined to frequencies less than M_t times the blade-passing frequency.

(b) $M_t^2 << 1$.

(c) The rotor disk is large compared with the wavelength of the radiated sound.

Within these limitations, the spectrum of the radiated sound may be approximated by a series of discrete frequencies, and a criterion analogous to cutoff determines the range of turbulence wavenumbers which contribute to the radiation at a particular frequency:

$$(k_p \pm k_y)^2 + k_z^2 < \left(\frac{\omega}{c}\right)^2 \quad , \quad (k_p = 2\pi|p|/d_R) \ . \tag{1}$$

Here k_y (tangential) and k_z (radial) are the turbulence wavenumber components in the rotor disk. The left-hand side of (1) is therefore a two-dimensional approximation to the square of the source wavenumber, where the source arises from interaction between the p^{th} harmonic component of the rotor field (wavenumber components $\pm k_p, 0$) and the turbulent velocity field (k_y, k_z).

7.1.1 Analogy with periodic-wake theory

Components of the turbulence (k_y, k_z) spectrum which satisfy condition (1) are equivalent to the wake harmonic components considered in Chapter 6, in that the resulting source pattern has a high radiation efficiency. It was assumed in Chapter 6 that the wake velocity decayed slowly in the streamwise direction, and a corresponding assumption will be made in the present analysis:

(d) The streamwise length scale of the turbulence is large enough for turbulent velocities to remain well-correlated, over a streamwise separation of up to a blade space.

The validity of this assumption is assured in practice by (a) and (b) above.

It follows under these conditions that the analysis of Chapter 6 for low-Mach-number interaction with a periodic velocity wake may be applied directly to the present problem, provided the mean square axial wake velocity in the sinusoidal case is replaced by

$$\iint F_u\,(k_y,k_z)\,dk_y\,dk_z \quad . \tag{2}$$

Here F_u is the (k_y,k_z) spectrum of the axial turbulent velocity component (u), and the integration is between the limits set by condition (1). The contribution of non-axial velocity perturbations is neglected, as in Chapter 6.

7.1.2 Evaluation of the wavenumber integral

Viewed as a restriction on k_y for given k_z, (1) gives (for $k_y > 0$)

$$|k_y - k_p| < \left[\left(\frac{\omega}{c}\right)^2 - k_z^2\right]^{\frac{1}{2}} \quad , \qquad \left(|k_z| < \frac{\omega}{c}\right) \quad . \tag{3}$$

If $\left(\frac{\omega}{c}\right)^2 \ll k_p^2$ (i.e. $M_t^2 \ll 1$), the integral over k_y for a given k_z may be approximated by

$$F_u(k_p,k_z).\quad \Delta k_y \tag{4}$$

(see Fig. 7.1).

The wavenumber spectrum is assumed in the form

$$F_u(k_y,k_z) = \frac{\langle u^2\rangle}{\pi^2} \cdot \frac{\ell_y \ell_z}{(1+k_y^2\ell_y^2)(1+k_z^2\ell_z^2)} \quad , \tag{5}$$

corresponding to a spatial cross-correlation coefficient ($\tau=0$) of $e^{-\ell_y^{-1}|\eta|} \times e^{-\ell_z^{-1}|\zeta|}$. The length scales ℓ_y, ℓ_z are left unspecified at this stage.

With this model of the turbulence, the k_y integration in (2) gives approximately, from (3) and (4),

$$\int F_u(k_y,k_z)\, dk_y \doteq \frac{2\langle u^2\rangle}{\pi^2} \cdot \frac{\ell_y \ell_z}{1+k_p^2\ell_y^2} \cdot \frac{2\left[\left(\frac{\omega}{c}\right)^2 - k_z^2\right]^{\frac{1}{2}}}{1+k_z^2\ell_z^2} \quad ; \qquad (6)$$

note that contributions from $k_y \sim -k_p$ are included in (6), as well as from $k_y \sim k_p$.

The second integration, over k_z, is simplified by substituting

$$\left.\begin{aligned} k_z &= \frac{\omega}{c}\sin\theta \\ dk_z &= \frac{\omega}{c}\cos\theta . d\theta \end{aligned}\right\}; \text{ range of integration } \theta = -\frac{\pi}{2} \text{ to } \frac{\pi}{2} . \qquad (7)$$

Thus

$$\iint F_u(k_y,k_z)\, dk_y\, dk_z = \frac{4}{\pi^2}\langle u^2\rangle \cdot \left(\frac{\omega}{c}\right)^2 \frac{\ell_y \ell_z}{1+k_p^2\ell_y^2} \cdot \int_{-\frac{\pi}{2}}^{\frac{\pi}{2}} \frac{\cos^2\theta .\, d\theta}{1+\left(\frac{\omega\ell_z}{c}\right)^2 \sin^2\theta} \quad . \qquad (8)$$

Evaluating the θ integral in (8) leads to the final result

$$\iint F_u\, dk_y\, dk_z = \frac{4}{\pi}\langle u^2\rangle \frac{\ell_y/\ell_z}{1+k_p^2\ell_y^2} \left\{\left(1+\frac{\omega^2\ell_z^2}{c^2}\right)^{\frac{1}{2}} - 1\right\} . \qquad (9)$$

The expression above represents that part of the turbulent-velocity wave-number spectrum which interacts with the p^{th} spatial harmonic of the rotor

field to produce radiating acoustic waves. It is therefore the equivalent in the wake interaction problem of $2|U_s|^2$, where U_s is the s^{th} spatial harmonic of the wake velocity field entering the rotor.

Equation (9) may be written in terms of the dimensionless parameters

$$k_p \ell_y = 2\pi |p| \frac{\ell_y}{d_R} \quad ,$$

and

$$k\ell_z = \frac{\omega \ell_z}{c} \quad .$$

Since $\frac{k}{k_p} = M_t$, it follows that

$$\iint F_u \, dk_y \, dk_z = \frac{4}{\pi} \langle u^2 \rangle \, M_t \, \frac{k_p \ell_y}{1+k_p^2 \ell_y^2} \cdot \frac{(1+k^2\ell_z^2)^{\frac{1}{2}} - 1}{k\ell_z} \quad . \tag{10}$$

The functions of $k_p \ell_y$ and $k\ell_z$ appearing in (10) are sketched in Fig. 7.2. For $k_p^2 \ell_y^2 << 1$ and $k_p^2 \ell_z^2 << 3/M_t^2$, equation (10) reduces to

$$\iint F_u \, dk_y \, dk_z \doteq \frac{2}{\pi} \langle u^2 \rangle \, M_t^2 . k_p^2 \ell_y \ell_z \quad ; \tag{11}$$

while the largest possible value of (10) occurs when $k_p \ell_y = 1$ and $k_p^2 \ell_z^2 >> 3/M_t^2$, and is

$$\left(\iint F_u \, dk_y \, dk_z \right)_{max} = \frac{2}{\pi} \langle u^2 \rangle \, M_t \quad . \tag{12}$$

7.1.3 Estimates of sound power output

In the periodic interaction analysis of Chapter 6, the stator wake harmonic components U_s are represented by

$$\left|\frac{U_s}{c}\right|^2 = K_w \cdot \frac{1}{4}\pi_S^2 M_x^2 \quad . \tag{13}$$

It follows that the substitution

$$K_w\pi_S^2 \rightarrow \frac{2}{c^2M_x^2} \iint F_u \, dk_y \, dk_z \tag{14}$$

permits the stator-rotor interaction results of that chapter - in particular mechanisms (b), (c) and (d) - to be used for estimates of rotor noise generation in low-frequency turbulence.

Estimates are presented below for a rotor in an axial mean flow ($\alpha_2 = 0$), in the special case where the turbulence length scales in equation (5) are chosen to give maximum sound output at the $|p|^{th}$ harmonic of the blade-passing frequency. Equations (12) and (14) then give

$$K_w\pi_S^2 \rightarrow \frac{4}{\pi} \cdot I_{turb}^2 M_t \tag{15}$$

to be substituted in equations (32), (36) and (39) of Chapter 6; the dimensionless quantity $I_{turb} = \langle u^2\rangle^{\frac{1}{2}}/cM_x$ is the turbulence intensity in the axial flow entering the rotor.

The results for the three different mechanisms are:

Rotor lift fluctuations due to turbulence

$$\frac{I_p}{\rho c^3} \doteq \frac{1}{4\pi|p|} I_{turb}^2 \sigma_R M_R^5 \cos^2\beta_1 \sin^4\beta_1 (1-\phi_R \cot\beta_1)^2 \quad . \tag{16}$$

Interaction of turbulence with rotor wake pattern

$$\frac{I_p}{\rho c^3} \doteq \frac{1}{2\pi} I_{turb}^2 \pi_R^2 M_R^7 \cos^6\beta_1 \sin\beta_1 \quad . \tag{17}$$

Interaction of turbulence with rotor potential velocity field

$$\frac{I_p}{\rho c^3} \doteq \frac{1}{4\pi|p|} I_{turb}^2 \sigma_R \phi_R^2 M_R^7 \cos^2\beta_1 \sin^3\beta_1 \quad . \tag{18}$$

These equations give the sound intensity radiated to either side of the rotor, in a frequency band centred on the $|p|^{th}$ blade-passing harmonic. Equation (16) is based on unsteady airfoil theory for high reduced frequencies, while equation (18) is based on a high-solidity model of the rotor potential field; both approximations are valid provided $\exp 2\pi|p|\sigma_R \gg 1$, except that if σ_R is much greater than 1, the isolated-airfoil approximation to the unsteady lift will break down.

It is sometimes useful to express the sound output as a fraction of the power required to drive the rotor. This will be done for the turbulence-potential velocity interaction, which is a mechanism inevitably associated with the development of a steady lift on the rotor blades in turbulent flow. The acoustic efficiency

$$\eta_p = I_p / (\tfrac{1}{2}\pi\sigma_R \phi_R \rho c^3 M_R^3 \sin\beta_1 \cos\beta_1) \quad , \tag{19}$$

which compares the $|p|^{th}$-harmonic sound power and the rotor power associated with lift, is given by (18) as

$$\eta_p \doteq \frac{1}{2\pi^2|p|} I_{turb}^2 \phi_R M_R^4 \cos\beta_1 \sin^2\beta_1 \quad . \tag{20}$$

For example, a rotor running in "optimum-scale" turbulence of 2% intensity, with a relative Mach number $M_R = 0.7$ and the typical values $\phi_R (= C_L/\pi) = 1$,

$\cos\beta_1 \sin^2\beta_1 = \frac{1}{3}$, has an acoustic efficiency according to (20) of order 2.10^{-6} at blade-passing frequency. This is certainly the same order of magnitude as found experimentally [54] when care is taken to avoid rotor-stator interactions of the type described in Chapter 6, but definite conclusions cannot be drawn without knowing the turbulence properties.

7.2. SUBSONIC ROTOR: RADIATION FROM STEADY LOADING AND THICKNESS

A rotor placed in a steady uniform flow (*i.e.* free from turbulence) can still radiate a certain amount of sound power at multiples of the blade-passing frequency, even if the tip speed is less than the speed of sound. This is the situation considered in the present section.

An immediate consequence of the subsonic tip speed is that for a ducted rotor, each acoustic mode associated with the steady blade loading and thickness is below cut-off. The radiation of sound under these conditions is controlled by the three-dimensional nature of the rotor; a two-dimensional model, as used previously for modes above cut-off, would predict *zero* sound power below cut-off. In the following analysis, the radial variation of blade profile area and loading is assumed to take a particular form which leads to the idea of a quasi-two-dimensional model.

Further assumptions made in the analysis are that the mean flow is axial, and that the rotor solidity is low enough for a blade-line model to apply ($\pi|p|\sigma_R << 1$; *cf.* section 7.1.3). The theory of Chapter 4 is then used to derive, for this model, the equivalent source strength and radiated power due to both thickness and loading. To obtain corresponding estimates for the high-solidity case, it is simply necessary to multiply the equivalent source strength by a factor $(2/\pi^2|p|\sigma_R)^{\frac{1}{2}}$ and to locate the source plane at

the rotor leading edge, as indicated in section 6.1.1.

The sound power output from a rotor in a free field is obtained from the present analysis by setting the duct length equal to zero.

7.2.1 Quasi-two-dimensional model

The acoustic duct modes associated with the $|p|^{th}$ blade-passing harmonic of a B-bladed rotor have modal orders ($|p|B,n$), if the excitation is due to steady loading or thickness and the blades are evenly spaced.

Although the source pattern for a given harmonic $|p|$ will in general consist of several modes, with radial orders n = 0, 1, 2 etc., the total power radiated from a radially uniform distribution is controlled by the n = 0 mode if the rotational tip speed of the pattern is subsonic. This is proved in Appendix IV for the case of a circular source distribution, and is expected to remain valid for an annular distribution of any hub-tip ratio.

It is also shown in Appendix IV that the free-field sound power radiated from an annular source distribution with zero radial variation can be estimated quite simply, for subsonic rotation of the source pattern. Adoption of such a source distribution as a model for the rotor blade loading and thickness therefore has the following advantages:

(a) Simplified radiation calculation in the short-duct limit, for any hub-tip ratio;

(b) Decay of the rotor field in a finite duct can be estimated as for a pure n = 0 mode, since the more rapid decay of the higher radial modes has negligible effect on the sound power radiated from the end of the duct.

Spanwise distributions of steady loading and thickness along each rotor blade are accordingly assumed as follows:

$$\begin{aligned}
&\text{Cross-sectional area of blade profile} \propto \text{radius} && (\text{tip value} = a) \ ; \\
&\text{Axial (thrust) component of blade loading} \propto \text{radius} && (\text{tip value} = \ell_x) \ ; \\
&\text{Tangential (torque) component of blade loading} \propto (\text{radius})^2 && (\text{tip value} = \ell_\theta) \ .
\end{aligned} \tag{21}$$

Each of the blade-line distributions defined by (21) can be analysed spatially into a series of circumferential harmonic components proportional to $e^{im\theta}$ ($m=pB$). The equivalent acoustic source distribution (cf. Chapter 4) which corresponds to each $e^{im\theta}$ component is radially constant. The essential three-dimensional nature of the sound radiation is then accounted for in the radiation efficiency τ_m of each $e^{im\theta}$ source component, as calculated in Appendix IV.

While the above source description leads to a straightforward analysis in the case $M_x = 0$, the presence of a mean flow through the rotor complicates the situation, to the extent that a two-dimensional approximation to the sound field in the duct becomes desirable. Fortunately this is possible without much loss of accuracy, provided the approximation is based on rotor tip conditions[†], and the resulting two-dimensional (m,0) mode is assigned the radiation efficiency τ_m mentioned above.

[†]For large m values, such as are found with a multibladed rotor, the (m,0) duct-mode shape function is concentrated at the outer radius.

This last step is essentially a geometrical approximation, of the same type as was used in Chapter 6 for modes above cut-off. The only difference is that the two-dimensional model of Chapter 6 was based on mean-radius conditions, while the outer radius is used here - on the grounds that higher-order radial modes in the rotor duct now make negligible contribution to the radiated power, as compared with the (m,0) mode.

7.2.2 Blade thickness radiation

In terms of the quasi-two-dimensional model, the blade-section distribution given by (21) leads to a displacement distribution in the plane of the rotor of

$$d = \sum_q a\ \delta(y-y_q) \quad ; \tag{22}$$

here $y_q = y_o + q\ d_R$ is the tangential position of the q^{th} blade at time t, and the summation is over all blades.

The displacement per unit area given by (22) may be analysed into spatial Fourier components :

$$d = D_o + \sum_p D_p \qquad (p = \pm 1,\ \pm 2\ \underline{\text{etc.}}) \quad , \tag{23}$$

where

$$D_p = \frac{a}{d_R} \exp\ i(2\pi p y'/d_R) \qquad (y' = y-y_o) \quad ,$$

<u>i.e.</u>

$$D_p = \bar{D}_p\ e^{-i\omega t}\ e^{ik_y y} \qquad (\bar{D}_p = a/d_R) \quad . \tag{24}$$

In equation (24), $y_o = cM_t t$ relates the 0^{th} blade position at time t to the tip Mach number M_t of the rotor blades; the radian frequency is

$\omega = cM_t k_y$, and $k_y = 2\pi p/d_R$ is the wavenumber in the tangential direction (positive in the direction of blade motion).

The spatial Fourier components D_p are also normalized mode components ($m = pB$, $n = 0$) in the present two-dimensional model. The theory of Chapter 4 gives the equivalent source coefficient $\bar{S}_p$, corresponding to the mode coefficient $\bar{D}_p$, as

$$\bar{S}_p = -\left(\frac{1-\alpha M_x}{1-M_x^2}\right)^2 \omega^2 \bar{D}_p \qquad (x > x_s) \qquad (25)$$

for radiation to the +x side of the source plane. Equation (25) is based on the assumption that reflected waves on the -x side may be neglected, which is reasonable since all modes are below cut-off.

The axial wavenumber parameter α, estimated on a two-dimensional basis, is

$$\alpha = \left(1 - \frac{1-M_x^2}{M_t^2}\right)^{\frac{1}{2}} = i\,\frac{(1-M_R^2)^{\frac{1}{2}}}{M_t} \qquad (M_R < 1)\ , \qquad (26)$$

where

$$M_R = (M_t^2 + M_x^2)^{\frac{1}{2}} \qquad (27)$$

is the flow Mach number relative to the rotor tip. Finally, the sound intensity radiated in the +x direction at $|p|$ times blade-passing frequency is related to these quantities by

$$\frac{I_p}{\rho c^3} = \frac{1}{2}\,\frac{q_s}{|\alpha|}\,\frac{1}{\omega^2 c^2}\left|\frac{1-M_x^2}{1-\alpha M_x}\right|^2 |\bar{S}_p|^2 \ ; \qquad (28)$$

the p and -p source components have been combined to give equation (28), since the source distributions S_p, S_{-p} are identical.

In order to estimate the modal energy transmission coefficient q_s at the source plane, the theory of Chapter 4 is used to relate q_s to the value q_o at the duct opening.

$$\frac{q_s}{q_o} = K_p = \exp \frac{-2|\alpha| k\ell}{1-M_x^2} \qquad (\ell = \text{length of duct measured from source plane})$$

$$= \exp \left\{ \frac{-4\pi |p| \ell}{d_R} \cdot \frac{(1-M_R^2)^{\frac{1}{2}}}{1-M_x^2} \right\} \quad . \tag{29}$$

Physically, the factor K_p accounts for the decay of the sound field between the rotor plane and the end of the duct.

It remains to estimate the value of $q_o/|\alpha|$, which as a first approximation will be calculated from the zero-flow theory of reference 27 (equation 3.10). For frequencies <u>below</u> cut-off, this gives

$$\frac{q_o}{|\alpha|} = \frac{4\,\tau_o}{(1+|\alpha|\chi_o)^2 + (|\alpha|\tau_o)^2} \doteq 4 \times (\text{radiation efficiency of opening}) , \tag{30}$$

since $|\alpha|\tau_o$ and $|\alpha|\chi_o$ are small for frequencies below cutoff. The radiation efficiency of the duct opening, as mentioned earlier, is to be taken as the value calculated in Appendix IV for an m-cycle phase variation around the opening; thus

$$\frac{q_s}{|\alpha|} \doteq 4K_p\,\tau_m \; ; \quad m = pB \quad . \tag{31}$$

Equation (31) must be regarded as a tentative estimate of the transmission coefficient in the presence of axial flow, although it reduces to the correct value when $M_x \to 0$.

Combining equations (25) to (28) with (31) gives the sound intensity in the quasi-two-dimensional model as

$$\frac{I_p}{\rho c^3} \doteq 2K_p \tau_n \frac{\omega^2}{c^2} \left(\frac{a}{d_R}\right)^2 \left|\frac{1-\alpha M_x}{1-M_x^2}\right|^2 \qquad (n = |p|B)$$

$$= 8\pi^2 p^2 K_p \varepsilon_R^2 \sigma_R^4 \frac{M_R^2}{1-M_x^2} \tau_n \qquad (a = \varepsilon_R b_R^2) \; ; \tag{32}$$

the parameter ε_R is the mean thickness-chord ratio of the rotor blade tip section. Equation (32) gives the intensity in either direction from the rotor, since the factor $(1-M_x^2)^{-1}$ which accounts for axial Mach number effects is an even function of M_x.

In terms of the actual rotor dimensions (tip radius a_o, hub-tip ratio μ), Appendix IV gives the following zero-flow approximation to τ_n (noting $ka_o = nM_t$).

$$\tau_n \doteq \frac{2}{1-\mu^2} \frac{(nM_t)^{2n+2}}{(n+2)^2 (2n+1)!} \frac{n^{\frac{1}{2}M_t^2}}{(\frac{3}{4})^{2nM_t^2}} \qquad (M_t^2 << 1, \; \mu^{n+2} << 1).$$

This may be written as

$$\tau_n \doteq \frac{2}{1-\mu^2} F(n).\; G(n,M_t) \quad , \tag{33}$$

where

$$F(n) = (\tfrac{3}{4})^{2n} \; n^{2n+\frac{5}{2}} / (n+2)^2 (2n+1)! \tag{34}$$

is a slowly-varying function of n, plotted in Fig. 7.3, and

$$G(n,M_t) = \left[n^{-\frac{1}{2}} \left(\frac{4}{3}\right)^{2n} \right]^{1-M_t^2} M_t^{2n+2} \qquad (G=1 \text{ when } M_t=1) \qquad (35)$$

contains the dependence on tip Mach number M_t.

From equations (32) and (33), it follows that the $|p|^{th}$-harmonic sound power due to blade thickness, radiated in either direction from a ducted subsonic rotor, is approximately

$$\frac{W_p}{\rho c^3 S_o} \doteq 16\pi^2 p^2 K_p \epsilon_R^2 \sigma_R^4 M_R^2 (1-M_x^2)^{-1} FG \qquad (M_t^2 \ll 1), \qquad (36)$$

where $S_o = \pi a_o^2$ is the area of the complete rotor disk. It is interesting to note that the sound power is unaffected by the hub-tip ratio μ, provided (as assumed above) μ^{n+2} is negligible.

7.2.3 Steady blade loading radiation

Again in terms of the quasi-two-dimensional model, the blade-loading distribution given by (21) leads to a force distribution in the plane of the rotor of the form

$$f_i = \sum_q \ell_i \quad (y-y_q) \quad , \qquad (37)$$

where $\ell_i = (\ell_x, \ell_\theta)$ are the blade force components per unit span at the rotor tip.

Spatial Fourier analysis gives, as in the preceding section,

$$f_i = (F_i)_o + \sum_p (F_i)_p \qquad (p = \pm 1, \pm 2 \text{ etc.}) \qquad (38)$$

where

$$(F_i)_p = (\bar{F}_i)_p \; e^{-i\omega t} \; e^{ik_y y} \quad , \qquad (39)$$

and the Fourier coefficients are given by $(\bar{F}_i)_p = \ell_i/d_R$.

The acoustic source distribution equivalent to the above distribution of forces is found by the methods of Chapter 4. If the steady force on the blade is perpendicular to the relative flow direction (so that $\ell_x = \ell_R \sin\beta$, $\ell_\theta = \ell_R \cos\beta$ where ℓ_R is the resultant blade loading at the outer radius), the p^{th} harmonic component of the force distribution leads to a source coefficient $\bar{S}_p$ for which

$$\left|\bar{S}_p\right|^2 = \frac{1-M_R^2}{1-M_x^2} \frac{\ell_R^2}{M_t^2} \left(\frac{\omega}{\rho c d_R}\right)^2 \quad . \tag{40}$$

An argument exactly parallel to the preceding section gives the following estimate for the sound intensity in the quasi-two-dimensional model.

$$\frac{I_p}{\rho c^3} \doteq \frac{1}{2} K_p \sigma_R^2 C_{LR}^2 M_R^2 (1-M_R^2) \tau_n \quad . \tag{41}$$

Here C_{LR} is the steady lift coefficient at the rotor tip, defined by $\ell_R = \frac{1}{2} C_{LR} \rho c^2 M_R^2 b_R$. Equation (41), like (32), gives the intensity on either side of the rotor; the compressibility factor $(1-M_R^2)$ reduces the sound power equally in both directions.

If the radiation efficiency τ_n is estimated from equation (33) as before, it follows that the $|p|^{th}$-harmonic sound power due to steady blade loading, radiated in either direction from a ducted subsonic rotor, is approximately

$$\frac{W_p}{\rho c^3 S_o} \doteq K_p \sigma_R^2 C_{LR}^2 M_R^2 (1-M_R^2) FG \qquad \text{(pure lift, } M_t^2 << 1\text{).} \tag{42}$$

7.2.4 Comparison with previous work

Equation (42), which is the main result of section 7.2, applies to rotors in which the steady blade loading acts predominantly in the lift direction. While this is a reasonable assumption for an aerodynamically designed rotor, the only previous analytical result available for comparison is the expression given by Embleton [55], which refers to the opposite case of pure drag forces.

When the steady loading analysis of section 7.2.3 is repeated using the assumption that the blade forces are parallel to the relative flow direction (i.e. $\ell_x = -\ell_R' \cos\beta$, $\ell_\theta = \ell_R' \sin\beta$), an expression similar to (42) is found in which C_{LR} is replaced by the tip drag coefficient C_{DR}, and the compressibility factor $1-M_R^2$ no longer appears:

$$\frac{W_p}{\rho c^3 S_o} \doteq K_p \sigma_R^2 C_{DR}^2 M_R^2 FG \qquad \text{(pure drag, } M_R^2 << 1\text{).} \tag{43}$$

Embleton's result, on the other hand, is based on Gutin's calculation [56] of the sound field radiated from an unducted rotor, which involves two assumptions not made in the foregoing analysis:

(a) The mean flow through the rotor disk is neglected ($M_x = 0$) ;

(b) The distributed loading on each blade is replaced by a point force acting at an effective radius.

These lead to the following expression for the $|p|^{th}$-harmonic sound power radiated either side of the rotor plane (total power = $2W_p$), in terms of the total torque Q acting on the rotor; the effective radius is taken as the tip radius a_o (*c.f.* Appendix IV).

$$\frac{W_p}{\rho c^3 S_o} = \frac{Q^2}{8\pi^2\rho^2 c^4 a_o^6} \cdot \frac{n}{M_t} \bar{J}_{2n}(2nM_t) \qquad \text{(Embleton [55])}. \tag{44}$$

For the torque force distribution assumed in the present calculation (equation 21), Q is given by

$$Q = \frac{1}{4} \pi\sigma_R C_{DR} \rho c^2 M_t^2 a_o^3 (1-\mu^4) \qquad (M_x = 0) \quad . \tag{45}$$

Combining (44) and (45), and noting the approximation for $\bar{J}_{2n}(x)$ given in Appendix IV, shows that Embleton's expression for W_p based on the Gutin model differs by a factor

$$\frac{1}{64}(1-\mu^4)^2 \left(\frac{n+2}{1-\mu^{n+2}}\right)^2 \quad , \quad \doteq \left(\frac{n+2}{8}\right)^2 \text{ unless } \mu \text{ is close to 1}, \tag{46}$$

from the value given by equation (43) with no flow ($M_x = 0$) and zero duct length ($K_p = 1$).

There are two reasons for this discrepancy. First, the assumption of zero reflection, *i.e.* outgoing waves, on the backward side of the source in the ducted-rotor analysis becomes inaccurate as the duct length tends to zero. This accounts for the factor of $\frac{1}{4}$ which remains in (46) as the hub-tip ratio tends to 1.

Second, and more important for large values of $n = |p|B$, is the error involved in the effective radius assumption. As explained in Appendix IV, treating a uniform circular source distribution as a ring concentrated at the outer radius overestimates the sound power output by a factor $(1 + \frac{1}{2}n)^2$. This accounts for the remaining difference between the two calculations.

7.3 CONCLUSIONS

(a) At low values of relative Mach number M_R, a rotor operating in low-frequency turbulence as described in section 7.1 generates a tone power output proportional to M_R^5. The sound is generated by fluctuating blade forces. At the blade-passing frequency, the sound output can be as high as

$$\frac{W_1}{\rho c^3 S} \sim 10^{-2} I_{turb}^2 M_R^5$$

for turbulence length scales of the same order as the blade chord and $\sigma_R \sim 1$.

(b) If M_R^2 is not small, two other turbulence interaction mechanisms become of comparable importance. These are interaction of turbulence with the rotor wake pattern, and interaction with the rotor potential velocity field.

(c) The turbulence-potential velocity interaction mechanism has an acoustic efficiency proportional to M_R^4 and given by equation (20), for turbulence length scales of the same order as the blade chord

and $\sigma_R \sim 1$. This result for a subsonic rotor becomes invalid as M_R approaches 1. On the other hand the inverse Mach number dependence found for this mechanism by Ffowcs Williams and Hawkings [51] is based on an approximation which becomes invalid when M_R is less than 1, so the two estimates cover different ranges of operation.

(d) The sound power radiated from steady blade loading in the absence of turbulence is given by equation (42), for a rotor of low solidity. This may be compared with equation (18) for turbulent flow entering a high-solidity rotor, if (42) is divided by $\pi^2 |p| \sigma_R$ and (18) expressed in terms of rotor-tip (rather than mean-radius) conditions.† Putting $K_p = 1$ (zero duct length) gives the ratio, for any blade-passing harmonic, as

$$\frac{W_{dir}}{W_{turb}} = K \frac{G(n,M_t)/M_t^5}{(\tilde{u}_{turb}/u_{blade})^2} \qquad (M_R^2 \ll 1)$$

where the constant $K, \doteq \frac{16\pi F}{(1+\mu^2)(1-\mu^4)}$, is of order 1.

It follows that the factor

$$\left(\frac{G}{M_t^5}\right)^{\frac{1}{2}} = \left[n^{-\frac{1}{4}} \left(\frac{4}{3}\right)^n\right]^{1-M_t^2} M_t^{n-\frac{3}{2}} \qquad (M_t = \text{blade tip Mach number})$$

may be interpreted as the ratio of r.m.s. turbulent velocity to blade

---

† Equation (18) is a two-dimensional approximation and probably best evaluated at the r.m.s. rotor radius. Since the expression given varies approximately as (radius)^4 for a constant blade chord, it should be multiplied by $\left(\frac{1+\mu^2}{2}\right)^2$ if tip values of M_t etc. are to be used.

tip speed which makes the sound power W_{turb}, due to interaction with turbulence, roughly equal to the power W_{dir} radiated directl from the steady loading in smooth flow. A plot of $(G/M_t^5)^{\frac{1}{2}}$ as a function of M_t and rotational harmonic number n is given in Fig. 7.4.

(e) In smooth flow, the ratio of the sound power due to blade thickness and that due to blade loading is

$$\frac{W_p(\text{thickness})}{W_p(\text{loading})} \doteq 16\pi^2 p^2 \left(\frac{\varepsilon\sigma}{C_L}\right)^2_{\text{rotor tip}} \qquad (M_R^2 << 1).$$

It follows that thickness noise becomes relatively more important at high harmonics of the blade-passing frequency. On the other hand turbulence interaction noise tends in practice to overwhelm both these mechanisms as the rotational harmonic number n increases (Fig. 7.4).

(f) Compressibility effects introduce a factor $(1-M_x^2)^{-1}$ in the thickness noise estimate and a factor $(1-M_R^2)$ in the steady-loading noise estimate, for a subsonic rotor in smooth flow. The latter corresponds to the quadrupole correction introduced in [51], although the order-of-magnitude estimate given there is incorrect: the effect of the mean flow is actually to <u>reduce</u> the sound power radiated by steady lift forces on the rotor†.

---

†With steady <u>drag</u> forces there is no mean-flow effect, as equation (43) shows.

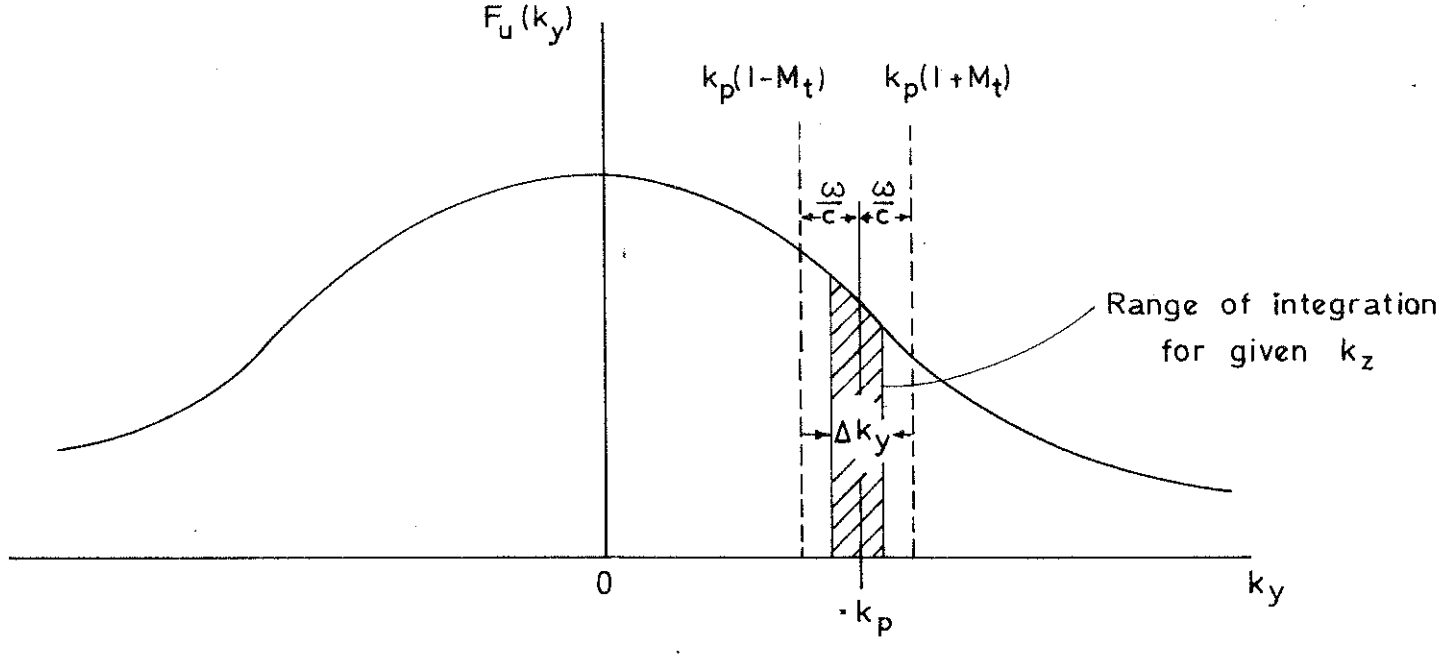

Fig. 7.1 Turbulence k_y spectrum.

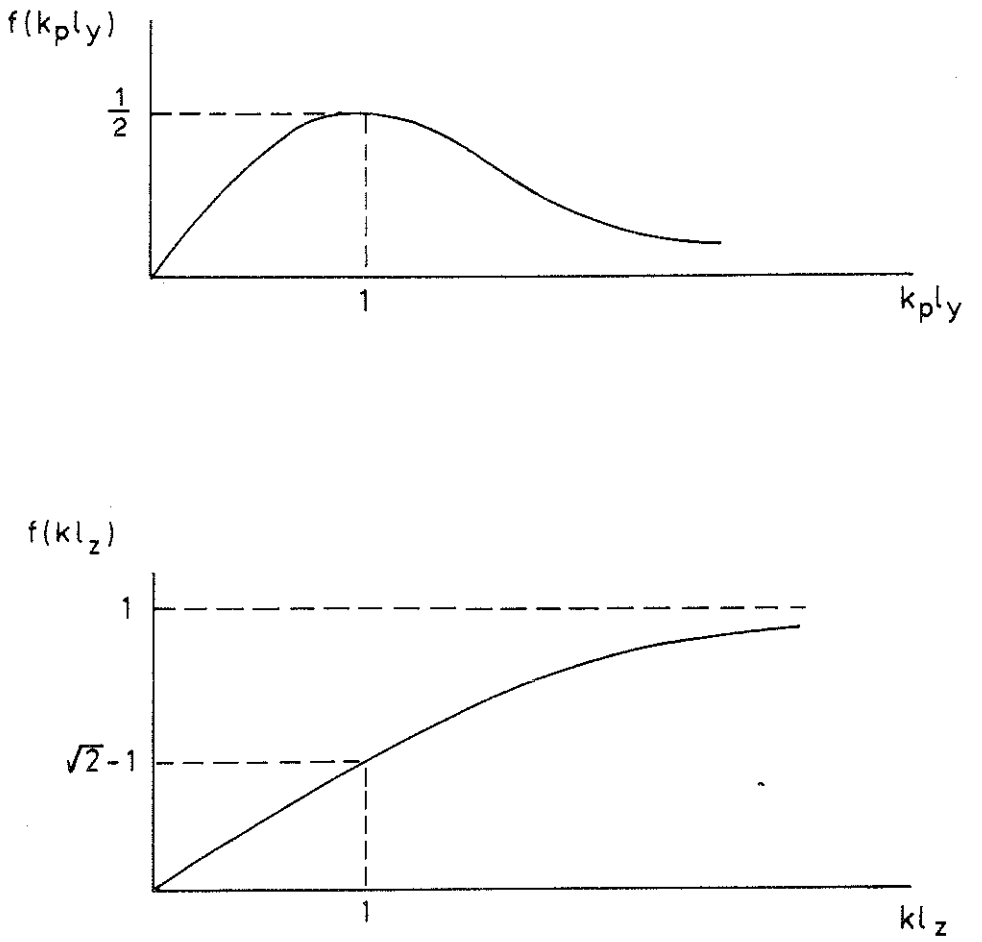

Fig. 7.2 Effect of tangential and spanwise length scales on wavenumber integral.

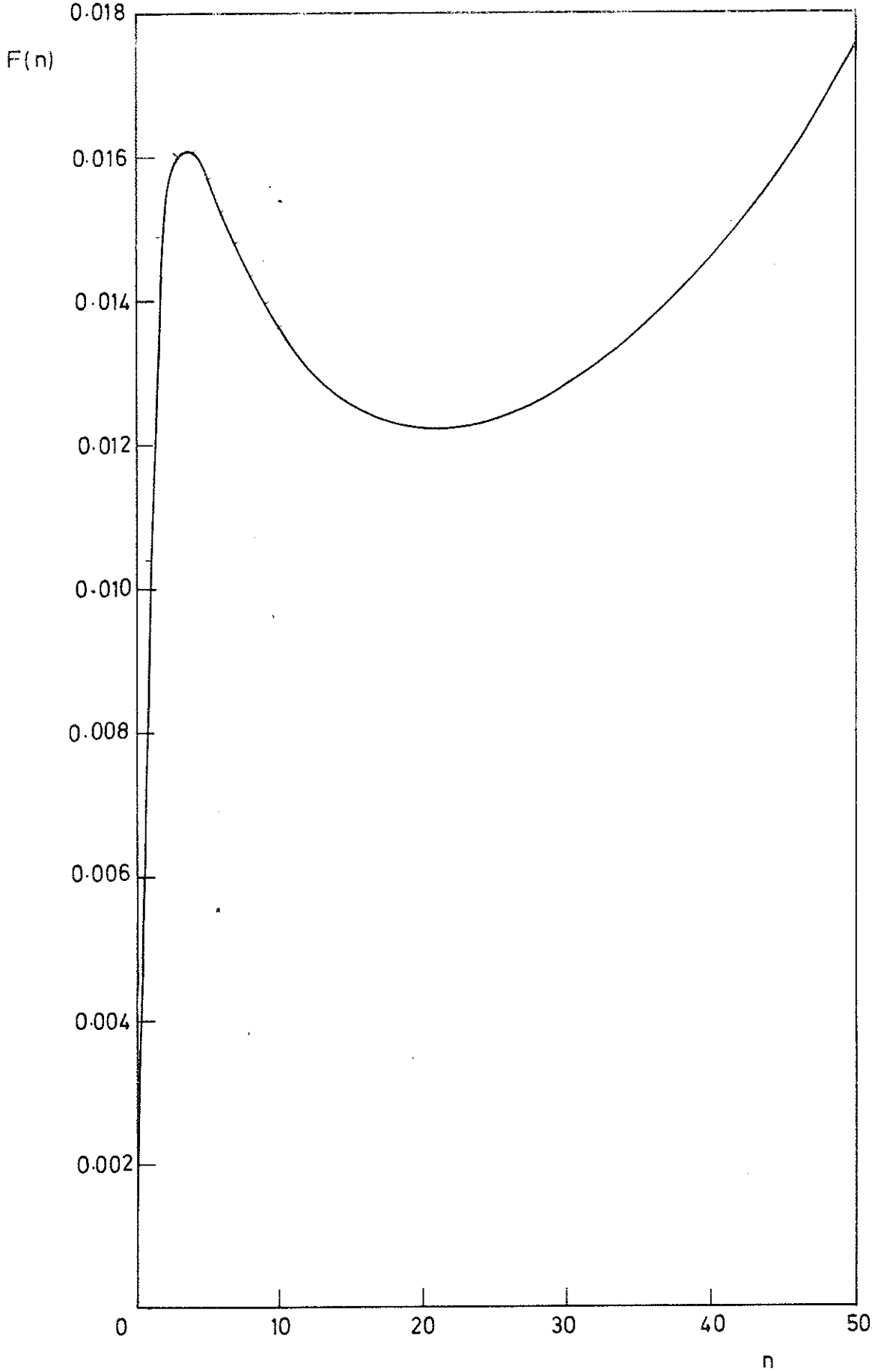

Fig. 7·3 The function $F(n) = \frac{(\frac{3}{4})^{2n}\, n^{2n+5/2}}{(n+2)^2 (2n+1)!}$.

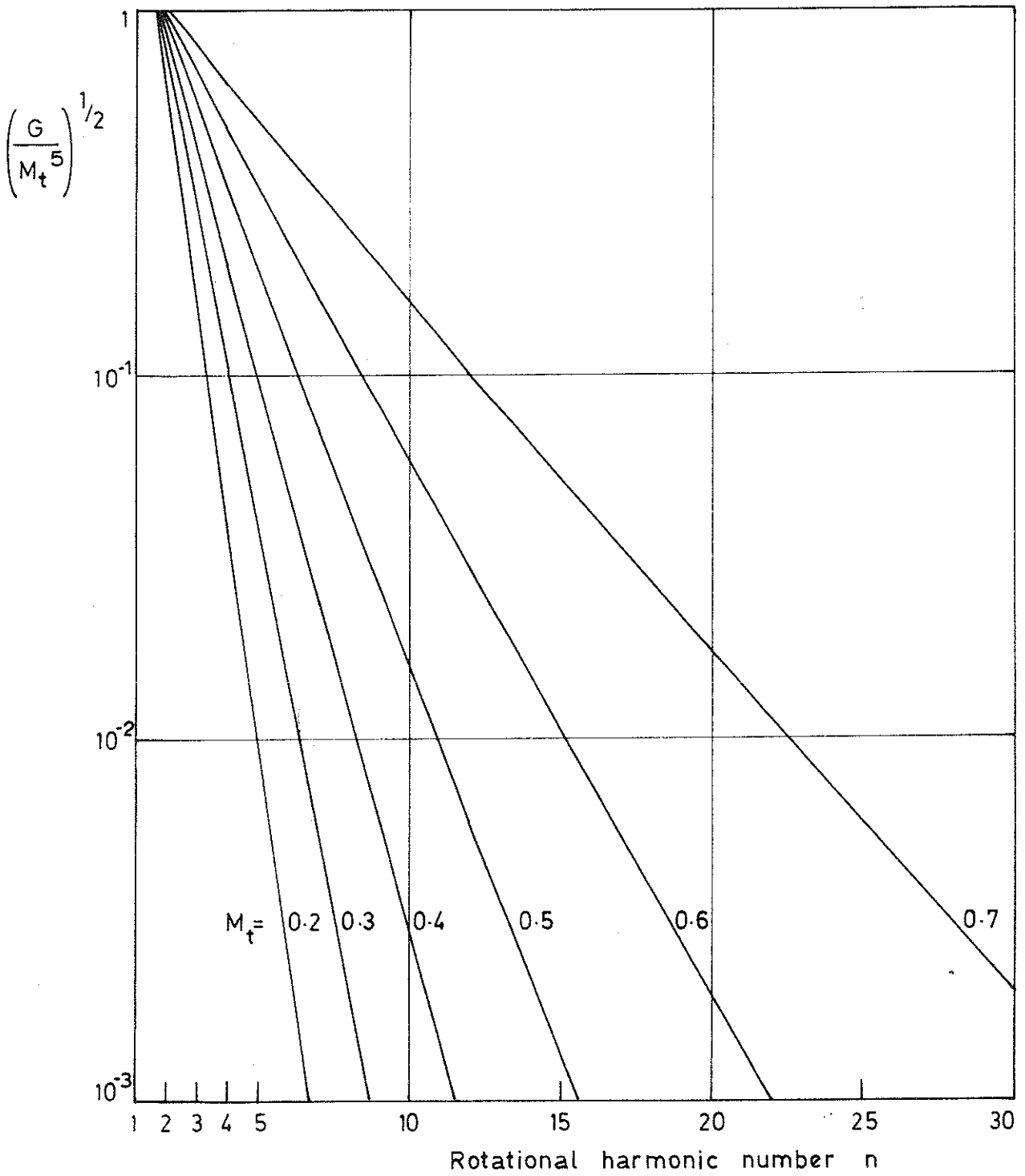

Fig. 7.4 Approximate intensity of optimum-scale turbulence which equalizes the turbulence-interaction sound power and direct sound power arising from steady rotor loading.

CHAPTER 8

SHOCK RADIATION FROM A SUPERSONIC ROTOR

Over the subsonic speed range considered in the preceding chapter, the pressure field of a ducted rotor decays rapidly with distance away from the rotor. It is possible to calculate the rotational speed above which this decay no longer occurs, by using the linearized theory of Chapter 4. What the linearized acoustic theory is unable to predict is the amplitude of the pressure field above the critical speed.

The aim of the following analysis is to estimate the rotor pressure field and sound power output under these conditions. Attention is restricted, as in Chapter 7, to the blade-passing harmonic content of the frequency spectrum; the rotor blades are accordingly assumed to be identical and equally spaced. As a further simplification, three-dimensional effects are neglected and the rotor with its duct replaced by a two-dimensional model. However, the equivalent two-dimensional rotor is arranged so that its pressure field propagates under the same conditions as the pressure field of the actual rotor.

8.1 EQUIVALENT TWO-DIMENSIONAL MACH NUMBER

The blade-passing pressure field of the actual rotor begins to propagate along the rotor duct, according to the linearized theory of Chapter 4, when

$$\frac{\omega}{c} = \frac{2\pi BN}{c} = k_{BO}\,(1-M_x^2)^{\frac{1}{2}}. \qquad (1)$$

In equation (1), N is the rotational speed of the rotor and k_{BO} is the cut-off wavenumber for the (m = B, n = 0) duct mode. For the fundamental blade-passing frequency of a B-bladed rotor, this is the lowest-order mode and is therefore the first to propagate as the speed is increased.

Equation (1) as it stands assumes axial flow in the rotor duct. If the duct contains a swirling flow, with solid-body rotation at angular velocity Ω in the rotor direction, a first approximation to the cut-off criterion is obtained from (1) by substituting

$$\omega \to (\omega - B\Omega), \qquad \underline{\text{i.e.}} \quad 2\pi N \to 2\pi N - \Omega. \tag{2}$$

In other words, the propagation relative to the swirl is unaffected by the swirl, for small swirl Mach numbers (cf. Appendix II). However, the mean flow is assumed to be axial in the following analysis.

The cut-off criterion (1) can be expressed in terms of an equivalent two-dimensional relative Mach number M_R, as

$$M_R = 1 \quad . \tag{2}$$

M_R is defined by the relation

$$M_R^2 = M_x^2 + (2\pi BN/ck_{BO})^2 = M_x^2 + \left(\frac{B}{g_o}\right)^2 M_t^2 \quad , \tag{3}$$

where M_t is the tip Mach number of the rotor blades, and $g_o = k_{BO}\, a_O$ is the dimensionless cut-off parameter for the (B,0) duct mode. In the limit as $\mu \to 1$ (two-dimensional rotor), $g_o \to B$ and M_R reduces to the

actual relative Mach number.†

In what follows, it is assumed that $M_R > 1$. Because according to linearized theory the blade-passing pressure field travels without attenuation along the rotor duct, and is of high amplitude close to the rotor, a dominant role is played by nonlinearity and shock formation. A simplified model of the rotor pressure field is therefore constructed in terms of repeated shock waves.

8.2 SHOCK AMPLITUDES UPSTREAM OF A SUPERSONIC ROTOR

Figure 8.1 showsa system of parallel shocks attached to the leading edge of a two-dimensional rotor. Because the shocks are non-uniform (being strongest near the rotor plane), they do not propagate in a truly one-dimensional manner. Nevertheless, the similarity is sufficiently close for one-dimensional theory to be illuminating.

The first-order theory of one-dimensional finite-amplitude waves [58, 59, 60] predicts that if a periodic waveform, of wavelength λ, has a sufficiently large initial amplitude to develop into a sawtooth shape within a distance x, its peak-to-peak amplitude at that distance is approximately

$$\frac{\Delta p}{p_o} = \left(\frac{2\gamma}{\gamma+1}\right) \frac{\lambda}{x} \qquad \text{(perfect gas, } \gamma \text{ constant).} \qquad (4)$$

Equation (4) sets an upper limit to the shock strength $\Delta p/p_o$ at distance x, regardless of the initial amplitude. It suggests that beyond a certain distance from the rotor leading edge, the shock strength will

†The significance of the (B,0) cut-off condition was pointed out by McCune [57] in the context of transonic flow through axial-compressor blade rows.

decay inversely with upstream distance, and will be insensitive to details of the blade shape and loading. A more detailed examination of the shock propagation, given below, supports the 1/x decay prediction; while comparison with experimental results indicates that shock amplitudes can be predicted, within a factor of 2, without knowing the blade profile geometry.

8.2.1 Two-dimensional analysis of shock propagation

Fig. 8.2 shows a sawtooth pressure waveform, assumed to be rotating with the rotor in the plane $x = x_s$ (starting plane). It is assumed in this analysis that the shocks are fairly weak and symmetrical about the mean pressure p_o, so that

(a) The shocks propagate relative to the mean flow at speed c_o normal to the shock front, corresponding to pressure p_o;

(b) Other points on the waveform propagate in the same relative direction, but with an additional velocity $\beta \frac{p-p_o}{\rho_o c_o}$; the coefficient $\beta = \frac{1}{2}(\gamma+1)$ for a perfect gas with γ constant (Appendix I).

Consider points P and Q on the initial waveform (Fig. 8.2). P will eventually overtake the shock ahead of it, and Q will be overtaken by the same shock. We wish to find at what distance upstream this occurs.

P starts at a perpendicular distance

$$\tfrac{1}{2}d_R \left[1 - \frac{2p'}{(\Delta p)_s}\right] \cos\phi \qquad (5)$$

from the shock front. The time taken to overtake the shock is therefore

$$t' = \frac{2}{\gamma+1} \cdot \frac{\rho_o c_o}{p'} \cdot \tfrac{1}{2} d_R \cos\phi \cdot \left[1 - \frac{2p'}{(\Delta p)_s}\right]$$

$$= \frac{\rho_o c_o}{\gamma+1} \cdot d_R \cos\phi \left[\frac{1}{p'} - \frac{2}{(\Delta p)_s}\right] \quad . \tag{6}$$

Similarly, point Q is overtaken after a time

$$t'' = \frac{\rho_o c_o}{\gamma+1} \cdot d_R \cos\phi \left[\frac{1}{p''} - \frac{2}{(\Delta p)_s}\right] \tag{7}$$

from starting at $x = x_s$.

The corresponding upstream distances x', x'' (from $x = x_s$) at which P and Q combine with the shock are given by

$$x' = c_o t'(\sin\phi - M_x) + \tfrac{1}{2} d_R \sin\phi \cos\phi \left[1 - \frac{2p'}{(\Delta p)_s}\right] \quad ; \tag{8}$$

$$x'' = c_o t''(\sin\phi - M_x) - \tfrac{1}{2} d_R \sin\phi \cos\phi \left[1 - \frac{2p''}{(\Delta p)_s}\right] \quad . \tag{9}$$

The first term is the distance travelled by the shock; the second term allows for the motion of P, Q relative to the shock.

We are concerned with the situation where P and Q <u>coincide</u> on meeting the shock. A necessary condition for this to occur is that

$$x' = x'' \quad ; \tag{10}$$

the other condition, that P and Q should arrive at the shock simultaneously, determines the departure-time interval at $x = x_s$ which is not required here.

Equations (8), (9) and (10) give

$$c_o(t''-t') \ (\sin\phi-M_x) = d_R \ \sin\phi \ \cos\phi \ \left[1 - \frac{p'+p''}{(\Delta p)_s}\right] \ ;$$

so from (6) and (7),

$$\frac{\rho_o c_o^2}{\gamma+1} \ (\sin\phi-M_x) \ (\frac{1}{p'} - \frac{1}{p''}) = \sin\phi \ \left[1 - \frac{p'+p''}{(\Delta p)_s}\right] \ . \qquad (11)$$

Equation (11) gives the required relation between p' and p''. If it is satisfied, the actual upstream distance may be taken as the average of the values x', x'' given by (8) and (9); i.e.

$$\bar{x} = \tfrac{1}{2}c_o(t'+t'') \ (\sin\phi-M_x) - \tfrac{1}{2}d_R \ \sin\phi \ \cos\phi . \ \frac{p'-p''}{(\Delta p)_s} \ ,$$

or, from (6) and (7),

$$\bar{x} = \frac{\rho_o c_o^2}{\gamma+1} \ d_R \ \cos\phi . (\sin\phi-M_x) \ \left[\frac{p'+p''}{2p'p''} - \frac{2}{(\Delta p)_s}\right] \ - \tfrac{1}{2}d_R \ \sin\phi \ \cos\phi . \ \frac{p'-p''}{(\Delta p)_s} \ . \qquad (12)$$

The substitutions

$$p'+p'' = \Delta p, \qquad p'-p'' = \delta p$$

give

$$p' = \tfrac{1}{2}(\Delta p+\delta p); \quad p'' = \tfrac{1}{2}(\Delta p-\delta p); \quad p'p'' = \frac{1}{4}\left[(\Delta p)^2-(\delta p)^2\right] \ . \qquad (13)$$

Equation (11) may therefore be written in terms of Δp and δp as

$$- \frac{\rho_o c_o^2}{\gamma+1}(\sin\phi-M_x) . \ \frac{4 \ \delta p}{(\Delta p)^2} \left[1 + \left(\frac{\delta p}{\Delta p}\right)^2 + \ldots\right] \ = \sin\phi \ . \left[1 - \frac{\Delta p}{(\Delta p)_s}\right] \ ,$$

i.e. if $\left(\frac{\delta p}{\Delta p}\right)^2$ is negligible compared with 1,

$$\frac{\delta p}{\Delta p} \doteq -\frac{\gamma+1}{4}\,\frac{\sin\phi}{\sin\phi - M_x}\left[1 - \frac{\Delta p}{(\Delta p)_s}\right]\frac{\Delta p}{\rho_o c_o^2} \quad . \tag{14}$$

Equation (14) shows that we are neglecting terms of order $\left(\frac{\Delta p}{\rho_o c_o^2}\right)^2$.

To the same accuracy, equations (12) and (14) give

$$\frac{\bar{x}}{d_R \cos\phi} \doteq \frac{\rho_o c_o^2}{\gamma+1}(\sin\phi - M_x)\left[\frac{2}{\Delta p} - \frac{2}{(\Delta p)_s}\right]$$

$$+ \tfrac{1}{2}\sin\phi \cdot \frac{\gamma+1}{4}\,\frac{\sin\phi}{\sin\phi - M_x}\left[1 - \frac{\Delta p}{(\Delta p)_s}\right]\frac{\Delta p}{(\Delta p)_s}\,\frac{\Delta p}{\rho_o c_o^2} \quad . \tag{15}$$

The above equation relates $\bar{x}/d_R$, the shock strength $z = \frac{\Delta p}{p_o}$ at a position $\bar{x}$ upstream of the starting plane, and the shock strength $z_s = \frac{(\Delta p)_s}{p_o}$ at the plane $x = x_s$. It may be written in terms of these variables as

$$\frac{\bar{x}}{d_R} = \frac{2\gamma}{\gamma+1}\cos\phi(\sin\phi - M_x)\left(\frac{1}{z} - \frac{1}{z_s}\right)\left\{1 + \left(\frac{\gamma+1}{4\gamma}\,\frac{\sin\phi}{\sin\phi - M_x}\right)^2 \frac{z^3}{z_s}\right\} \quad . \tag{16}$$

The second term in brackets is of order $\left(\frac{\delta p}{\Delta p}\right)^2$, and must therefore be neglected in the present approximation. It follows that to an accuracy of $(\Delta p/\rho_o c_o^2)$, the relation between shock strength z and upstream distance $\bar{x}$ is

$$\frac{\bar{x}}{d_R} = \frac{2\gamma}{\gamma+1}\left(\frac{1}{z} - \frac{1}{z_s}\right) F(M_R, M_x) \quad . \tag{17}$$

The function $F(M_R,M_x) = \cos\phi.(\sin\phi - M_x)$ is determined by the relative Mach number M_R entering the rotor and its axial component M_x, and is evaluated in the following section.

Equation (17) may also be written as

$$\left(\frac{\gamma+1}{2\gamma}\right) z = \eta / \left(1 + \frac{2\gamma}{\gamma+1}\,\frac{\eta}{z_s}\right) \quad , \qquad (\eta = Fd_R/\bar{x}) \tag{18}$$

which gives the shock strength z explicitly in terms of the parameter $\eta = Fd_R/\bar{x}$. This result shows that for small η (large distances), z varies linearly with η and is independent of z_s. At small distances, as expected, z tends to the starting value z_s.†

8.2.2 The shock-propagation function $F(M_R,M_x)$

The shock-front inclination ϕ (Fig. 8.1) may be calculated from the relation

$$\beta + \phi + \mu = \pi \quad , \tag{19}$$

where $\beta = \cos^{-1}(M_x/M_R)$ is the flow angle relative to the rotor, and $\mu = \sin^{-1}(1/M_R)$ is the Mach angle. It follows that

$$\cos\phi = \frac{1}{M_R^2}\left[M_t - M_x(M_R^2-1)^{\frac{1}{2}}\right] \quad , \quad \sin\phi = \frac{1}{M_R^2}\left[M_x + M_t(M_R^2-1)^{\frac{1}{2}}\right] \tag{20}$$

where $M_t = (M_R^2 - M_x^2)^{\frac{1}{2}}$ is the tangential Mach number of the rotor.

Values of the function $F(M_R,M_x) = \cos\phi.(\sin\phi - M_x)$ obtained from equation (20) are plotted in Fig. 8.3. Physically, Fd_R is the distance travelled upstream in the axial direction by a point on the shock, as the

† The value of z_s in the leading-edge plane of a supersonic rotor may be roughly estimated as the strength of a normal shock corresponding to an upstream Mach number M_R.

shock front advances by one "wavelength" $d_R \cos\phi$ relative to the fluid. Thus when M_x approaches 1, F becomes small because a point on the shock is swept downstream almost as fast as it advances relative to the fluid.

When $M_R^2 >> 1$, ϕ approaches $\pi/2$ and F is given approximately by $(1-M_x)^2/M_R$, as may be checked from Fig. 8.3.

8.2.3 Comparison of simplified theory with measurements

Shock measurements from two experimental supersonic fan rotors [61, 62], of widely different hub-tip ratios (approx. 0.8 and 0.3) are plotted in Fig. 8.4, in the form suggested by equation (18). The initial shock strength z_s was taken for this purpose as the normal-shock strength for a Mach number M_R. Values of M_R in the tests ranged from 1.16 to 1.37.

The four sets of data points correspond to upstream measuring positions whose distances from the leading-edge plane ranged from 2.2% to 90% of the rotor blade space.† In every case the measurements fall within a factor of 2 of the simplified theory, which is represented in Fig. 8.4 by a straight line of unit slope.

Considerably closer agreement is found when the simplified theory is compared with exact calculations based on a two-dimensional isentropic model, for a rotor of similar geometry to the $\mu = 0.8$ design. This suggests that assumptions common to both calculations - such as two-dimensional flow and exact uniformity of the shock pattern - are a more serious source of error in predicting the shock strength than any subsequent assumptions used in obtaining equation (18).

---

†A value of d_R corresponding to the effective radius, i.e. (B/g_o) times the casing radius, is used throughout the calculations.

8.3 SOUND POWER RADIATED UPSTREAM AT BLADE-PASSING FREQUENCY

A supersonic rotor running in an open-ended duct will radiate an amount of sound power governed by the strength of the shock patterns at the upstream and downstream ends of the duct. This is because nonlinear effects are comparatively unimportant once the sound has left the duct and is able to spread three-dimensionally. If the theory of section 8.2 is used to estimate the pressure field at, say, the inlet end of the duct, the corresponding sound power can be calculated provided the energy transmission coefficient for the inlet opening is known.†

Attention is concentrated here on the sound radiated at blade-passing frequency. For this purpose we require the fundamental Fourier component of the sawtooth pattern assumed in the previous section, which gives a pressure amplitude $\Delta p/\pi$. The corresponding upstream sound power, which for a two-dimensional rotor is confined to the (B,0) mode, is given by equation (4.22) as

$$\frac{W_1}{S} = \frac{1}{2\rho_o c_o}\left(\frac{\Delta p}{\pi}\right)^2 \alpha q_o \left(\frac{1-M_x^2}{1+\alpha M_x}\right)^2 \quad , \quad (M_x > 0). \tag{21}$$

Provided the shock strength at the inlet face is small compared with the initial strength leaving the rotor - as will generally be the case for duct lengths $\ell > \frac{1}{2}d_R$ - equation (18) can be simplified to give Δp at the end of the duct as

---

†It is assumed that the pressure field reflected back to the rotor from the inlet will not affect the shock pattern generated at the rotor. In view of the axial decay of the shock pattern, this is reasonable for duct lengths of order d_R or greater.

$$\frac{\Delta p}{p_o} \doteq \left(\frac{2\gamma}{\gamma+1}\right) \frac{Fd_R}{\ell} \quad . \tag{22}$$

It follows from (21) that

$$\frac{W_1}{\rho_o c_o^3 S} = \frac{2}{\pi^2(\gamma+1)^2} \left(\frac{d_R}{\ell}\right)^2 R \quad ,$$

where (23)

$$R = \alpha q_o \left(\frac{1-M_x^2}{1+\alpha M_x}\right)^2 F^2 \quad .$$

A realistic estimate of the transmission coefficient q_o in this situation is obtained by assuming a modal admittance ratio of unity at the inlet opening, i.e. $\beta_o = 1$ (cf. section 4.3.3). This gives

$$q_o = \frac{4\alpha}{(1+\alpha)^2} \quad , \tag{24}$$

which tends to 1 as required for high rotational Mach numbers, and is zero at cut-off (where $\alpha = 0$).

The relative sound power function $R(M_R, M_x)$ given by (23) and (24) is plotted in Fig. 8.5. The upstream sound power depends strongly on the axial Mach number of the flow; at high rotor Mach numbers, the power is proportional to $(1-M_x)^6/M_R^2$.

Also shown in Fig. 8.5 is a scale of absolute sound intensity W_1/S, calculated for a duct length $\ell = d_R$. If the fluid stagnation properties are taken as those of air at standard sea-level conditions, equation (23)

gives the intensity as

$$\frac{W_1}{S} = \frac{1.7 \cdot 10^6}{(1+0.2M_x^2)^4} \; R(M_R, M_x) \qquad \text{watt/m}^2 \quad . \tag{25}$$

The coefficient of R does not vary much over the range $M_x = 0$ to 1, and has been approximated by 10^6 watt/m^2 in Fig. 8.5.

8.4. CONCLUSIONS

(a) If a rotor is operating supersonically according to the definition given in equation (3), its associated pressure field is expected to form shock waves and cannot be described by linearized theory.

(b) A simplified weak-shock theory has been developed to predict shock strengths upstream or downstream of a supersonic rotor, on the basis of a two-dimensional model.

(c) The theory has been compared with shock measurements on two different rotors, at upstream positions within one blade space of the rotor leading-edge plane. The measurements fall within a factor of 2 of the predicted shock strengths, and are mostly below the predicted value.

(d) The sound power radiated upstream at blade-passing frequency, from a supersonic rotor with identical blades and spacing, has been estimated from the theory. There is a rapid fall-off as the axial Mach number approaches 1 (Fig. 8.5).

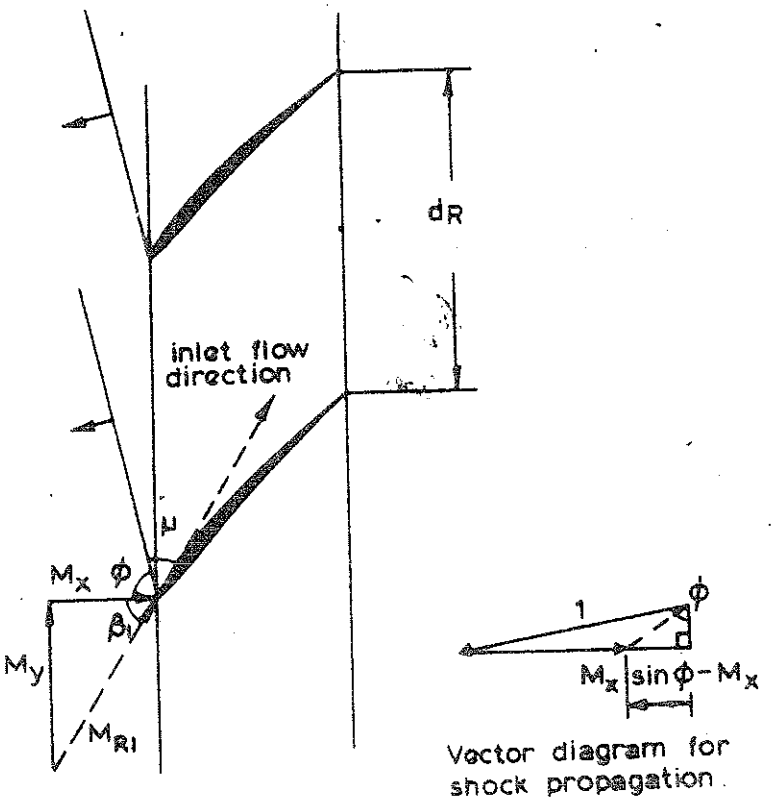

Fig. 8.1 Shock waves upstream of a two-dimensional rotor.

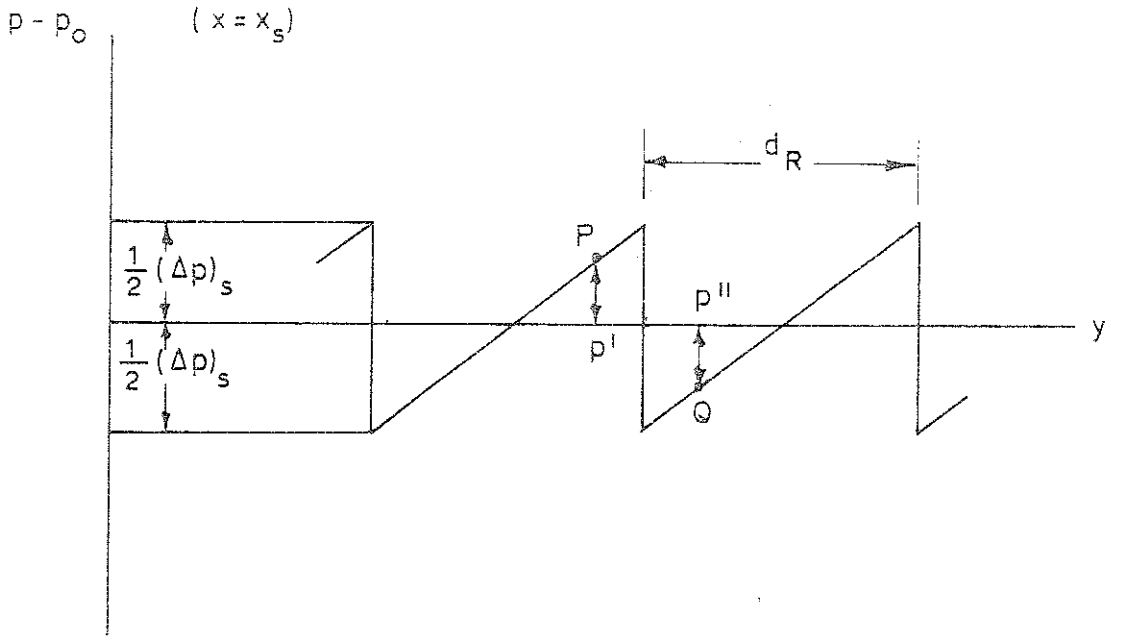

Fig. 8.2 Sawtooth pressure waveform in starting plane.

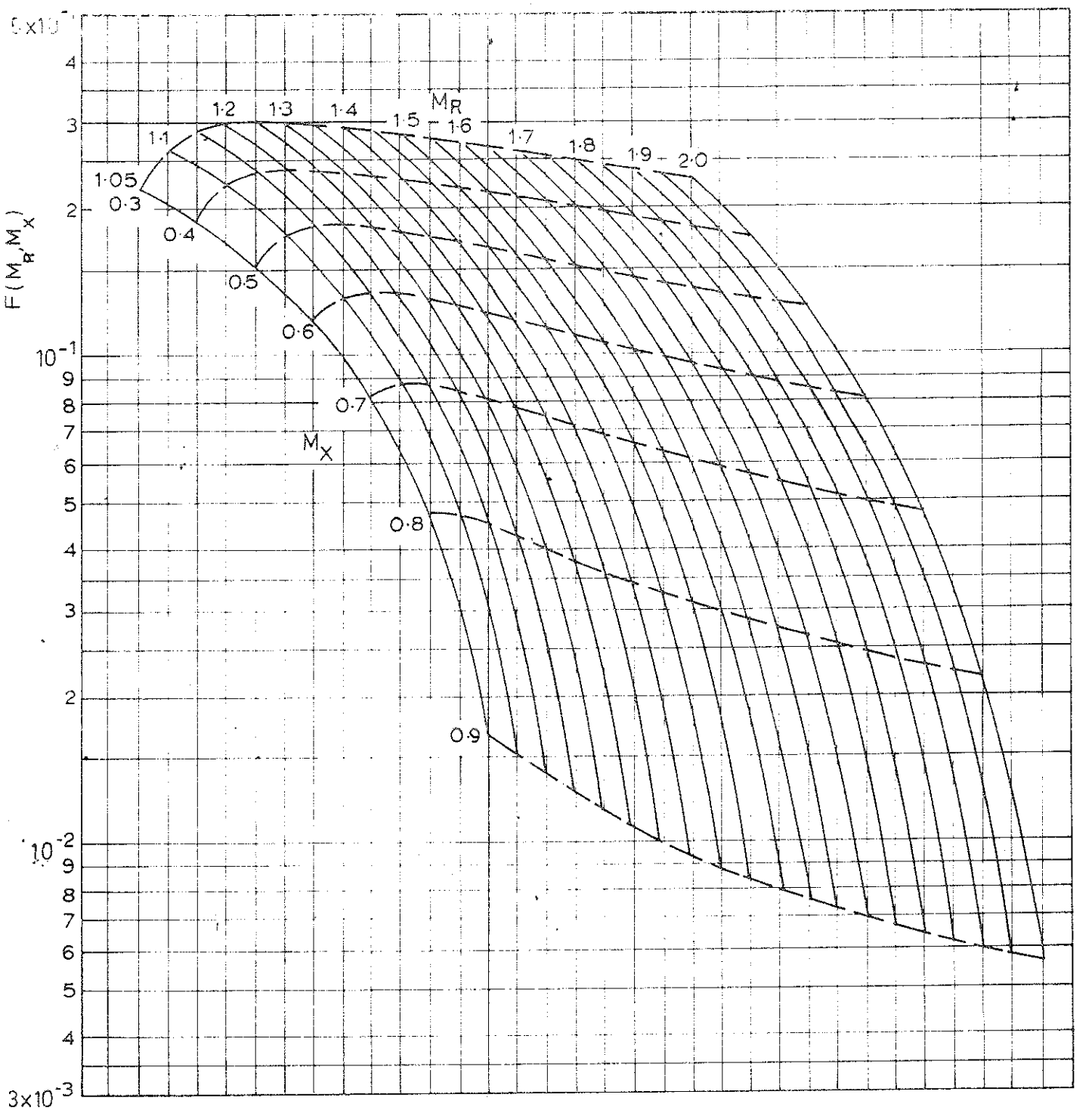

Fig. 8.3 Shock-propagation function $F(M_R, M_X)$ [approx. $(1-M_X)^2/M_R$]

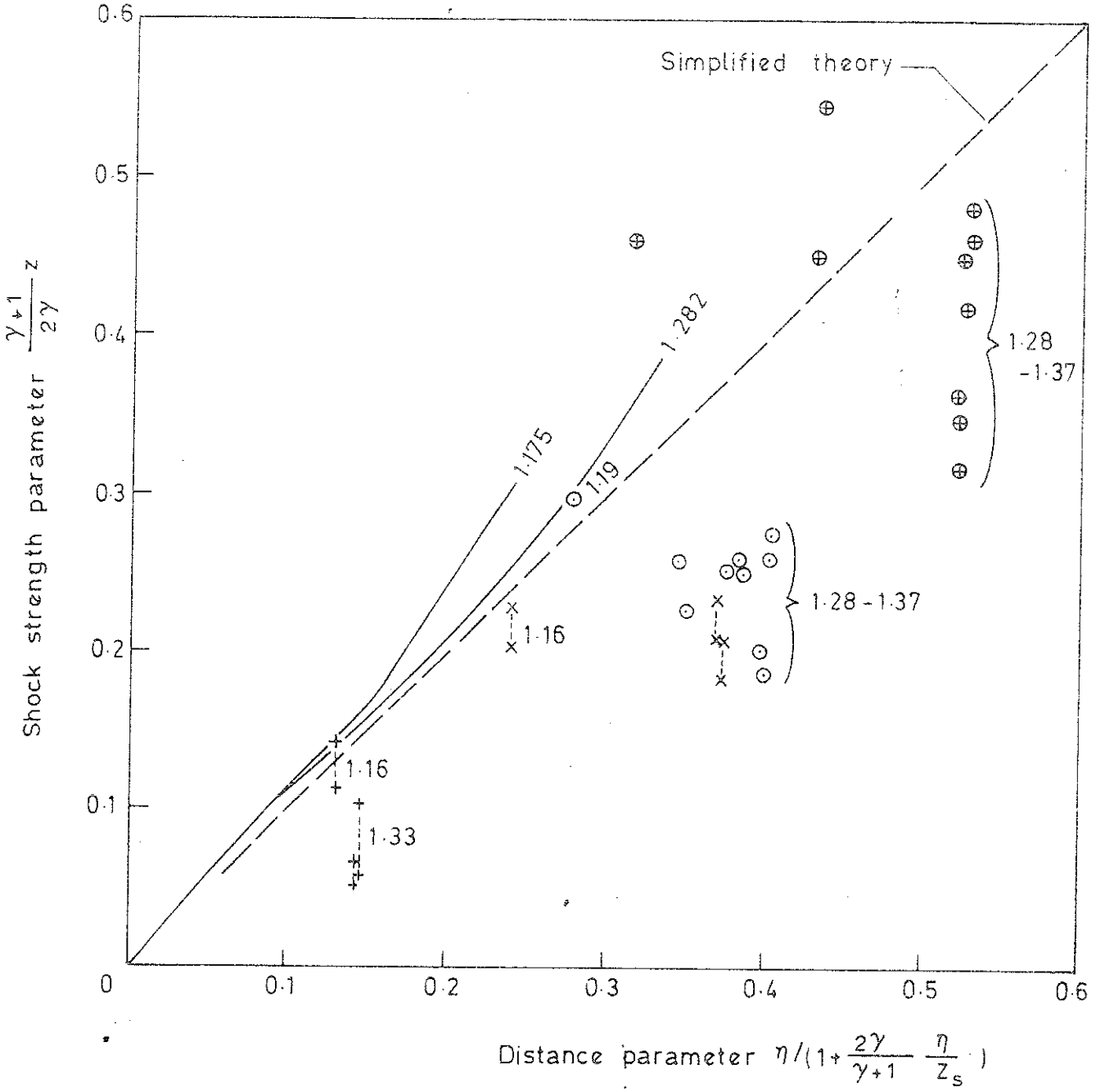

Gauge distances upstream from L.E. rotor tip

- ⊕ 2·2% d_R } $\mu \sim 0.8$
- ⊙ 12% d_R }
- × 14·5% d_R } $\mu \sim 0.3$
- \+ 90% d_R }

×
:
× Denotes range covered by data

Relative Mach. numbers marked: +1·19

Relative flow angles $\beta = 60° - 70°$

(Rotor inlet values)

Fig. 8·4 Comparison of shock measurements with theory.

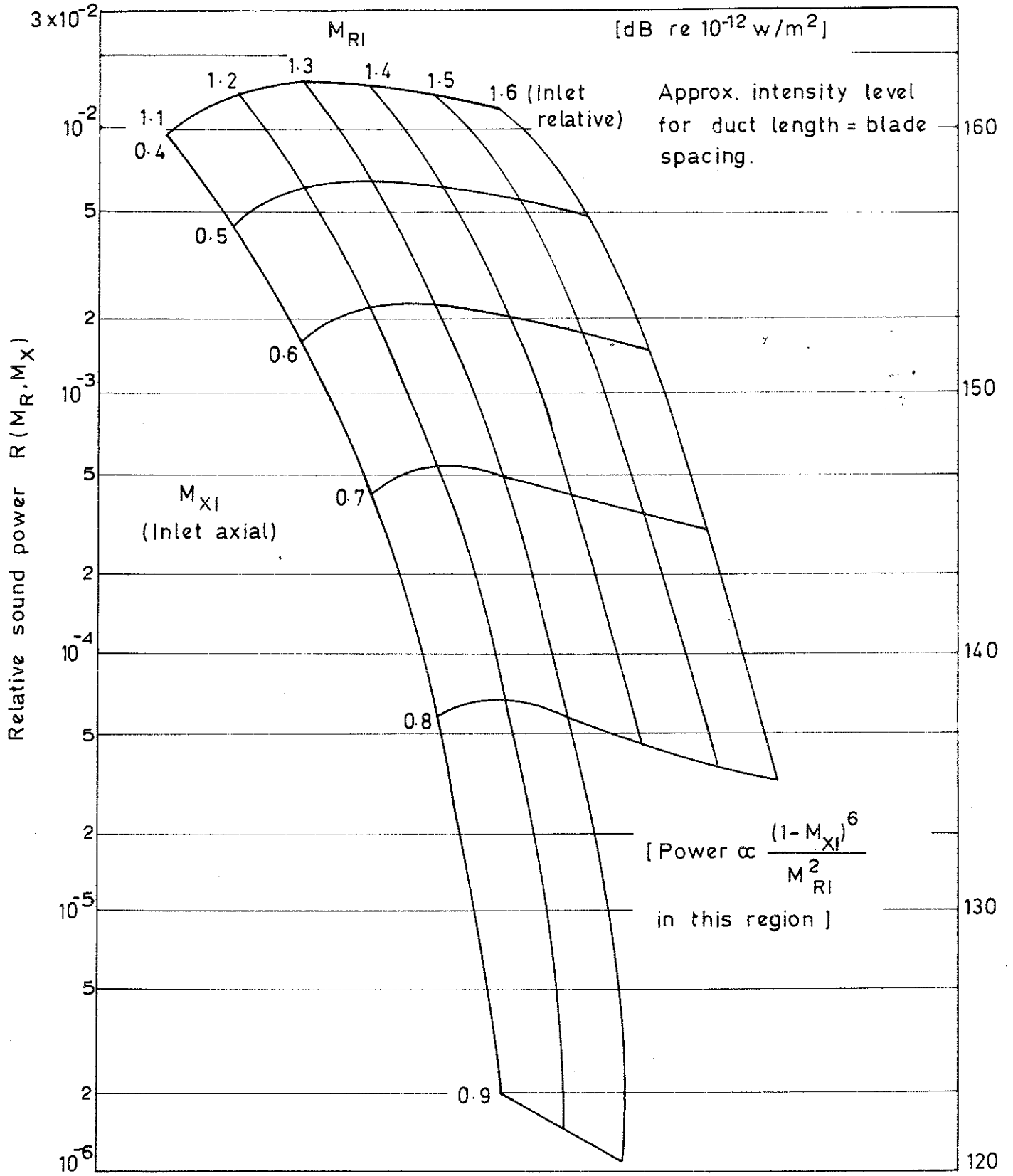

Fig. 8.5 Sound power function $R(M_R, M_X)$.

CHAPTER 9

REVIEW AND SUMMARY OF CONCLUSIONS

The preceding chapters have brought together acoustic and aerodynamic theory with the primary goal of estimating, from first principles, the sound power output of axial-flow machines. Among the practical situations to which the theory is relevant - in addition to the jet-engine noise problem which motivated the work - are heating and ventilating systems, nuclear reactor coolant circuits, and the noise of helicopter rotors, heat-exchanger fans and propellers.

The main conclusions are outlined below, together with suggestions for further research in the area of turbomachinery noise.

(A) - Basic Theory

1. The continuity property of sound power can be extended to non-dissipative irrotational flows, if the classical definitions of acoustic energy flux and energy density are modified. For more general types of flow, use of the modified definitions given in Chapter 2 leads to an acoustic energy balance equation which exhibits acoustic energy production within the flow. The production rate (which may be negative) is determined by certain local correlations between fluctuating quantities.
2. The generalization of acoustic energy mentioned above finds its main use in situations where the production of acoustic energy is negligible. In certain other cases the production rate is significant, but can be estimated; for this purpose a description of the sound

field is required in the production region.

3. The excitation of sound in ducted flows is conveniently described by a convected wave equation for the pressure. Chapter 3 shows that perturbations to a uniform steady flow give rise to source terms in the wave equation, and these are evaluated to second order in the perturbations. Among the acoustic source terms identified in this way are second-order interactions between the flow perturbations (pressure, entropy, velocity) and external forcing terms (volume, momentum and entropy input to the flow).

4. A linearized theory is developed in Chapter 4 to describe the transmission and generation of sound in hard-walled ducts with flow. Given the spatial and time dependence of an acoustic source distribution contained in a finite duct, together with the modal reflection properties of the duct terminations, it is possible to calculate the sound power radiated from the source. Mode coupling at the terminations is neglected, and the duct is assumed uniform between the terminations.

(B) - Applications to Turbomachinery

1. Several different sound-generating mechanisms in subsonic turbomachinery involve the interaction of a blade row with a disturbance field which is unsteady relative to the blades. These interaction mechanisms, identified in Chapter 5 and evaluated in Chapter 6, supplement and often outweigh the direct radiation of sound from steady rotor loading and thickness which occurs in an undisturbed flow.

2. The interaction of a subsonic rotor with turbulent velocity disturbances can radiate either a broad-band or an almost-discrete spectrum of sound frequencies, depending on the frequency spectrum of the turbulence as viewed in a fixed reference frame. For low-frequency turbulence (compared with the blade-passing frequency) the radiated spectrum is concentrated around multiples of the blade-passing frequency; Chapter 7 compares the interaction sound output in this case with the steady-loading sound output in the absence of turbulence. It is found that when the radiated frequency exceeds twice the rotor revolution rate, the steady-loading sound power is negligible at low rotor Mach numbers. As the frequency ratio is increased (above 2), the break-even point moves to higher tip Mach numbers.

3. Sound radiation from a supersonic ducted rotor is dominated by shock-wave formation and decay within the duct. The 1-dimensional theory of weak sawtooth wave propagation predicts shock strengths upstream of two different rotors within a factor of 2 of the measured values, if applied at an effective radius which accounts for the cylindrical geometry of the rotor duct. The same theory predicts that the upstream sound power at blade-passing frequency should vary with the approach-flow Mach number M_x approximately as $(1-M_x)^6$.

4. The theory of turbomachinery noise is still at a primitive stage, in that very few successful comparisons have been made with measurements. Further analytical work is needed to fill gaps in the theory,

together with more detailed aerodynamic measurements than are available at present. Some of the particular topics which require investigation are listed below.

- Refinement of unsteady airfoil theory for incompressible flow, to account for viscous boundary layer effects.
- Computer solutions for unsteady compressible flow in cascades, for cases where incompressible isolated-airfoil theory breaks down.
- Simplified theoretical models for sound transmission through blade rows.
- Propagation of nonuniform rotor shock patterns.
- Measurements of temperature inhomogeneities in turbine flows.
- Measurements of turbulence spectra and scales in multi-stage turbomachinery.
- Experimental verification of theory for rotor noise generation in turbulent flow.

REFERENCES

1. MORSE, P.M. and INGARD, K.U. 1961 Handbuch der Physik, ed. S. Flügge (Springer-Verlag, Berlin), Vol. XI/1. Linear acoustic theory.
2. WALKER, L.R. 1955 J. Appl. Phys. 26, 1031. Power flow in electron beams.
3. ANDREEV, N.N. 1955 Sov. Phys. Acoust. 1, 2. Concerning certain second-order quantities in acoustics.
4. MARKHAM, J.J. 1952 Phys. Rev. 86, 712. Second-order acoustic fields: energy relations.
5. MARKHAM, J.J. 1953 Phys. Rev. 89, 972. Second-order acoustic fields: relations between energy and intensity.
6. SCHOCH, A. 1953 Acustica 3, 181. Remarks on the concept of acoustic energy.
7. BERGMANN, P.G. 1946 J. Acoust. Soc. Am. 17, 329. The wave equation in a medium with a variable index of refraction.
8. BLOKHINTSEV, D.I. 1946 Acoustics of a nonhomogeneous moving medium (Gostekhizdat). Transl: NACA Technical Memorandum 1399 (1956).
9. CANTRELL, R.H. and HART, R.W. 1964 J. Acoust. Soc. Am. 36, 697. Interaction between sound and flow in acoustic cavities: mass, momentum and energy considerations.
10. MORFEY, C.L. 1965 Paper K15 in Proc. of 5th Int. Cong. on Acoustics, Liège, ed. D.E.Commins. (Impre. Georges Thone, Liège). Sound fields and acoustic energy in non-uniform flows.
11. LANDAU, L.D. and LIFSHITZ, E.M. 1959 Fluid Mechanics (Pergamon Press Ltd., Oxford), section 77.

12. MORSE, P.M. and INGARD, K.U. 1968 Theoretical Acoustics (McGraw-Hill Book Co., New York), section 6.4.

13. WHITEHEAD, D.S. 1968 J. Sound Vib. 8, 262. Non-linear acoustic oscillations in a spherical cavity.

14. CHU, B.T. and KOVASZNAY, L.S.G. 1958. J. Fluid Mech. 3, 494. Non-linear interactions in a viscous heat-conducting compressible gas.

15. TEMKIN, S. 1968 Physics of Fluids 11, 960. Nonlinear gas oscillations in a resonant tube.

16. TEMKIN, S. 1969 J. Acoust. Soc. Am. 45, 224. Propagating and standing sawtooth waves.

17. RIBNER, H.S. 1957 J. Acoust. Soc. Am. 29, 435. Reflection, transmission and amplification of sound by a moving medium.

18. LIGHTHILL, M.J. 1956 Surveys in Mechanics, ed. G.K.Batchelor and R.M.Davies (Cambridge Univ. Press.) Viscosity effects in sound waves of finite amplitude (see section 3.1).

19. HAYES, W.D. 1968 Physics of Fluids, 11, 1654. Energy invariant for geometric acoustics in a moving medium.

20. RIBNER, H.S. 1958 Inst. of Aerophysics, Univ. of Toronto, UTIA Tech. Note 21. Note on acoustic energy flow in a moving medium.

21. RYSHOV, O.S. and SHEFTER, G.M. 1962 PMM 26, Transl: J. Appl. Math. Mech. 26, 1293. On the energy of acoustic waves propagating in moving media.

22. GUIRAUD, J.P. 1964 C.R. Acad. Sc. Paris 258, 4425. Geometric acoustics and ballistic shock waves (in French).

23. PRIDMORE-BROWN, D.C. 1958 J. Fluid Mech. 4, 393. Sound propagated in a fluid flowing in an attenuating duct (see Appendix).

24. LIGHTHILL, M.J. 1952 Proc. Roy. Soc. A 211, 564. On sound generated aerodynamically: I. General theory.

25. CURLE, N. 1955. Proc. Roy. Soc. A 231, 505. The influence of solid boundaries upon aerodynamic sound.

26. FFOWCS WILLIAMS, J.E. 1969 Ann. Rev. Fluid Mech. 1, 197. Hydrodynamic noise.

27. MORFEY, C.L. 1964 J. Sound Vib. 1, 60. Rotating pressure patterns in ducts: their generation and transmission.

28. MANI, R. 1969 ASME Applied Mechanics and Fluids Engineering Conference (June 1969), paper No. 69 FE-12. Discrete frequency noise generation from an axial flow fan blade row.

29. MORFEY, C.L. 1969 J. Sound Vib. 9, 367. A note on the radiation efficiency of acoustic duct modes.

30. CARRIER, G.F. 1956 Quarterly Appl. Math. 13, 457. Sound transmission from a tube with flow.

31. MECHEL, F., SCHILZ, W. and DIETZ, J. 1965 Acustica 15, 199. Acoustic impedance of an opening carrying airflow (in German).

32. MORFEY, C.L. 1969 ASME Winter Annual Mtg. (Nov. 1969), paper No. 69-WA/FE-4. Sound generation in subsonic turbomachinery.

33. DOAK, P.E. 1968 Noise and Acoustic Fatigue in Aeronautics, ed. E.J. Richards and D.J.Mead (J. Wiley & Sons Ltd., London.) An introduction to sound radiation and its sources.

34. LOWSON, M.V. and OLLERHEAD, J.B. 1969 J. Sound Vib. 9, 197. A theoretical study of helicopter rotor noise.

35. MORFEY, C.L. 1969 Proceedings of UTIAS/AFOSR Symposium on Aerodynamic Noise (May 1968), ed. H.S. Ribner (Toronto Univ. Press), p.299. A review of the sound-generating mechanisms in aircraft-engine fans and compressors. [Note equations (8) and (10) of Appendix II are incorrect; they are superseded by the results given in Chapter 4.]

36. FAHY, F.J. and PRETLOVE, A.J. 1967 J. Sound Vib. 5, 302. Acoustic forces on a flexible panel which is part of a duct carrying airflow.

37. TYLER, J.M. and SOFRIN, T.G. 1962 S.A.E. Transactions 70, 309. Axial flow compressor noise studies.

38. MORFEY, C.L., SHARLAND I.J. and YEOW, K.W. 1968 Noise and Acoustic Fatigue in Aeronautics, ed. E.J.Richards and D.J. Mead (J. Wiley & Sons Ltd., London). Fan noise.

39. BERNDT, S.B. 1966 J. Fluid Mech. 26, 433. The vorticity jump across a flow discontinuity.

40. BATCHELOR, G.K. 1967 An Introduction to Fluid Dynamics (Cambridge Univ. Press).

41. DAVIES, H.G. and FFOWCS WILLIAMS, J.E. 1968 J. Fluid Mech. 32, 765. Aerodynamic sound generation in a pipe.

42. LOWSON, M.V. 1968 J. Acoust. Soc. Am. 43, 37. Reduction of compressor noise radiation.

43. HETHERINGTON, R. 1963 AIAA Journal 1, 473. Compressor noise generated by fluctuating lift resulting from rotor-stator interaction.

44. KEMP, N.H. 1952 J. Aero. Sci. 19, 713. On the lift and circulation of airfoils in some unsteady-flow problems.

45. KEMP, N.H. and SEARS, W.R. 1953 J. Aero. Sci. 20, 585. Aerodynamic interference between moving blade rows.

46. KEMP, N.H. and SEARS, W.R. 1955 J. Aero. Sci. 22, 478. The unsteady forces due to viscous wakes in turbomachines.

47. BRAGG, S.L. and BRIDGE, R. 1964 J. Roy. Aero. Soc. 68, 1. Noise from turbojet compressors.

48. SLUTSKY, S. 1969 Proceedings of UTIAS/AFOSR Symposium on Aerodynamic Noise (May 1968), ed. H. S. Ribner (Toronto Univ. Press), p.331. Discrete noise generation and propagation by a fan engine.

49. LILLEY, G.M. 1961 Rolls-Royce Ltd. Noise Panel Report (limited circulation). On the vortex noise from airscrews, fans and compressors.

50. SHARLAND, I.J. 1964 J. Sound Vib. 1, 302. Sources of noise in axial flow fans.

51. FFOWCS WILLIAMS, J.E. and HAWKINGS, D.L. 1969 J. Sound Vib. 10, 10. Theory relating to the noise of rotating machinery.

52. LIEBLEIN, S. and ROUDEBUSH, W.H. 1956 NACA Technical Note 3662. Theoretical loss relations for low-speed two-dimensional-cascade flow.

53. HORLOCK, J.H. 1968 Trans. ASME (Journal of Basic Engineering) 90 D, 494. Fluctuating lift forces on aerofoils moving through transverse and chordwise gusts.

54. MORFEY, C.L. 1964 Engineering 198, 782. How to reduce the noise of jet engines.

55. EMBLETON, T.F.W. 1962 J. Acoust. Soc. Am. 34, 862. Relation of mechanical power of a propeller to radiated power of the resulting acoustic sources.

56. GUTIN, L. 1936 Phys. Z. SowjUn. 9, 57. Transl: NACA TM 1195 (1948). On the sound field of a rotating propeller.

57. McCUNE, J.E. 1958 J. Aero. Sci. 25, 616. The transonic flow field of an axial compressor blade row.

58. RUDNICK, I. 1953 J. Acoust. Soc. Am. 25, 1012. On the attenuation of a repeated sawtooth shock wave.

59. BLACKSTOCK, D.T. 1966 J. Acoust. Soc. Am. 39, 1019. Connection between the Fay and Fubini solutions for plane sound waves of finite amplitude.

60. MORFEY, C.L. 1968 J. Acoust. Soc. Am. 44, 300. Finite-amplitude plane waves: the weak-shock method.

61. MORFEY, C.L., BIES, D.A. et al. 1968 Bolt Beranek and Newman Inc., Report No. 1617, submitted to General Electric Co. Investigation of discrete-frequency noise generation by aero-engine compressors and fans.

62. Data supplied by Rolls-Royce Ltd., Advanced Research Laboratory, Sept. 1969.

63. SOZOU, C. 1969 J. Fluid Mech. 36, 605. Adiabatic transverse modes in a uniformly rotating fluid.

64. SALANT, R.F. 1968 J. Acoust. Soc. Am. 43, 1302. Symmetric normal modes in a uniformly rotating fluid.

65. SOZOU, C. and SWITHENBANK, J. 1969 J. Fluid Mech. 38, 657. Adiabatic transverse waves in a rotating fluid.

66. EMBLETON, T.F.W. and THIESSEN, G.J. 1962 J. Acoust. Soc. Am. 34, 788. Efficiency of circular sources and circular arrays of point sources with linear phase variation.

67. LOWSON, M.V. 1969 NASA Contractor Report 1287. Theoretical studies of compressor noise.

LIST OF SYMBOLS

a	cross-sectional area of blade profile, equation (7.21)
a_o, a_1	outer, inner radii of annulus
B	number of rotor blades
$\underset{\sim}{B}$	phasor vector potential
b, b_x	blade chord, axial chord
$\underset{\sim}{b}$	vector potential for velocity field induced by vorticity
C_L	steady-state lift coefficient
C_p	constant-pressure specific heat of fluid
c	sound speed in fluid
D	mean acoustic energy density
D_p	spatial Fourier components of displacement distribution
d	displacement distribution in rotor plane (Chapter 7)
d	tangential spacing of blades
E^*	acoustic energy density
E_N, E_{mn}	duct-mode shape functions (normalized): $\int_S E_N E_N^* \, dS = S$
e	internal energy of fluid per unit mass
e_{ij}	components of rate-of-strain tensor, $\frac{\partial V_j}{\partial x_i} + \frac{\partial V_i}{\partial x_j}$
$e_R, \bar{e}_R$	displacement, momentum thickness of rotor wake in tangential direction
$F(M_R, M_x)$	shock propagation function $\cos\phi(\sin\phi \pm M_x)$ (− upstream, + downstream)
$F(n)$	defined by equation (7.34)

$F_u(k_y,k_z)$	wavenumber spectrum of axial turbulent velocities
F_x	phasor force component in x direction, per unit area.
$\underset{\sim}{f}$; f_i	force distribution over duct section; cartesian components
$G(n,M_t)$	defined by equation (7.35)
$G(x,x_s)$	single-frequency mode response function
g	Re(q) (Appendix III)
g_o	mode eigenvalue $k_{mn}a_o$
$\underset{\sim}{g}$; g_i	force applied to fluid per unit mass; cartesian components
H	entropy input rate per unit volume
h	enthalpy of fluid per unit mass
h	Im(q) (Appendix III)
I	interaction source terms in wave equation
$\underset{\sim}{I}$; I_i	acoustic intensity vector; cartesian components
I_p	total sound intensity due to interaction between turbulence and rotor at $\|p\|$ × blade-passing frequency
I_{ps}, I_{sp}	modal sound intensity due to interaction between blade rows at $\|p\|$ × blade-passing frequency (radiated from stator, rotor)
I_{turb}	turbulence intensity entering rotor
J	stagnation enthalpy per unit mass
J*	defined by equation (2.15)
K_p	pressure-field decay factor, equations (6.5) and (7.29)
K_w	wake decay factor, equation (6.12)
k	thermal conductivity of fluid (Chapter 2)

$k(\xi)$	circulation distribution over blade chord
k; k_x	acoustic wavenumber (ω/c); axial wavenumber in duct
k_N, k_{mn}	mode characteristic wavenumbers (cut-off value for no flow)
k_p	$2\pi\|p\|/d_R$
k_y, k_z	tangential, radial wavenumber components in rotor disk (2-dimensional model)
L, L_x	unsteady blade lift per unit span, axial component
ℓ	length of duct between source and open end
ℓ_R	resultant steady loading on rotor blade
ℓ_x, ℓ_θ	thrust, torque components of steady blade loading, equation (7.21)
ℓ_y, ℓ_z	turbulence length scales in tangential, radial directions (2-dimensional model)
M_R, M_S	Mach number of flow relative to rotor, stator
M_t	tangential Mach number of rotor, $M_x(t_1 + t_2)$
M_x, M_θ	components of flow Mach number in duct
m	mass flow per unit disk area (Chapter 4)
m	circumferential mode number (number of cycles round disk)
m_i	components of mass flux, ρV_i
m_i^*	defined by equation (2.15)
N	rotor revolution rate
$\underset{\sim}{N}$; N_i	energy flux vector; cartesian components
N_i^*	components of acoustic energy flux, $J^* m_i^*$

n	radial mode number
n	reduced frequency in fluctuating lift calculation
n	ratio of sound frequency to rotor revolution rate, $\|p\|B$
$\underset{\sim}{n}$	unit vector normal to disk
P	rate of acoustic energy production per unit volume (Chapter 2)
P; $\bar{P}(x)$	phasor sound pressure; modal coefficient
P_{ij}	components of fluid stress tensor
P_S	entropy production rate per unit volume
Pr	Prandtl number of fluid
p; p^*	pressure; dimensionless fluctuation $p'/\rho c^2$
p	rotor spatial harmonic number ($p = \pm 1, \pm 2$ etc.); $\|p\|$ = blade-passing harmonic number
Δp	pressure rise across shock wave
δp	defined by equation (8.13)
Q	three-dimensional acoustic source distribution
Q	total torque on rotor (Chapter 7)
$Q^{(o)}, Q_i, Q_{ij}$	define source distributions of monopole, dipole, quadrupole order
q	modal energy transmission coefficient
q	reduced chordwise wavenumber in fluctuating lift calculation
q	blade index number (Chapter 7)
q_i	components of heat flux vector
$R(M_R, M_x)$	sound power function, equation (8.23)

R_j	defined by equation (2.17)
R_{mn}	radial mode shape function (normalized)
r	radial co-ordinate
r	modal pressure reflection coefficient
S	defined by equation (2.17)
S	area of annulus or duct cross-section
S_o	area of complete rotor disk
$S^{(o)}, S_x, S_{xx}$	phasor axial source moments corresponding to $s^{(o)}$ etc.
$S^{(x)}, S^{(xx)}$	equivalent zero-order axial moments corresponding to S_x, S_{xx}
$\bar{S}^{(o)}$	modal coefficient of $S^{(o)}$; similarly for other source moments
s	entropy of fluid per unit mass
s	spatial harmonic number for stator vane disturbances ($s = \pm 1, \pm 2$ etc.)
s	distance from source (Appendix IV)
$s^{(o)}, s_x, s_{xx}$	successive axial moments of acoustic source distribution Q
s_i, s_{ij}	defined by equation (4.54)
T	absolute temperature
t	time
t_1, t_2	$\tan \alpha_1$, $\tan \beta_2$
U, U_v	phasor axial velocities (sound field, vorticity field)
U_o, U_S	amplitude of longitudinal velocity fluctuations at mid-chord, stator LE
$\bar{U}$	spatial r.m.s. value of velocity amplitude
u	axial component of turbulent velocity fluctuation (Chapter 7)

$\tilde{u}_{turb}$	r.m.s. axial component of turbulent velocity
$\underset{\sim}{u}$; u_i	$\underset{\sim}{v}$-$\underset{\sim}{w}$; cartesian components
V	number of stator vanes
V	phasor tangential velocity (Appendix II)
V_o, V_S, V_R	amplitude of upwash fluctuation at mid-chord, stator LE, rotor TE
$\underset{\sim}{V}$; V_i	fluid velocity; cartesian components
$\bar{\underset{\sim}{V}}$; $\bar{V}_i$	velocity in unperturbed flow; cartesian components
$\underset{\sim}{v}$; v_i	fluid velocity perturbation; cartesian components
W	sound power
W_p	sound power radiated to either side of a ducted rotor, at $\|p\|$ × blade-passing frequency
$\underset{\sim}{w}$; w_i	vorticity-induced velocity perturbation; cartesian components
X	wake coordinate x/b_x (x = 0 at TE)
x	axial co-ordinate in duct
$\bar{x}$	blade-row separation (Chapter 6)
$\bar{x}$	axial distance from starting plane (Chapter 8)
x_i, x_j	cartesian coordinates (i,j = 1,2,3)
y	tangential co-ordinate in two-dimensional rotor model
$\underset{\sim}{y}$; y_i	position vector in duct cross-section; cartesian components
$\underset{\sim}{Z}$	phasor vorticity field
z	volume displacement per unit volume
z	shock strength $\Delta p/p_o$ (Chapter 8)

α	axial wavenumber parameter
α_1, α_2	stator inlet, exit flow angles
α_T	thermal expansion coefficient
β, β_o	modal admittance ratio in x direction, value at duct opening
β	nonlinearity coefficient (Appendix I)
β_1, β_2	rotor inlet, exit relative flow angles
γ	specific-heat ratio
ε	ratio f_θ/f_x at outer radius $r = a_o$
ε	mean thickness-chord ratio at blade tip
ζ	vorticity
ζ_{ij}	components of vorticity tensor, $\frac{\partial V_j}{\partial x_i} - \frac{\partial V_i}{\partial x_j}$
η	$\mathrm{Im}\psi$ (Chapter 4)
η	shock distance parameter, equation (8.18)
η_p	acoustic efficiency defined by equation (7.19)
θ; θ_p θ_s	$\ln\rho$; derivatives with respect to pressure, entropy
θ	angle in cylindrical co-ordinates
θ_R	temperature defect parameter for rotor wake
λ	wavelength of periodic pattern
μ	viscosity of fluid (Chapter 2)
μ	radius ratio a_1/a_o for annular duct; hub-tip ratio of rotor

μ	Mach angle (Chapter 8)
ξ	Reψ (Chapter 4)
ξ	dimensionless chordwise coordinate
π_R, π_S	stagnation-pressure loss coefficient of rotor, stator
ρ	fluid density
σ	Axial conductance ratio, Re β
σ	blade-row solidity
τ_o	modal radiation efficiency at duct opening
τ_m	radiation efficiency of annular source with zero radial variation
τ_{mn}	radiation efficiency of annular source in (m,n) mode
ϕ	Axial susceptance ratio, Imβ
ϕ	C_L/π (2-dimensional model)
ϕ	shock angle (Fig. 8.1)
χ_o	modal reactance ratio at duct opening
ψ, ψ_o	reflection phase, value at x = 0
ψ	angle to disk axis (Appendix IV)
Ω	angular velocity of mean swirl
ω, ω_o	radian frequency (relative to mean swirl, absolute value)

Subscripts

i,j	cartesian components (i,j= 1, 2, 3 ; repeated subscripts indicate summation)
N	general mode index
n	normal to chord (Chapter 6)
n	normal to surface or wavefront
p,s	harmonic components of rotor, stator disturbances

q	q^{th} blade around disk
R,S	rotor, stator
s	source position
s	value in starting plane (Chapter 8)
t	transverse component (normal to axis)
t	tangential to wavefront (Chapter 2)
v	component due to vorticity
0	unperturbed value
+, −	+x, −x side of source plane

Superscripts

'	perturbation
(0)	simple source
+, −	value just downstream, upstream of actuator disk
+, −	indicates direction of progressive waves along duct (Chapter 4)

Functions

C(n)	Theodorsen function
D/Dt, $\bar{D}$/Dt	$(\partial/\partial t + V_i\ \partial/\partial x_i)$, $(\partial/\partial t + \bar{V}_i\ \partial/\partial x_i)$
$e^{-i\omega t}$, $e^{i\underset{\sim}{k}.\underset{\sim}{x}}$	time, space factors corresponding to radian frequency ω and wavenumber $\underset{\sim}{k}$
$J_q(x)$	Bessel function of order q
$\bar{J}_q(x)$	Bessel function integral $\int_o^x J_q(t)\ dt$

$K_L(n,q)$	Kemp-Sears lift response function
L	$\bar{D}^2/Dt^2 - c_o^2\nabla^2$
Re, Im	real, imaginary part
$\delta( )$	delta function
∇, ∇_t	gradient operator, transverse component
$< >$	time average

APPENDIX I : THERMODYNAMIC RELATIONSHIPS

The thermodynamic properties of any homogeneous substance are determined by an equation for the specific enthalpy in the form $h=h(p,s)$, provided the only means available for transferring energy to the substance (under equilibrium conditions) are compression work and heat transfer. Such an equation of state is expected to hold for a fluid which is free from chemical or electromagnetic effects.

Under these conditions, the thermodynamic properties at equilibrium are linked by the differential relationship

$$dh = \rho^{-1}\, dp + T\, ds \quad ;$$

it follows that the partial differential coefficients of $h(p,s)$ are given by

$$h_p = \rho^{-1} \quad ; \qquad h_s = T \quad .$$

Differentiation with respect to s gives:

$$T_p = h_{ps} = \left(\frac{\partial \rho^{-1}}{\partial s}\right)_p = \left(\frac{\partial \rho^{-1}}{\partial T}\right)_p \left(\frac{\partial T}{\partial s}\right)_p = \frac{\alpha_T\, T}{\rho\, C_p} \quad ;$$

$$h_{ss} = \left(\frac{\partial T}{\partial s}\right)_p = T/C_p \quad ,$$

where $C_p = \left(\frac{\partial h}{\partial T}\right)_p$;

here,

$$\alpha_T = \rho\left(\frac{\partial \rho^{-1}}{\partial T}\right)_p$$

is the coefficient of thermal expansion. Alternatively,

$$h_{ps} = \left[\frac{(\gamma-1)T}{\rho^2 c^2 C_p}\right]^{\frac{1}{2}} ,$$

where $\gamma = C_p/C_v$ is the ratio of specific heats.

From the basic relationships given above, the following partial differential coefficients of $\theta(p,s)=\ln \rho$ are obtained:

$$\theta_p = \frac{1}{\rho c^2} \quad ; \qquad \theta_s = -\frac{\alpha_T T}{C_p}$$

$$\theta_{pp} = (1-2\beta)\,\theta_p^2 \quad , \qquad = -\left[\frac{(\gamma-1)T}{c^2 C_p}\right]^{\frac{1}{2}}$$

where β is a "nonlinearity" coefficient given by

$$\beta = \frac{1}{2}\rho^3 c^4 h_{ppp} = \frac{1}{c}\left(\frac{\partial \rho c}{\partial \rho}\right)_s \quad .$$

For a perfect gas, $\alpha_T T=1$, so $\theta_s=-(1/C_p)$. If the gas has constant specific heats, it follows that

$$\theta_{ps} = 0, \quad \theta_{ss} = 0 \quad .$$

The nonlinearity coefficient β for such gas is $\beta = \frac{1}{2}(\gamma+1)$.

APPENDIX II : EFFECT OF MEAN SWIRL ON SOUND TRANSMISSION IN AXISYMMETRIC DUCTS

If the mean swirl is represented by solid-body rotation of the flow at angular velocity Ω , a first approximation to the sound field in the duct is obtained by applying the zero-swirl solution to a co-ordinate system rotating with the flow.

However, this procedure neglects the coupling of the unsteady pressure and vorticity fields caused by the mean vorticity in the flow (Ω effect), as well as the presence of radial density and sound-speed gradients in the mean flow (rotational Mach number effect). The continuity property of acoustic energy moreover ceases to hold when the mean-flow vorticity becomes comparable with the radian frequency (cf. section 2.).

The range of validity of the rotating-co-ordinate approximation is explored below, by examining the effect of solid-body rotation on mode cut-off frequencies. An expression for acoustic intensity is then derived on the assumption that this approximation can be applied.

Cut-off frequencies in a rotating flow

Sozou [63] has calculated (m,n) mode cut-off frequencies in a fluid with solid-body rotation bounded by a hard-walled circular duct, for modes with $m \geq 1$. The fluid was taken as a perfect gas, with $\gamma = 1.4$ and uniform mean entropy. In addition, Salant [64] has calculated (0,n) cut-off frequencies under similar conditions except that γ was taken as 1.

From these numerical results it is clear that the cut-off frequencies ω_{mn} relative to the rotating fluid are influenced by the rotation, particularly for the (1, 0) mode. However, provided the fluid rotates at subsonic speeds,

and this mode is excluded,† it appears that the ratio $\omega_{mn}(\Omega)/\omega_{mn}(0)$ always lies between 1 and $1 - \Omega/\omega_o$. Here ω_o is the cut-off frequency in fixed co-ordinates, and Ω is taken as positive if the fluid is rotating in the same direction as the acoustic wave††. The zero-swirl cut-off frequency $\omega_{mn}(0)$ is calculated using the sound speed in the rotating fluid at the r.m.s. radius, for purposes of comparison.

Sozou and Swithenbank [65] have subsequently extended these calculations to study the effect of non-uniform rotation on the (1,0) and (2,0) modes. A Rankine vortex is assumed, which reduces to the previous case when the core fills the cylinder. Exactly the same conclusions may be drawn as before concerning the effect of fluid rotation on cut-off frequencies, provided the uniform angular velocity Ω is replaced by a mean value

$$\Omega = \int \Omega(r) . r^3 dr / \int r^3 dr \qquad (1)$$

in the calculations. Equation (1) would correspond to an angular-momentum average of $\Omega(r)$ if the fluid density were uniform; it is introduced here as a convenient definition, in order to generalize the uniform-rotation results.

Footnotes: † The upper bound is slightly exceeded when the (1,0) mode rotates in the direction opposite to the fluid. The same applies in the Rankine vortex case; but the discrepancy does not exceed 10% provided the flow is locally subsonic over the whole cross-section.

†† For $m = 0$, Ω is taken as negative (the cut-off frequencies are increased by fluid rotation).

It follows that

$$\Omega \ll \omega_o \quad (\omega_o = \text{radian frequency in fixed co-ordinates}) \tag{2}$$

is a sufficient condition for mode cut-off frequencies, relative to a subsonically rotating fluid, to be approximated by neglecting the rotation and using a typical sound speed as described above. The same condition ensures the continuity of acoustic energy, and is assumed to hold in the analysis which follows.

Acoustic intensity in a uniformly rotating flow

In terms of (x, θ, r) velocity components, equation (2.13) gives the axial component of the acoustic intensity as

$$I_x = \langle p'v_x \rangle + \frac{\bar{V}_x}{\rho_o c_o^2} \langle p'p' \rangle + \frac{\bar{V}_x^2}{c_o^2} \langle p'v_x \rangle + \rho_o \bar{V}_x \langle v_x v_x \rangle + \frac{\bar{V}_x \bar{V}_\theta}{c_o^2} \langle p'v_\theta \rangle + \rho_o \bar{V}_\theta \langle v_x v_\theta \rangle . \tag{3}$$

For a single frequency and duct mode, the tangential velocity fluctuations $v_\theta = \mathrm{Re}(V)$ corresponding to waves travelling in the $+x$ and $-x$ directions are

$$V^+ \doteq \frac{mP^+}{\rho_o \omega r}\left(\frac{1 - M_x^2}{1 - \alpha M_x}\right), \quad V^- \doteq \frac{mP^-}{\rho_o \omega r}\left(\frac{1 - M_x^2}{1 + \alpha M_x}\right) \qquad (\Omega \ll \omega_o); \tag{4}$$

these follow from the linearized momentum equation in the θ direction (cf. equation 4.13). The radian frequency ω is measured relative to the mean swirl; i.e.

$$\omega = \omega_o - m\Omega \tag{5}$$

where ω_o is the frequency in fixed co-ordinates.

Adding the forward and backward wave components, and using equations (4.10) & (4.14), gives the combined tangential velocity as

$$V = \frac{mP}{\rho_o \omega r}(1 + \beta M_x) .$$

If the values

$$\left.\begin{aligned} &\bar{V}_x = c_o M_x , \quad \bar{V}_\theta = \Omega r, \\ &v_x = \mathrm{Re}\left\{\frac{\beta P}{\rho_o c_o}\right\} , \quad v_\theta = \mathrm{Re}\left[\frac{mP}{\rho_o \omega r}(1 + \beta M_x)\right] \end{aligned}\right\} \tag{6}$$

are substituted in (3), the intensity is obtained as

$$I_x = \frac{\omega_o}{\omega} \cdot \frac{1}{2} \frac{|P|^2}{\rho_o c_o} \{(1 + M_x^2)\,\mathrm{Re}\,\beta + M_x (1 + |\beta|^2)\} . \tag{7}$$

Comparison with equation (4.16) shows that to the present approximation ($\Omega \ll \omega_o$, subsonic flow), the effect of the mean swirl is to multiply the axial intensity in each mode by the factor

$$\frac{\omega o}{\omega} = 1 + \frac{m\Omega}{\omega} = \left(1 - \frac{m\Omega}{\omega_o}\right)^{-1} . \tag{8}$$

APPENDIX III: RESULTS FROM UNSTEADY AIRFOIL THEORY

A theory due to Kemp [44] gives the fluctuating lift response of a stationary two-dimensional airfoil to small upwash-velocity fluctuations superimposed on the mean free-stream velocity V_∞ . Effects of airfoil thickness, camber, and interference from neighboring blades are all neglected; the theory is restricted to incompressible inviscid flow, and the Kutta condition is applied at the trailing edge (i.e. the pressure is assumed continuous).

A basic upwash distribution is taken in the form

$$v = \mathrm{Re}\left[V_o\, e^{i(q\xi-\omega t)}\right] , \tag{1}$$

where ξ is the distance rearward from the mid-chord point normalized by the half-chord (b/2).

The corresponding complex lift L per unit span is given by

$$L = \pi\rho b V_\infty V_o\, e^{-i\omega t} \cdot K_L(n,q). \tag{2}$$

Here K_L is the Kemp-Sears lift function, related to the Theodorsen function C(n) by

$$K_L(n,q) = \left[J_o(q) + iJ_1(q)\right] C(n) - i\left(\frac{n}{q}\right) J_1(q) , \tag{3}$$

and n is the reduced frequency $\omega b/2V_\infty$.

Typically n is of order 3 throughout the operating range of a compressor. The Theodorsen function C(n) can then be closely approximated by $\frac{1}{2}$.

In addition to the upwash-induced lift fluctuations described above,

the airfoil will respond to longitudinal (i.e. chordwise) velocity fluctuations u in a similar manner. The lift response is no longer frequency-dependent, but is governed by q. It may be calculated for airfoils of negligible camber by noting that the steady-state distribution of circulation over the blade chord is unaltered by longitudinal gusts of small amplitude, in contrast to the upwash case analysed by Kemp.

The calculation for an airfoil with a flat-plate steady lift distribution, subjected to a longitudinal gust pattern

$$u = \mathrm{Re}\left[U_o\, e^{i(q\xi-\omega t)}\right] , \tag{4}$$

gives

$$L = \pi\rho b V_\infty U_o\, e^{-i\omega t} \,.\, H_L(q); \tag{5}$$

the unsteady-lift response function in this case is†

$$H_L(q) = \frac{C_L}{2\pi}\left[J_o(q) - i\, J_1(q)\right] . \tag{6}$$

The function H_L, unlike K_L, depends on the steady lift coefficient of the airfoil.

Approximation to longitudinal response function

For $|q|^2 >> 1$, equation (6) gives approximately

$$H_L(q) \doteq \frac{C_L/\pi}{(2\pi q)^{\frac{1}{2}}}\; e^{h}\, e^{i(\frac{1}{4}\pi-g)}, \quad (q=g+ih\,;\ |q|^2 >> 1);$$

i.e.

$$H_L'(q) \doteq (2\pi q)^{-\frac{1}{2}}\, \phi\, e^{i\frac{1}{4}\pi} \quad \text{(referred to leading edge;}\ \ \phi = C_L/\pi) . \tag{7}$$

† Equation (6) can be shown to agree with Horlock's calculation [53], if his gust parallel to the mainstream is resolved into longitudinal and upwash components.

Approximations to upwash response function

Three particular cases are of interest.

(a) Frozen convected gust pattern

Here $g = n$, $h = 0$. If we further assume $n > 1$ so that $C(n) \doteq \frac{1}{2}$, equation (3) gives

$$K_L(n,n) \doteq \tfrac{1}{2}\left[J_o(n) - i\, J_1(n)\right] = (1/\phi)H_L(n) \quad , (n > 1); \qquad (8)$$

or from (7)

$$K'_L(n,n) = (2\pi n)^{-\frac{1}{2}}\, e^{i\frac{1}{4}\pi} \text{ (referred to leading edge; } n^2 >> 1). \qquad (9)$$

(b) Pattern decaying towards trailing edge

If the upwash disturbances decay strongly, so that $e^h >> 1$, then (3) can be approximated at high reduced frequencies by

$$K_L(n,q) \doteq \frac{n}{(2\pi q^3)^{\frac{1}{2}}}\, e^h\, e^{i(\frac{1}{4}\pi - g)} \doteq \frac{n}{q}(1/\phi)H_L(q), (e^h >> 1, n > 1); \qquad (10)$$

i.e.

$$K'_L(n,q) \doteq \frac{n}{q}(2\pi q)^{-\frac{1}{2}}\, e^{i\frac{1}{4}\pi} \text{ (referred to leading edge).} \qquad (11)$$

(c) Pattern amplifying towards trailing edge

If $e^h << 1$ and $n > 1$, equation (3) gives

$$K_L(n,q) \doteq \frac{q-n}{(2\pi q^3)^{\frac{1}{2}}}\, e^{-h}\, e^{i(g-\frac{1}{4}\pi)}, \quad (n > 1,\ e^h << 1);$$

i.e.

$$K''_L(n,q) \doteq \left(1-\frac{n}{q}\right)(2\pi q)^{-\frac{1}{2}}\, e^{-i\frac{1}{4}\pi} \text{ (referred to trailing edge).} \qquad (12).$$

It follows in this case that

$$K_L(n,q) >> H_L(q). \qquad (13)$$

Conclusions

If the disturbance has a much greater velocity amplitude at the trailing edge than at the leading edge, the fluctuating lift is dominated by the upwash component and can be estimated (for $n > 1$) from (12).

Otherwise, the upwash and longitudinal velocity contributions are comparable. Equations(8) and (10) indicate the following approximate relationship for this case:

$$\frac{H_L(q)}{K_L(n,q)} \doteq \phi \cdot \frac{q}{n}, \quad (n > 1);$$

the absolute value of K_L follows from (10) or (11).†

† The errors involved in using (11) or (12) for $|K_L|$ are in fact of order e^{-2h}, e^{2h} respectively at high reduced frequencies, so that the modulus is given more accurately than the phase by these expressions.

APPENDIX IV

SOUND RADIATION FROM AN ANNULAR SOURCE DISTRIBUTION WITH LINEAR PHASE VARIATION CIRCUMFERENTIALLY.

The following analysis provides an estimate of the radiation efficiency for a subsonically rotating source pattern, either in a free field or in a duct. The source is taken as being uniformly distributed over an annular region of arbitrary radius ratio, with a circumferential phase variation around the annulus. A feature of the analysis is that no appeal is made to the effective radius concept.

Circular source distribution: radiation efficiency for (m,n) modes

Consider a source distribution confined to a circular disk of radius a_o, with volume velocity 2U per unit disk area. The quantity U corresponds to the normal velocity of each face of the disk. If U is taken as

$$U = \tilde{U}\, E_{mn}(r,\theta).\ e^{-i\omega t} \qquad , \qquad (m \geq 1) \tag{1}$$

where E_{mn} is the normalized (m,n) mode shape function for a circular cross-section and $\tilde{U}$ is the spatial r.m.s. value of the velocity amplitude, the far-field radiation can be obtained from reference 29 (see Appendix).

The result for the far-field pressure amplitude, at angle ψ to the disk axis and distance s, is

$$|P| = \frac{\rho\omega |U(a_o)| S}{2\pi s} \left| \frac{G_m(z_o)}{g_o^2 - z_o^2} \right| \qquad , \qquad (z_o = ka_o \sin\psi) \tag{2}$$

where $U(a_o)$ is the modal velocity at the outer radius ($r = a_o$). The function

$$G_m(x) = 2xJ'_m(x) = 2mJ_m(x) - 2xJ_{m+1}(x)$$

may be approximated for small values of x by

$$G_m(x) \doteq 2mJ_m(x) \qquad (x^2 << \tfrac{1}{2}m^2 + \tfrac{1}{2}m) \ . \tag{3}$$

Thus provided $k^2a_o^2 << \frac{1}{2}m^2$ (which implies that the frequency is below the mode cut-off value), equation (2) can be approximated by neglecting z_o^2 in comparison with g_o^2 and using (3).

It follows that

$$|P| \doteq \frac{\rho\omega|U(a_o)|S}{\pi s} \cdot \frac{m}{g_o^2} J_m(ka_o \sin\psi) \quad , \quad (k^2a_o^2 << \tfrac{1}{2}m^2). \tag{4}$$

Comparison of (4) with equation (5.18) of [27] gives the power radiated from each side of the disk as

$$W_{mn} \doteq \frac{\rho\omega|U(a_o)|^2 S^2}{2\pi a_o} \frac{m^2}{g_o^4} \bar{J}_{2m}(2ka_o) \quad , \quad (k^2a_o^2 << \tfrac{1}{2}m^2) \tag{5}$$

where $\bar{J}_q(x)$ stands for $\int_o^x J_q(t)\,dt$. (The total power radiated from the modal volume-velocity distribution 2U is $2W_{mn}$.)

The outer-radius velocity amplitude is related to the spatial mean square amplitude by

$$|U(a_o)|^2 = |\tilde{U}|^2/(1 - \frac{m^2}{g_o^2}) \ . \tag{6}$$

It follows from (5) and (6) that the modal radiation efficiency τ_{mn}, defined by

$$W_{mn} = \tfrac{1}{2}\rho c \tau_{mn} |\bar{U}|^2 S \quad , \tag{7}$$

is approximately

$$\tau_{mn} \doteq \frac{k a_o m^2}{\left(1-\frac{m^2}{g_o^2}\right) g_o^4} \bar{J}_{2m}(2ka_o) \qquad (k^2 a_o^2 << \tfrac{1}{2}m^2). \tag{8}$$

For (m,0) modes, an approximation to (8) which is accurate to within 5% for $m \geq 1$ is

$$\tau_{m0} \doteq 0.53\ (m+2)^{-4/3}\ ka_o\ \bar{J}_{2m}\ (2ka_o) \quad , \quad (k^2 a_o^2 << \tfrac{1}{2}m^2). \tag{9}$$

Radiation efficiency τ_m for annular source with zero radial variation

Consider next the radiation from a volume-velocity distribution 2U such that

$$U = U_o e^{i(m\theta - \omega t)} \qquad (m \geq 1) \quad , \quad (U_o = \text{const.}) \tag{10}$$

over an annulus of arbitrary radius ratio $a_1/a_o = \mu$. The far-field pressure amplitude is given by equation (5.16) of [27] as

$$|p| = \left| \frac{\rho\omega U_o}{s} \int_{a_1}^{a_o} r\ J_m\ (kr \sin\psi).\ dr \right| \quad . \tag{11}$$

As before, the analysis is restricted to low frequencies, such that

$$k^2 a_o^2 \ll m^2 \quad ; \tag{12}$$

this implies that all (m,n) modes are excited below their cut-off frequency. The integral in (11) may then be estimated using the asymptotic approximation to the variation of J_m :

$$J_m(x) \propto x^m \quad \text{(index approximately valid for } x^2 \ll m^2\text{)}. \tag{13}$$

It follows that

$$\int_{a_1}^{a_o} r\, J_m(kr \sin\psi).\, dr \doteq \frac{a_o^2}{m+2} (1 - \mu^{m+2})\, J_m(ka_o \sin\psi) \ . \tag{14}$$

From (11) and (14),

$$|P| = \frac{\rho\omega |U_o| S}{(m+2)\pi s} \cdot \frac{1-\mu^{m+2}}{1-\mu^2} \cdot |J_m(ka_o \sin\psi)|, \quad (k^2 a_o^2 \ll m^2). \tag{15}$$

This result may be compared with the narrow-annulus approximation given by equation (5.17) of [27]. The equations coincide when $\mu \to 1$, as expected, and also when $m = 0$ (radiation from an annular piston). In general, however, the effect of finite annulus width on the radiated sound power is represented by the factor

$$\left(\frac{2}{m+2} \cdot \frac{1-\mu^{m+2}}{1-\mu^2}\right)^2 \quad , \qquad (\to 1 \text{ as } \mu \to 1) \tag{16}$$

which is the ratio of the actual power, given by (15), to the power radiated from a ring source of radius a_o having the same value of the radially integrated source strength $\int_{a_1}^{a_o} Ur.dr$ (i.e. the power is compared with the limiting case $\mu \to 1$, holding $U_o S$ constant).

For annular distributions of finite width (μ not close to 1), and $m \geq 1$, it is clear from (16) that to concentrate the whole source in a ring at the outer radius is generally a poor approximation. In the extreme case where $\mu = 0$, for example, the power is thereby overestimated by a factor $(1 + \frac{1}{2}m)^2$.

Equation (15) gives the sound power radiated from each side of the disk as

$$W_m \doteq \frac{\rho\omega |U_o|^2 S^2}{2\pi a_o (1-\mu^2)^2} \left(\frac{1-\mu^{m+2}}{m+2}\right)^2 \bar{J}_{2m}(2ka_o) \quad , \tag{17}$$

so the corresponding radiation efficiency is

$$\tau_m \doteq \frac{ka_o}{1-\mu^2} \left(\frac{1-\mu^{m+2}}{m+2}\right)^2 \bar{J}_{2m}(2ka_o) \qquad (k^2 a_o^2 << m^2), \tag{18}$$

for any radius ratio μ. In practice the quantity μ^{m+2} can often be neglected compared with 1.

Power radiated from (m,0) component of uniform circular distribution.

The radially-uniform source distribution studied above may be regarded as a sum of (m,n) modal distributions, all values of n being

present to some extent. It is relevant to inquire how much of the radiated power given by (17) is accounted for by direct radiation from the (m,0) component alone, under the present low-frequency restriction (12) which ensures that all modes are radiated below cut-off. If this is the dominant contribution - as in fact turns out from the following analysis - then the presence of the higher-order radial modes is evidently immaterial as far as the radiated power is concerned. It follows that equation (17) may be used to estimate the sound power, even if the modal components $n \geq 1$ of the original uniform distribution have been suppressed (e.g. by placing the source in a duct.)

For simplicity a circular source distribution ($\mu = 0$) is assumed; this is expected to maximize the higher-mode contribution to W_m. The normalized (m,n) mode coefficient of the radially-uniform distribution (10) is then given by

$$\bar{U}S = 2\pi U_o \int_o^{a_o} r\, R_{mn}\, dr \quad , \tag{19}$$

where

$$R_{mn}(r) = \frac{J_m(g_o r/a_o)}{\left(1-\frac{m^2}{g_o^2}\right)^{\frac{1}{2}} J_m(g_o)} \quad . \tag{20}$$

Evaluation of the integral $I_{mn} = \frac{1}{a_o^2} \int_o^{a_o} r\, R_{mn}\, dr$, for $n = 0$ and a range of m values ($m \geq 1$), leads to the approximation

$$I_{m0} \doteq 0.85\ (m+4)^{-1/3} \qquad \text{(within 5\% for } m \geq 1\text{)}. \tag{21}$$

Hence

$$\bar{U} \doteq 1.7\ (m+4)^{-1/3}\ U_o \qquad (m \geq 1) \tag{22}$$

is the approximate spatial r.m.s. value of the (m,0) component of (10). Combining this result with the radiation-efficiency estimate (9) gives the power radiated directly from the (m,0) component as

$$W_{m0} \doteq \frac{3}{4} \frac{\rho\omega |U_o|^2 S^2}{\pi a_o} (m+2)^{-4/3}\ (m+4)^{-2/3}\ \bar{J}_{2m}(2ka_o), \qquad (k^2 a_o^2 << \tfrac{1}{2}m^2,\ m \geq 1)\ . \tag{23}$$

The ratio of this power to the total radiated power, as given by (17) for $\mu = 0$, is

$$\frac{W_{m0}}{W_m} \doteq \frac{3}{2} \left(\frac{m+2}{m+4}\right)^{2/3} \qquad (m \geq 1)\ , \tag{24}$$

which lies between 1 and 1.5. At frequencies low enough for all modes to be below cut-off, therefore, a radially uniform source distribution as given by (10) radiates energy predominantly through the (m,0) mode component. This is in contrast to the high-frequency situation, where several modes contribute to the radiated power when m is large.

Approximation to the Bessel function integral

The integral $\bar{J}_{2m}$ appearing in (8) and (18) is difficult to evaluate for large m (cf. [27], Sec. 5.2). The following approximations are useful when rough estimates are required.

For small values of the argument, the asymptotic value of $\bar{J}_q(x)$ is

$$\bar{J}_q(x) \doteq \frac{2(\frac{1}{2}x)^{q+1}}{(q+1)!} \qquad (x^2 << q + 3) \; . \tag{25}$$

The small-argument limitation in (25) is unduly restrictive for present purposes, however; condition (12) requires only $x^2 << q^2$ for the radiation efficiency estimate (18) to be valid. By noting that $\bar{J}_q(j'_{qo})$ is approximately independent of q and lies between 0.7 and 0.8 (where j'_{qo} is the smallest positive root of $J'_q(x) = 0$), the following modification of (25) is arrived at:

$$\bar{J}_q(x) \doteq (\tfrac{1}{2}q)^{\frac{x^2}{2q^2}} (\tfrac{3}{4})^{\frac{x^2}{q}} \frac{2(\frac{1}{2}x)^{q+1}}{(q+1)!} \quad , \qquad (x^2 << q^2). \tag{26}$$

This reduces to (25) when $x^2 << q$, as required, and agrees well with published values given by Embleton [66, Fig. 8] and Lowson [67, Fig. 10].

The corresponding value of τ_m from (18), neglecting μ^{m+2} compared with 1, is

$$\tau_m \doteq \frac{2}{1-\mu^2} \frac{m^{(ka_o)^2/2m^2} (\frac{3}{4})^{2(ka_o)^2/m}}{(m+2)^2 \; (2m+1)!} (ka_o)^{2m+2} \quad , \quad (k^2a_o^2 << m^2). \tag{27}$$

Application of results to radiation from an annular opening

Equations (18) or (27) may be used directly to give the radiation efficiency for a radially-uniform distribution of fluctuating normal velocity, corresponding to (10), over a baffled annular opening. If there is no baffle, or the baffle is small compared with the wavelength, τ_m may be overestimated by a factor of up to 2.